1. A brief account of airglow study

1.1 A brief historical and scientific introduction to airglow study

The existence of the phenomenon of 'airglow' was probably discovered before 1800 [1]. Yntema [1] was the first person to photometrically establish the phenomenon of 'airglow' which is termed as Earthlight. Following the suggestion of Otto Struve, Silvey[2] introduced the name 'airglow' for the first time. The two main facts that led scientists to the discovery of 'airglow' were as follows:

(i) Insufficiency of scattered starlight or galactic light for explaining the then observed increase of light intensity towards horizon.

(ii) Brightness of the night sky was found to be more towards other direction than towards the Milky-Way.

After Yntema [1], Newcomb [3] and Burns [4] measured that extra brightness of night sky by means of visual aids following which the same was measured photographically by Townley [5] and Fabry [6]. Oxygen green line ($\lambda = 5577$Å) was the first of all kinds of auroral emissions, as known now, to be detected in all parts of the sky and this was found to exist for all time. Yntema called that emission as a permanent aurora which was termed as nonpolar aurora by Rayleigh. Van Rhijn [7] was the first to give a precise mathematical expression of airglow intensity :

$$I = I_0 \Big/ \left\{1 - [a/(a+z)]^2 \sin^2 \Psi\right\}^{1/2} \qquad (1.1)$$

where a – radius of Earth, z – height of the emitting layer, Ψ – the angle of declination towards the direction of incidence. VanRhijn considered a very simple case of a homogeneous, thin layer of emission for a completely transparent spherical atmosphere.

There was a major problem at that time with the percentage contribution of different sources to the total brightness of the night sky. The main sources of emissions, as was known at that time, are broadly classified as

(i) Zodiacal light,

(ii) Galactic light,

(iii) Self luminescence of the upper atmospheric gases.

The main problem at that time was to distinguish separately the contributions of purely galactic light, galactic light scattered by interplanetary gas and dust and purely terrestrial atmospheric emissions to night sky brightness. Rayleigh [8] was the first person to succeed at least partially in this regard. Babcock and Dufay [9] used the polarization property of light in their observation of night sky brightness and inferred about amount of light coming in certain direction of observation. It was Rayleigh [8] who made for the first time, the absolute measurement of intensity of green line emission from night sky and was the first to express it in terms of the number of atomic transitions per second in a column along the line of sight as

$$I = 4\pi\, \mathcal{N} = 4\pi \int_0^{\infty} F(r)dr \quad \text{and}$$

$$I = (A\Omega/4\pi) \int_0^{\infty} F(r)dr, \qquad (1.2)$$

where F(r) – No. of photons / c.c. sec. observed in an arbitrary direction of line of sight at a distance of 'r' from the source of emission,

A - The effective areal aperture of the photometer,

Ω - The effective angular range of clear vision for the diameter of the lense of the photometer expressed in terms of the unit of solid angle *i.e.* steradian. This is actually small enough relative to the angular range of irregularities of emitting layer.

$\mathcal{N}$ - No. of incident photons / cm^2 sec. sterad.

E - No. of incident photons / cm^2 sec. (column).

I - Total radiation striking the photometer per second (photons/sec.)

Amongst many other scientists who helped in establishing a standard theoretical basis of the science of airglow, the followings are noteworthy : J Dufay, H Vogel, A J Angstrom, E Wiechert, W W Campbell, H D Babcock, V M Slipher, L Vegard, J C.Melennan, J H Mc.Leod, G M Shrum, W Brunner, S Chapman, J Cabane, J S Bowen [9] identified for the first time some of the forbidden lines in the spectra of planetary nebula. S Chapman [10] was the first person who attempted to explain theoretically, the phenomenon and different features of airglow in general. Radiations emitted from the atmosphere and induced by extra-atmospheric atomic or subatomic particles, comprise what is known as Aurora. Regarding different characteristic features, there is similarity between the aurora and the airglow. For example, although the aurora is specifically produced by the interactions of particles, radiations emitted within the lower atmosphere by the interactions of cosmic rays are regarded as airglow emissions. Although light from auroral origin is much brighter in general, than light from airglow emissions, in some cases like that of λ 5577Å green line, there is little difference between the two. Non-thermal radiations emitted by terrestrial atmosphere are mainly the airglow emissions, although similar radiations produced by lightning, meteor trains or similar phenomena like explosions within the atmosphere are considered as auroral emissions. Considering all, a component of airglow is sometimes termed as permanent aurora or nonpolar aurora [10].

The whole of the terrestrial atmosphere is continuously being excited by the flux of energy which are coming from the cosmos. Those agencies of cosmic origin are very broadly known as cosmic rays. Cosmic rays constitute of electromagnetic radiations ranging from very large wavelength background radiations down to very small wavelength characteristic radiations and streams of high energy particles such as proton, electron, meson, hyperon *etc*. As major part of the cosmic energy flux comes in the form of electromagnetic radiation for which the collision crosssection is also very high within the terrestrial atmosphere, we consider electromagnetic radiation as the only responsible agent of excitation of atmospheric constituents. Moreover, we know that most of this electromagnetic energy flux comes from the Sun. Hence, solar energy plays a vital role in the overall excitation of the constituents of the terrestrial atmosphere.

Molecules and atoms throughout the atmosphere are excited by solar energy in presence of the Sun in the sky and these excited atmospheric molecules and atoms return to their ground-state emitting electromagnetic radiation in space which becomes clearly observable in the absence of the Sun from the sky [11]. Thus, the atmospheric excitation must bear a relation with the Sun's appearance in and disappearance from the sky. The airglow is accordingly very broadly classified as twilight airglow, night airglow and day-airglow. The twilight airglow is further classified as : Morning twilight airglow and Evening twilight airglow.

The proportional amount and wavelength of radiations in the absorption and emission by atmospheric molecules depend on the molecular concentration, reaction rate and scattering crosssection of those molecules, respectively. The thermal excitation and emission by atmospheric molecules, which eventually take place in the lower part of the atmosphere, are of special interest to geophysicists and meteorologists. The spectral range is from near infrared to far ultraviolet. This phenomenon eventually happens in the ionosphere where molecules are continuously dissociated by incident radiation to produce ions and the ions are continuously recombined with electrons to produce excited atoms. Emission by these excited atoms comprises what is known as the airglow. Thus, an airglow researcher is primarily concerned with the ionosphere. Depending on the ionospheric content and the characteristics of response to radio waves propagation, the ionosphere has been subdivided into finer layers such as E-layer, F-layer, D-layer , and so on. Which layer should we be interested in, depends mostly on which characteristic wavelength range do we study. For example, if we study the 6300 Å Oxygen red line, we would be interested in F_2-layer. Subdivision of sublayers such as F_1,F_2, occurs only in day time whenceforth these two sublayers merge together in absence of solar energy-flux at night and produce one single layer which is the F-layer.

Different areas of research in 'Airglow study' :

Among so many areas of research in airglow study, the followings are the most important :

(i) Verification of different mechanisms such as Chapmann's mechanism, Barth's mechanism *etc* which are proposed for explaining the production of various airglow lines.

(ii) Verification of the validity of some empirical equations, such as the equation due to Barbier, which connects intensity of a particular line and the critical frequency and virtual height of the layer responsible for producing that line.

(iii) Chemical modelling by means of proposing some kind of reaction for the interpretation of various observed physicochemical properties of a particular line.

(iv) Seasonal variation of intensity of a particular line.

(v) Latitudinal variation of intensity of a particular line.

(vi) Discovery of new airglow lines.

(vii) Effect of lunar tidal variation on the airglow line intensity.

(viii) Effect of various solar activities on the airglow line intensity.

(ix) Speculation about the possible airglow mode in the Martian, Venusian, and Jovian atmospheres.

(x) Discovering the influence of ozone depletion on the mode of variation of some specific line intensity.

(xi) Examining the possibility of and searching for airglow lines of very short wavelengths such as X-rays and gamma rays.

Besides, there may be many other interesting features concerning airglow that one may encounter while performing research in airglow.

1.2 Classification of airglow phenomena :

Airglow spectra may in general be of three different types :

i) Airglow lines ,

ii) Airglow band system ,

iii) Airglow continuum.

Specific ones of each type that are observed in different hours during a day, are named after the particular period of a day in which it is observed. [Fig. 1]

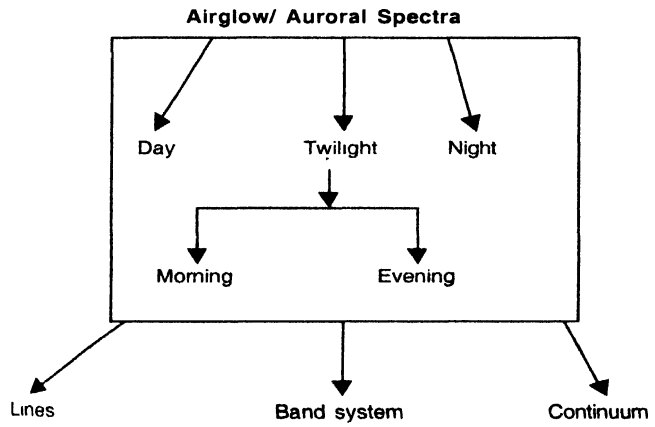

Figure 1. Classificatioin of Airglow Spectra awording to their time of occurrence and nature

Examples :

(1) Continuum :

4000 Å – 6000 Å (Approx.) Height of Peak Emission Layer is about 100 km. This continuum system was detected by both Barbier [12] and Chuvayev [13]. A possible mechanism was proposed by Krassovsky [14] which is as follows :

$$NO + O \longrightarrow NO_2 + h\nu, \quad \text{Radiative}$$

$$NO_2 + O \longrightarrow NO + O_2 \quad \text{association}$$

Krassovosky's mechanism was verified by Becker *et al* [15] .

(2) Band System :

i) Meinel (Hydroxyl) Band System (Rotational – Vibrational – Band , $\Delta v = 1$ sequence)

Height of peak emission Layer is 90 km.This system was first discovered by Lytle & Hampson [15] . A possible mechanism was proposed by Bates and Nicolet [16,17] .

Chemiluminescence cycle

$$H + O_3 \longrightarrow OH(v \leq 9) + O_2 ,$$

$$OH + O \longrightarrow O_2 + H.$$

(ii) Oxygen Band System (1.58μm (0.1))

Band of IR Atmospheric System $^1\Delta_g - X\,^3\Sigma_g^-$ was first detected by Vallance Jones and Harrison [18] .

Height of Peak Emission Layer is about 50 – 60 km.

A possible mechanism, given by Jones and Gattinger [15] is as follows :

$$O_3(^1A) + h\nu\,(2000\,A < \lambda < 3100Å) \longrightarrow$$

$$O(^1D) + O_2(a^1\Delta g).$$

According to Gauthier and Snelling [15] , this process is photodissociation of O_3 is followed by

$$O(^1D) + O_2(X^3\Sigma_g) \longrightarrow O(^3P) + O_2(b^1\Sigma_g^+).$$

Wallace and Hunten [15], on the basis of their consideration of resonant scattering and energy-transformation (Schuman–Runge Dissociation and Hartley dissociation), verified the above-mentioned mechanism of production of this band system [15].

(iii) Lyman-Birge- Hopfield Nitrogen band system.

LBH system, defined by the transition $a\,^1\Pi_g \rightarrow X\,^1\Sigma_g^+$ of N_2 appears in UV spectra whose midlatitude intensity is as high as 1KR. This band was first discovered by Borth and Schaffner [19] in the dayglow.

3) Lines [15,20,21] :

(i) Forbidden Red Doublet of oxygen 6300 – 6364 Å ,

(ii) Forbidden Green Doublet of nitrogen 5198 – 5201 Å.,

(iii) Forbidden Green 5577 Å and UV 2972 Å line of oxygen,

(iv) Sodium D_1 and D_2 lines 5896 Å and 5890 Å ,

(v) Intercombination lines of OI, OII, NI and NII λ 1304, λ 1356, λ 1152, λ 7990, λ 1134, λ 1200, λ 1493, λ 990, λ 834, λ 538, λ 539

(vi) Helium line λ 10,830 ($2p^3P \longrightarrow 2s^3S$)

(vii) Forbidden 7320 and 7330 Å doublet of OII and 5755 Å line of NII,

(viii) O^+ $2p-4s$ λ 2470 UV [15, 19]

(ix) Li (6708 Å) [15, 19]

(x) Fe (3860 Å) [15],

(xi) Mg^+ Doublet λ 2796, λ 2803 [19],

(xii) HI 1216 Å [15, 19];

1.3 Different atmospheric physical parameters, observational methods and instrumentation:

The most fundamental physical parameters which play vital roles in various features of terrestrial atmosphere are as follows ;

(i) Temperature, (ii) Pressure, (iii) Density, (iv) Composition, (iv) Radiation (Corpuscular), (v) Radiation (electromagnetic specially radiowave, microwave, UV, EUV, X-ray, γ-ray), (vi) Wind system, (vii) Humidities, (viii) Electron - and ion-density and (ix) Vertical distribution of ozone.

The main sources and probes for collecting information about the above-mentioned characteristic physical parameters related to upper atmosphere in early 50's were as follows [20] :

(i) Gun shell explosions (ii) Rocket observations, (iii) High altitude balloons (iv) Noctilucent clouds (v) Meteor observations, (vi) Emission from the sky (vii) Propagation of sound waves, (viii) Propagation of radio waves, (ix) Searchlight measurements and (x) Theoretical studies.

Among those all possible probes for collecting information about upper atmosphere, the 'Emission from the sky' and 'theoretical studies' are mainly dealt with in this work and are briefly mentioned below.

Emission from the sky :

Observations of emitted radiations from the night and twilight sky mainly through spectroscopes and photometers were taken and information regarding the upper atmospheric glow were obtained. The various sources of emission and the average percentages of their contributions to the total brightness of the sky that can be observed in a moonless night may be given as follows :

Star light (direct and scattered)	- 30% (G) (1)
Zodiacal light	- 15% (B) (2)
Galactic light	- 5% (Y) (3)
Luminescence of the night sky (Air glow)	- 40% (R) (4)
Scattered light from the last three sources	- 10% (W) (5)

π-chart showing percentage contribution of differe sources of emissions from the sky in the visible region

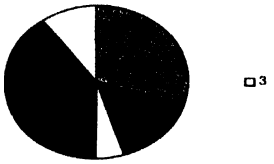

Comprehensive surveys on emissions from night sky, know as airglow, were made in the early 20th century by Prof's. E Hulburt [21], S K Mitra [22], P Swings and A B Meinel [23],

Theoretical studies :

Empirical method is one of the most significant pillars of scienc which is again based mainly on theoretical concepts. In case c upper atmospheric investigation, theoretical study may b broadly classified into two categories :

(i) Analysis of data from direct observation ,

(ii) Synthesis of concepts to match the observed dat and thereby explaining relation among differer features.

The method of synthesis necessarily creates physic models of terrestrial atmosphere which successively undergoin rectification and modifications, may take a final form so that a least some features of atmosphere can be explained to satisfactory level.

The range of heights for an application of theoretical analys may be considered to extend from the ground level up to 100,00 kms. and beyond that terrestrial atmosphere is a meaningles term.

Different important features of terrestrial atmosphere an theories concerned (as was reported in the Geophysical Researc papers No. 43, Methods and Results of Upper Atmospher Research, Geophysics Research Directorate, Air Forc Cambridge Research Centre, Air Research and Developmer Command) are :

(a) Atmospheric Tidal Oscillations,

(b) Dynamo theory,

(c) Theories of the Exosphere,

(d) General circulation model.

(a) Atmospheric tidal oscillations :

Diurnal and semi-diurnal barometric surface oscillations ar observed to occur within the atmosphere on both hemisphere Harmonic analysis of barograms alongwith statistical analys of ionospheric observations, auroral height data and signa intensity measurements have been made to isolate solar tid

from lunar tide. The fact that semi-diurnal barometric variation due to the Sun is 16 times that due to Moon while tide raising force of the Moon is twice that of the Sun, was first pointed out by Sir William Thomson [20] and was tentatively explained by himself on the basis of his proposition that the terrestrial atmosphere, having a period of free oscillation of nearly 12 hrs., produces resonance. Analogously with the Thomson's proposition, Taylor- Pekeri's theory tells that for a particular temperature, the height-distribution of terrestrial atmosphere may have two modes of free oscillation. Gerson [20] found that although tidal variations in the terrestrial atmosphere caused by the Sun is greater than that caused by the Moon; the solar tidal effect can not be easily isolated from the strong semi-diurnal harmonics of atmosphere while lunar tidal effect can readily by determined.

Any proposed model giving the altitudinal variation of temperature can easily be tested by means of calculations of its periods of free oscillation. According to the tidal theory, the pressure distribution generates a world-wide wind system. Wind systems play important role in upper atmospheric process because its average speed is much higher than that within the troposphere. Lunar tidal variations have been detected in D, E, F_1 and F_2 layer while solar tidal influence leaves its signature mainly in F_2-layer. The general theory of tidal oscillations, developed by Martyn [20] which is also known as 'electrodynamical theory', is based primarily on the postulate that the ions and electrons move only along geomagnetic field lines even if the tidal motions are mainly horizontal. Kirkpatrick and Mitra [20] made significant contributions in this field.

(b) Dynamo theory :

On regular undisturbed or quiet day, diurnal variations in the Earth's magnetic field and associated parameters that necessarily includes the upper atmospheric current system can be explained by the Dynamo theory first proposed by Stewart and Schuster [20]. There are two other theories ; namely, Diamagnetic theory of Ross Gunn [20] and Chapman's [20] Drift current theory. These two theories can not explain most of the ionospheric phenomena satisfactorily. The two basic requirements, common for both the diamagnetic and drift current theories are high temperature and high electron density that prevail in source-region of terrestrial ionosphere while the motion of the whole atmosphere is not at all a necessary requirement for either of these theories. But the Dynamo theory is consistent with the electrical and thermal properties of ionosphere as mentioned above and with the wind system. World-wide regular wind systems in the ionospheric region is presumably, partly due to variation in temperature and partly due to tidal forces.

With the help of Dynamo theory, Vestine [20] showed that a simple monthly mean wind system of geomagnetic disturbance agrees fairly with Kellog - Schilling model [20] of upper atmosphere-circulation (to be discussed later). Dynamo-theory also reveals the fact that the main phase of a magnetic storm is consistent with diurnal features of atmospheric motion deduced from radio-star scintillations and auroral motion.

According to the Dynamo theory, electrical conductivity of the ionosphere was found out to be much higher than that due to electron density obtained only from Radio wave measurements. Rocket measurements confirmed the existence of a very high ion density and of a horizontal current sheet and thus, the requirement of dynamo theory was found to be truly realistic.

Ionosphere comprises of equal number of positive and negative ions embedded in a neutral gas which at some height, moves mainly by solar and lunar tidal forces. This motion of ionospheric region is presumably eased or mobilized by internal motion caused by thermal energy. Bulk of charged particles within the ionosphere moves as a whole in permanent steady geomagnetic field and this fact is obviously analogous to the case of a dynamo in which a conductor moves within a magnetic field and produces emf. That is why the production of some amount of atmospheric emf and consequent atmospheric current caused by this kind of motion of ionospheric charged particles is known as the Atmospheric Dynamo Effect [24]. Ionospheric current caused by the atmospheric dynamo effect on the other hand, produces another magnetic field which interacts with the primary magnetic field of the Earth. This interaction follows successively the trio of Ampere's circuital law, Faraday's law and Lenz's law and produces a repulsive force between the sources respectively of the primary and the secondary magnetic field *i.e* the Earth and the ionospheric conducting sheet. As a result of this repulsion, the electron-ion plasma in the ionosphere moves as a whole, to the range of strong geomagnetic field. This is again some kind of effect that occurs within an electrical motor. Thus, this effect is called the Atmospheric Motor effect.

It has been found that as a first approximation, the 'dynamo' is situated in E-region and the 'motor' in the F-region [24] .

(c) Theories of Exosphere :

Terrestrial atmosphere, being gravitationally bound by Earth, rotates with Earth's axial rotation and it experiences the influences primarily of the following factors :

(i) Earth's Gravitational force,

(ii) Centrifugal force due to Earth's axial rotation,

(iii) Thermal energy which manifests mostly in the form of mean molecular kinetic energy within the atmosphere (mean free path, density, pressure),

(iv) Conservation of angular momentum ,

(v) Influence of external gravitating cosmic bodies (mainly the 'Sun' and the 'Moon'),

(vi) Incidence of electromagnetic radiation and cosmic ray particles from outside.

(vii) Effect of geomagnetic field, Atmospheric Dynamo and Motor *etc*

Amongst these, the first four determine the limit of some atmospheric equilibrium at which density becomes minimum and molecular mean-free-path becomes very very large. The order of magnitude of this limiting height of the terrestrial atmosphere is about 35500 kms above sea level for the equatorial plane. At this height, the mean free paths of molecules become very large and collisions become infrequent Consequently, gas particles are subjected to the gravitational force only. Those particles at this height, move in conic sectional orbits. Some of the particles fall back to denser region of the atmosphere but escape entirely from the Earth's vicinity after free flight for a while. This region is called the fringe region of the atmosphere or the exosphere. Various information regarding the density and temperature associated with the degrees of dissociation and ionization and also the rates of escape of different gas-molecular species can be derived from calculations based on some suitable model.

(d) General circulation Models (GCMs) :

On the basis of consideration of general convective and other type of circulation, some appropriate model has been constructed and with the help of those models, attempts have been made to know about various features of terrestrial atmosphere.

Instrumentation

The basic physical observable of greatest concern in the study of airglow is the intensity (*i.e* the brightness, total or specific line emission) of radiations. Methods of observations are mainly of two types, each of which is subdivided on the basis of technological means of observation into three categories [Fig. 2]

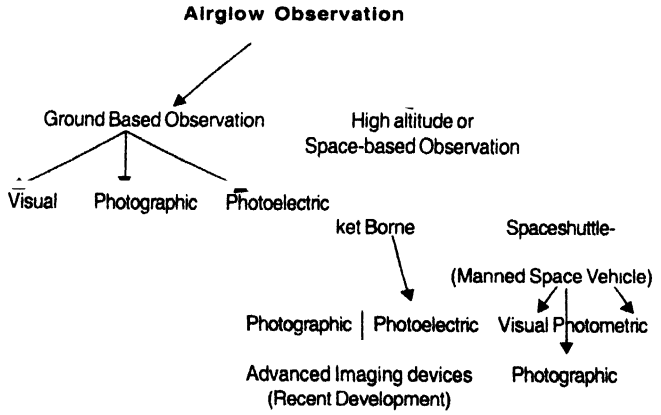

Figure 2. Different methods of airglow observation are shown categorically.

The instrument, devised mainly for the measurement of intensity is called photometer which, according to the mechanical or technological devices may be of three different types:

(i) Visual photometer,

(ii) Photographic photometer,

(iii) Photoelectric photometer,

Scientists like Dufay, Lord Rayleigh and S.K. Mitra [22] used to observe the total brightness or specific spectral emission intensity and their corresponding variation with the help of visual and photographic photometer. Schematic diagrams of such photometers are being shown in Figure 3 [22,25]

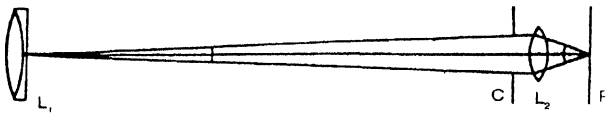

Figure 3(a). Photographic method for measuring the brightness of the night sky [L_1-Objective, C- Circular Opening in the focal plane of L_2, L_2 Converging lens, P Photographic plate]

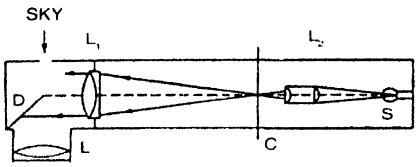

Figure 3(b). Visual photometer as devised by Dufay [22] [O – Observer's eye, L- Exit lens, D – Screen reflector, S – Lamp as an artificial source of light, C - absorbing wedge in the focal plane of L_2, the Telescopic system L_1 - collimator lens system, Light from the source S is made to pass through a filter of a dilute ammoniacal $CuSO_4$ solution].

Later on, scientists all over the world started observation of airglow and in a rapid progress, they developed photoelectric method, automatic recorder and a number of other devices including most advanced imaging devices. Sophisticated interference filter with very narrow bandwidth are usually used in photoelectric photometer. Various groups of observers used several set of such modified instruments for airglow observations some of which are shown in Figures 3 and 4 [25,26]. For details one may consult the Ref. [27,28]. Schematic view of some other Rocket borne photometers alongwith block- diagrams of the electronics are shown in Figure 5 [29]. The instrumentation consists of nine photometer units in two concentric rings of three and six and associated electronics distributed inside the

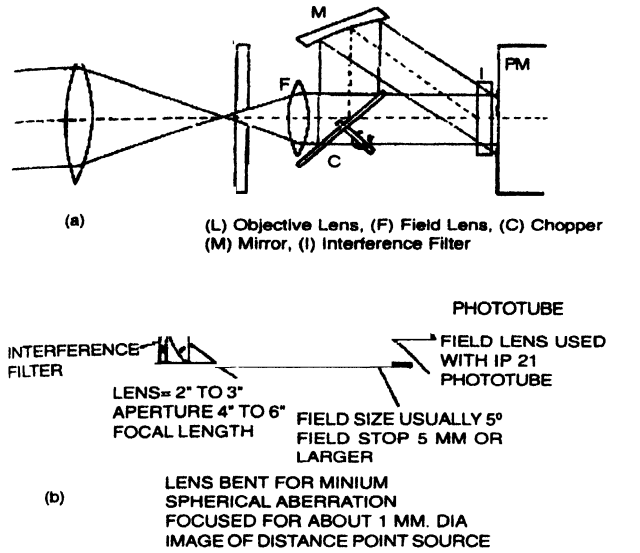

Figure 4. (a)&(b) Schematic representations of different opto-photometric setup used for this purpose of continuum subtraction and minimization of aberrations [L–Objective, A- Aperture, F-Field lens, C-Chopper, M- Mirror I - Inferfernece Filter].

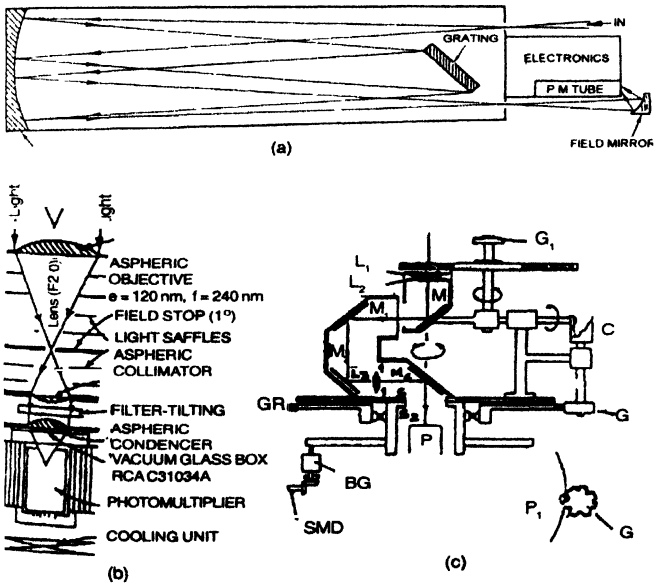

Figure 5. (a) Sketch of a rocket spectrometer. (b) Experimental arrangement of Misawa and Takeuchi [26] for measuring nightglow intensity. (c) An automatic photometer of Choudhuri and Tillu [26] for measuring nightglow intensity. [L_1, l_2 – Lenses forming objective

- Field lens, M, M_1, M_2, M_3, M_4 – Mirrors, F- Filter, S- Diaphragm G_1- seven sector geneva wheel, P- Revolving Pin.

ir-Guide Ring, C-A can, BG-Beval Gear

MD- Synchronus Motor Drive. T-Telescope Mount (Rotatable)]

ose cone and forward compartment of the Rocket Skylark VII sl. No. SL39 Figures 6 and 7 [Ref. 29].

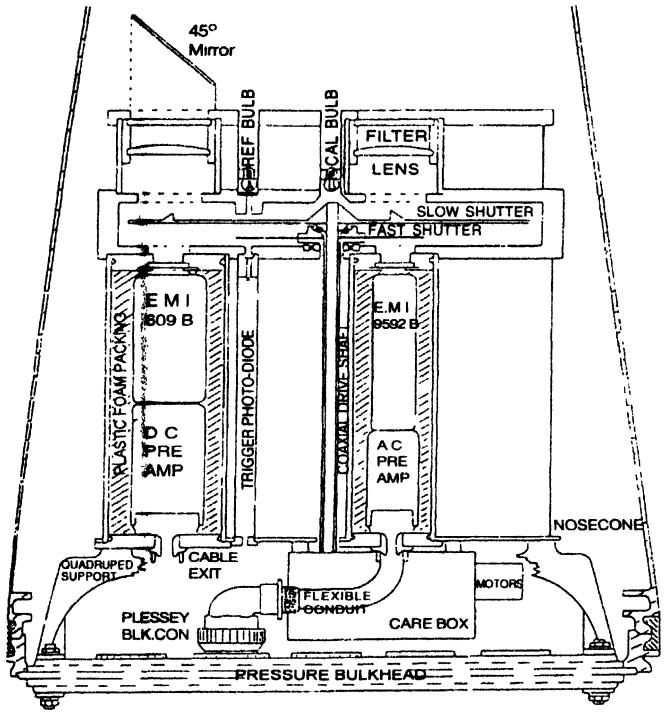

Figure 6. Simplified section view of photometer housing mounted on quadruped support inside nose cone

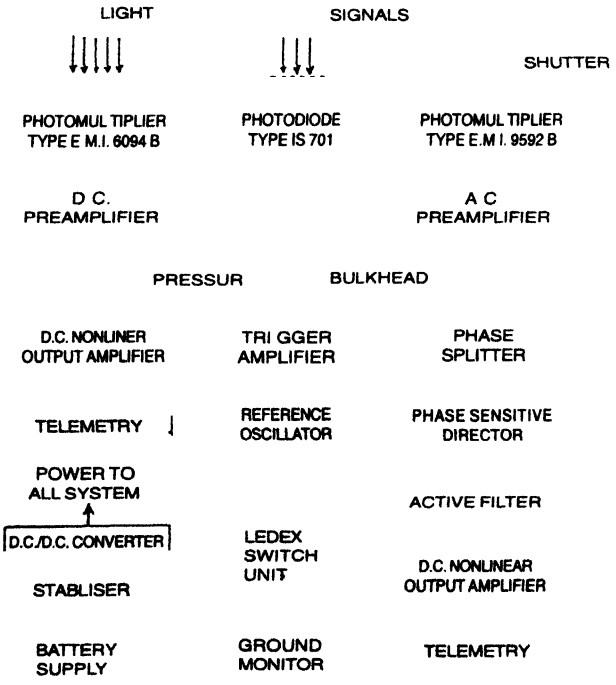

Figure 7. Block diagram of system electronics.

The MULTIFOT scientific rocket payload contained six longitudinally placed and four transversely placed photometers, all with interference filters for selection of emission line and a lens and diaphragm to determine the field of view. In all photometers, the photomultipliers are used in the photon counting mode with charge-sensitive preamplifier. Absolute laboratory calibrations of all photometers were made using two MgO diffusers illuminated by a standard light source. Multi 2 six channel multicolour tilting-filter photometer retained the capacity to measure zenith intensities of OI 5577 Å, Na D 5890 Å, OI 6800 Å, OH(9.4) band, Q (7750 Å) and R (7720 Å) branches and the O_2 atmospheric (0,1) band at 8600 Å. A photomultiplier with GaAs cathode was used to cover a broad spectral range. With the help of transportable lidar system, the vertical profiles of atmospheric sodium density and NaD airglow emission were simultaneously measured.

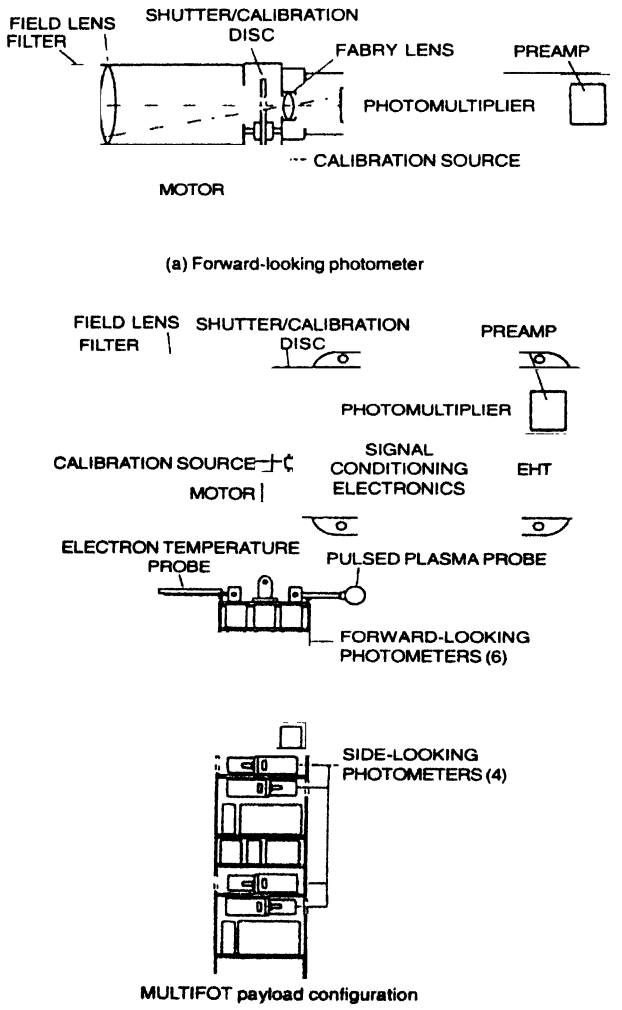

Figure 8. (a) Schematic representation of forward-looking photometer carried aboard rocket in MUL TIFOT - 92 campaign.

Imaging systems have been used very successfully in the study of equatorial aeronomy . A schematic diagram of such an imaging system is shown in Figures 8 and 9 [30 - 32].

Multi-Instrumented Studies of Equatorial Thermospheric Aeronomy (MISETA) is a program of exploiting imaging science to obtain various aeronomical observations. It was made with the help of Charged Coupled Device (CCD)-based all sky airglow imaging system set to operate on a continuous basis from an equatorial site. This program has multi-diagnostic capabilities including an incoherent scatter radar and a Fabry-Perot interferometer [33, 34].

A pair of photometers, specially devised to scan the sky continuously within a wide range of latitude for some specific airglow lines, is known as scanning-photometers–system. Such a system of scanning photometers was used by Sobral *et al* [35] to detect gravity wave perturbations of 6300 Å airglow at low latitudes.

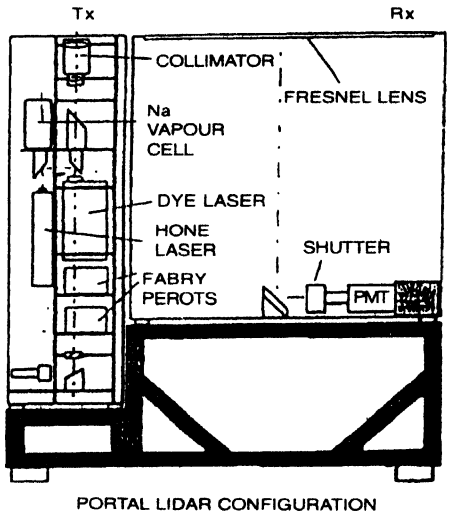

Figure 9. PORTAL Lidar configuration

Cosmovici *et al* [36] proposes the use of International Ultraviolet Hitchiker (IE) to obtain 2D images of EUV-FUV (400 – 1380 Å) optical phenomena which usually take place in the neighbourhood of tethered satellite system (TSS). Far Ultraviolet (1400 – 1800 Å) photon–counting imaging telescope FAUST was developed to provide precise photometry of extended astronomical objects and it has a wide FOV (7.6°) and an angular resolution of 2 arc minutes [36]. OGLOW (orbiter glow) experimental set up consists of a simple photographic imager combined with a series of high resolution interference filters. Fabry-perot interferometers and grating spectrometer and it was used to detect space-craft glow and atmospheric emissions [37].

Consisting of a narrow-band interference filter, a lens for focussing and a focal plane array (CCD) to record the spectral images in digital form, the interference filter spectral imager has two fields of view, one for the zenith and the other for 20° above the horizon [38].

High Resolution Airglow and Aurora Spectroscope (HIRAAS) experiment on the Advanced Research and Global Observing Satellite (ARGOS) demonstrates the accuracy of the UV technique for sensing the ionospheric state [39].

Dual etalon Fabry-perot spectrometer is also being used for airglow intensity measurement with high precision [40].

Cryogenic Infrared Radiance Instrumentation for Shuttle (CIRRIS) is another sophisticated instrumentation in which infrared imaging system is employed to detect rotation of radical like NO^+ in nonlocal thermal equillibrium (NLTE) [41].

Among the other useful instrumentation techniques that are in vouge, are Czerny-Turner Scanning spectrometer [42], Divided mirror technique with Fabry Perot and Michelson's interferometer [43] and Wind Imaging interferometer (WINDII) [44] Novel optical measurements of F-region ion temperatures have been made in conjunction with thermospheric neutral temperature with the help of a ground based F-B interferometer. Important results were obtained therefrom [45].

It is extremely important to mention a few words about the unit of intensity and its calibration for the purpose of measuring airglow intensity.

Rayleigh, the internationally adopted unit for upper atmosphere emissions is defined as

$$1 \text{ Rayleigh} = 10^6 \text{ quanta cm}^{-2} \text{ sec}^{-1}.$$

If B_λ is the specific radiance in 10^6 quanta cm^{-2} sec^{-1} $^{-1}$ $Å^{-1}$ then $B = \int_0^\infty B_\lambda d\lambda$ over the emission line (or over the domain of a filter in the case of a continuum) and the total flux (in Rayleighs) is $4\pi B = 4\pi \int_0^\infty B_\lambda d\lambda$) [46].

Calibration of airglow photometers means standardizing the instrument for obtaining directly the measurement of the concerned physical quantity (brightness or intensity here) in terms of a standard unit. Calibration of airglow photometers is usually made in two steps ; (i) the measurement of the relative spectral characteristics of all elements of the photometer and (ii) the measurement of the sensitivity of the photometer in absolute units.

One of the several methods of calibrating a detector or a complete photometer in absolute units in case of a line source, is to first obtain the relative spectral response and then to perform a measurement at one wavelength with a calibrated source of line emission. This source is chosen for its emission at a wavelength within the spectral region desired. The line should be one that can be isolated readily with filters and should also be intense enough to permit accurate measurement with a standardized thermopile and then to calibrate a secondary standard photo-detector for use as a monitor of the line source. Procedure of calibration in case of continuous source is a bit different [25].

The brief description of specific instrumentation of the experimental set up used by Midya *et al* for the observation of airglow intensity is given below [25,47].

The photometer

An automatic portable Dunn-Manring filter photometer was used to measure the intensity of twilight and night airglow for 6300 Å and 5893 Å line emissions. Flux of light is allowed to fall on the cathodes of photoelectric detector which, being integrated over a fraction of a second, produces a measurable photocurrent. Band- pass filters of narrow bandwidth are centred on the specific line emission under consideration, for study. If the band pass is made sufficiently narrow as compared to the extent of spectrographic slit, the emission feature of a specific line can reasonably be discriminated from the astronomical background. The photometer is usually operated through a power supply consisting of a 6.4 H.P portable motor generator. The diagram of the appartus is shown in Figure 10.

The Telescope

The Telescope part of the photometer consists of an interference filter, a lens, a field stop and a photomultiplier cathode system. The filter selects a narrow wavelength region at a specific wavelength. The lens collects and converges the incident light flux to magnify its intensity at the focus while the field stop restricts the viewing area of the telescope. The photomultiplier tube multiplies electrically the photo-flux, keeping its variation pattern completely unaltered. The interference filter is approximately 6" in diameter and has a band-width equal to 20 Å approximately. The associated OH continuum is subtracted by tuning and detuning the filter at the specific wavelength of concern. The filter is rotated about 10° at 5 cycles per second by a Bodini 30 rpm motor (Model NSY - 12R) from its normal position to the optical axis of the telescope. An AC signal of frequency approximately equals to 20 Hz is obtained from the photomultiplier detector which is a Du Mont 6292 tube. The field stop restricts the viewing area of the telescope so that it subtend, a solid angle with semi-vertical angle equal to 5.7° in

the focal plane of the lens. As the photometer is an all-sky scanning apparatus above the horizon, the telescope is capable of rotation through 360° in the horizontal plane and through 90° in the vertical plane. The zenith drive motion is controlled by a geneva gear, which is driven by a 56 rpm Borg motor, type 1004 SY. As each notch in the gear changes the zenith position by a step of 5°, the telescope can be made to assume any angle of elevation from O° to 90°.

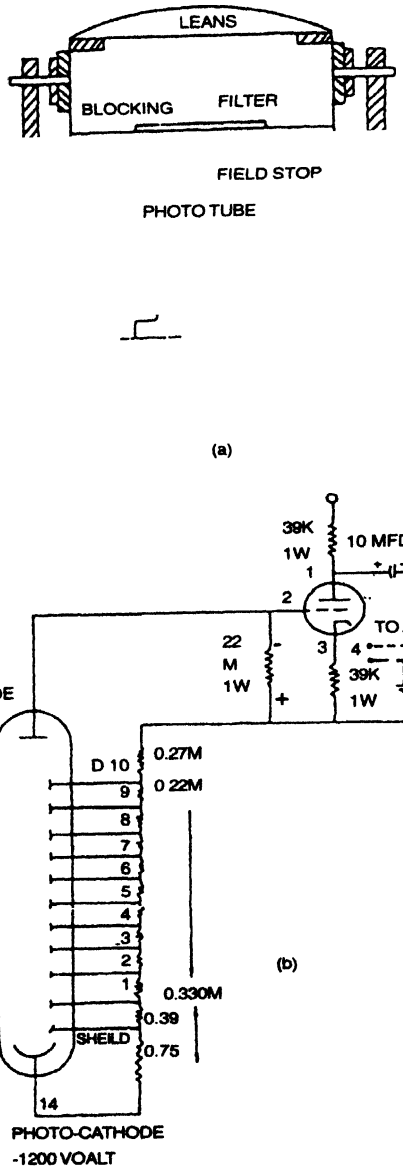

Figure 10. (a) Optical arrangement of the photometer telescope. (b) Phototube and cathode follower preamplifier circuit of the photometer telescope.

The Interference Filter

It consists of one or a series of Fabry Perot etalons. If a collimate beam of light is incident normally on a Fabry Perot etalon, onl wavelength satisfying the relation $2d = n\lambda$, are transmitte By reducing 'd' the interval between two such transmitte wavelengths can be increased. Choosing sufficiently small valu of 'd', a single maximum can be obtained in a specific spectr region. If 'd' is slightly larger than the etalon thickness, the filte is tuned to the specific wave length by tilting . On tilting th etalon, the effective etalon thickness is reduced to 'd cos , where ' θ ' is the angle of tilt. Consequently, the peak is shifte toward the shorter wavelength (Figures 11a and 11b). Therefore an etalon can be tuned by varying ' θ ' so that the peak is shifte to a slightly shorter wavelength.

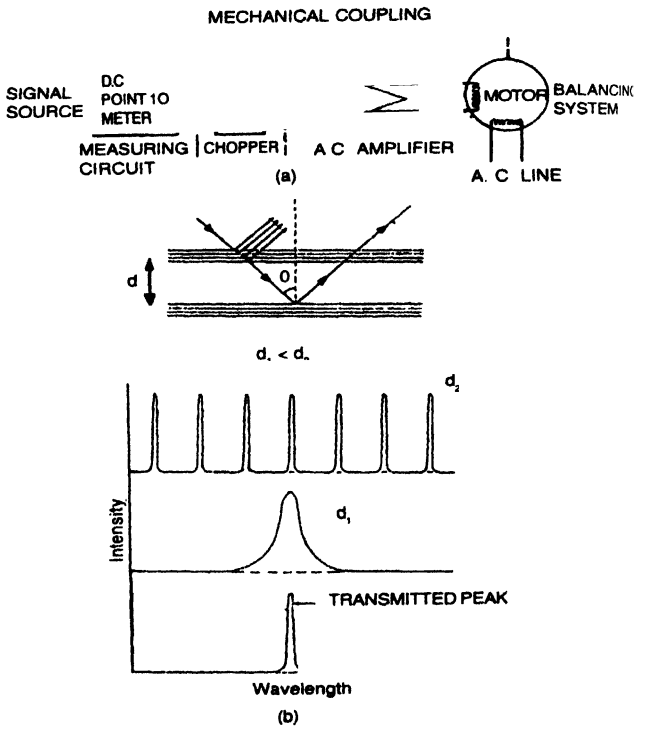

Figure 11. (a) Block diagram of the Varian G 10 graphic recorder. (b) Interference filter, a combination of Fabry Perot Etalons in series.

1.4 Most important airglow emissions and other emissions; chemical reactions , kinetics and excitation mechanisms for main airglow emissions :

The main airglow emissions are four in number ; they are :

(i) OI 6300 Å (ii) OI 5577 Å (iii) Na 5893 Å (iv) OH band emission (Hydroxyl emissions).

Table 1. Different airglow emission lines and their specific features.

Specific feature / Emissions	OI 6300 Å	OI 5577 Å	Na 5893 Å	OH emission
Nature and source of emission	Produced as specific emission line in combination with 6364 Å line conjugately known as forbidden Red Doublet $O^1D_2 \rightarrow O^3P_2$ (6300Å) $O^1D_2 \rightarrow O^3P_1$ (6364Å) [48]	Produced as a specific emission line known as forbidden Green line of oxygen O^1S_0 - O^1D_2 [48]	Produced as a specific emission line. Actually sodium doublet D1 &D2 are produced coherently according to the following scheme of transition; $3p^2P_{3/2} \rightarrow 3s\ ^2S_{1/2}$ (5896Å) $3p^2P_{1/2} \rightarrow 3s^2S_{1/2}$ (5890Å) This doublet is centred at 5893Å and emerges as a single line [15].	Produced as rotational vibrational band known as Meinel Hydroxyl Band system. Transition with different probabilities follow different vibrational transition schemes; OH(9,2), (6,0), (6,2), (7,1), (8,2) (9,3) (10,4), (5,0), (6,1), (5,1) (7,2) (8,3) (9,4) (4,0), (7,3) (8,4) *etc*. Among all these (8,3), (7,2), (9,4), (6,2), (5,1) bands are most important [49].
Average nightglow intensity (in unit of Rayleigh) [19]	35 R	250 R	120R	1000R
Average twilightglow intensity (R) [47]	1000R	400R	2500R	1000R
Average dayglow intensity (R) [47]	10000R	1500R	15000R	1000R
Peak emission height (Approx) [15,47]	245 km	95km(Nigh), 95 km and 200km (Twilight & Day)	92 km(Night), 90 km (Twilight & Day)	92 km (Night), 85 km or below (Twilight & Day)
Thickness of emitting layer (Approx) [24,47]	100 km - 600km ≈ 500km	15 km (Night) 15 km (Twilight) 25km (Day)	7 km (Night) 4-16km (Twilight)	10 km(Night) 12km (Twilight) 20km (Day)
Diurnal variation [24,47]	Nightglow intensity varies significantly at mid and high latitude sector ; Day glow intensity varies significantly	Nightglow intensity show different degree of variation for different latitudinal sector	Starting to decrease from twilight period intensity falls to a minimum at local midnight ; Appreciable variation occurs in case of day- glow	Different types of variation have been observed in case of nightglow ; Occasional decrease at twilight period has also been observed.
Latitudinal & longitudinal variation [47]	It shows prominent latitudinal variation being minimum near equator.	Both latitude and longitude dependence of intensity are observed, the minimum being near the equator.	This shows a prominent latitude- dependence, the minimum being at the geographic equator.	It has some kind of latitude variation.
Seasonal variation [24,47]	Oscillatory mode of variation with significant amplitude observed in case of 6300 Å line. Nightglow intensity maximum occurs in autumn and with the minimum being in summer.	It shows appreciable seasonal variation being maximum in spring and autumn equinoxes and minimum in summer and winter solstices.	Maximum in winter and minimum in summer. The Na 5893Å line airglow intensity shows peak at the autumn equinoxes	Seasonal variation takes place, being themaximum in winter and autumn the minimum in summer.

Airglow lines ;

Line specification (λ)	Features including origin	Reported by
2470Å	$^2P \rightarrow {}^4S$ forbidden transition (UV) Medium Intensity	Feldman [50]
7330Å , 7320 Å	$(^2P) \rightarrow (^2D)$ Forbidden Transitions	Misawa [51]
	$O^+(2P)$ near IR doublet. Major source of $O^+(2P)$ is direct photo ionization of $O(3P)$. Scale height 500 km (Approx.). Correlated with solar 10.7 cm solar flux and geomagnetic activity.	Meriwether *et al* [52]
8640 Å	Morning twilight enhancement exceeds evening twilight enhancement	Noxon [53]

Table 1. (*contd*)

O_2(0-1) 8645 Å		High correlation with 5577 Å indicates that its origin is the same as that of 5577 Å line.	Misawa [54]
Inter combination lines of OI & OII	834 Å	$2s2p^4(4P) \longrightarrow 2p^4(^4S^o)$	Fastie *et al* [58]
	538 Å	$2p^4(2P) \longrightarrow 2p^3(^2D^o)$	Brune *et al* [59]
	539 Å	$3s\ (4P) \longrightarrow 2p^3(^4S^o)$	Christensen [60]
	1304 Å	Triplet (1304) $2p^43s^4(S^o) - 2p^4(^4P)$	Feldman *et al* [61]
	8446 Å	(1356) $3s^5(S^o) - 2p^4(^4P)$	
	4368 Å	(1152) $3s^1(^1D^0) - 2p^4(^1D)$	
	1356 Å	(990) $3s^2\ (^1D^o) - 2p^4(3P)$	
	7774 Å	Quintet (7990) $3s^2(^1D^o) - 3p(^4P)$	
	9264 Å	Shows geomagnetic anomaly .	
	6157 Å	Low intensity , shows altitude variation	
	1152 Å		
	990 Å		
	7990 Å		
NI 5200 Å		Produced at F-region, quenched by free electron and atomic oxygen .	Federick [62]
$N_2$4278 Å		Photoionization of N_2 by scattered solar radiation at 340 Å and 584 Å, shows little variation over nights	Meriwetter [63]
$N_2(C^3\Pi)$ 3371 A		N_2 ($C^3\Pi$) is excited by low energy electrons	Frederick *et al* [64]
		Observed in the polar region	
NO (1-0) 2150 Å		NO *(1-0) (* band at 2150 Å	Beran *et al* [65]
OH 6329 Å		Shows twilight enhancement	Misawa [66]
6563 Å		This line has got its annual and semiannual components of seasonal variation	Fishkova [67]
Fe 3860 Å		Resonance Scattering , observed in twilight spectrum	Broadfoot [68]
Ca^+ 3933-3968 Å		Resonance Scattering of solar radiation Observed in lower thermospheric intermediate layers	Tepelay [69] Dufay [70] Vallence Jones[71]
Mg^+		Resonance Scattering	Naricsi [72]
MgI 2852 Å		Observable in F-region, mostly in late afternoon	Young *et al* [73]
MgII 2800 Å			
Mg 2796 Å & 2803 Å		Doublet i) $3s^2S_1$-$3p^2P_{1/2}$	Gerand and Monfils [74]
		ii) $3s^2S_{1/2}$ - $3p^2P_{3/2}$	
		Equatorial airglow lines indicate the presence of Mg^+ ions in the evening twilight F-region	
HI 1216 Å		Photon - electron radiative recombination excites neutral hydrogen to the 2nd quantum level which causes the emission line	Kazakov(75]
		Observed in twilight glow	Sullivan and Hunten [76]
N(^{2}D) 5198 Å-5201 Å		$O^+ - N_2$ ion-atom interchange process followed by NO^+ dissociative recombination.	Blackwell *et al* [15]
		Low intensity night airglow lines	
2972 Å		UV , Forbidden transition of oxygen atom (^{1}S —> ^{3}P)	Cohen-Sabban and Vuillemin [15]
Intercombination line of NI and NII	1134 Å	$2s2p^4(4P) - 2s^22p^3(4S^o)$	Takacks and Feldman [77]
	1200 Å	$2p^23s(^4P) - 2p^3(4S^o)$	Meier *et al* [15]
	1493 Å	$3s\ 2p^2(^2P) - 2p^3(^2D^o)$	Hudson and Kieffer [15]
		Impact dissociative excitation	
		and photodissociative excitation	

Table 1. (*contd.*)

He 10830 Å HeI 584 Å	$2p\ ^3P^o$ - $2s\ (^3S)$ High twilight intensity value, (Resonance scattering by metastable He)	Shefov [15] Teixeire *et al* [15] Donahaue *et al* [78]
NII 5755 Å	(^1S)- (^1D) forbidden transition dissociative ionization by EUV radiation and low intensity twilight glow	Torr *et al* [15]
I 6708 Å	Impact dissociative excitation $LiO^* + O \longrightarrow Li^* + O_2$ $Li^* - Li + hf(6708\ A)$ Height distribution of intensity is similar to that of NaD line intensity; Low intensity line	Delannoy and Weill [79] Henrikson [80]

Various important features of these four emissions in relation to the phenomenon of airglow, especially of nightglow, are tabulated in Table - 1 [15, 19, 24, 26]:

For some more spectral lines that are of low or medium intensity in cases of airglow emissions, one may consult the following references [Refs. 19,49,78-80].

Interrelations amongst the lines

Covariation of 5577 Å green line and 6300 Å red line intensity has been observed to exist with some certainty [15,19,51,55]. Midya and Ghosh [82] too have shown that there exists a strong correlation between the OI 6300 Å and OI 5577 Å (F-layer) airglow emissions intensities Q_{6300} and $Q_{5577}(F)$. They give the equation as

$$Q_{6300}/Q_{5577}(F) = (0.76\varepsilon/A'\varepsilon')/(1 + K_2 n(N_2)/A)$$

$$= 5.67/\left(1 + 3.3\times10^{-9} n(N_2)\right)$$

where ε and ε' are the probabilities of OI(^{1}D) and OI(^{1}S) atoms, respectively, A and A′ are the Einstein coefficients for OI 6300Å and OI 5577 Å line emissions, respectively, K_2 is the quenching rate constant of O(^{1}D) for N_2 molecules. The 7774Å line airglow intensity is correlated strongly with the 6300 Å red line airglow intensity through their common strong dependence on F-layer peak electron density [83]. Vertical distribution of sodium density and the intensity of OH (8,3) airglow emission show that nocturnal variation of the emission is strongly correlated with the density of sodium at about 85 km [51,52].

Sahai *et al* [84] showed that the ratio of OI 6300 Å and OI 5577 Å airglow emission intensity follows a particular equation

$$R = I_{6300}/I_{5577} = \{I_{5577}(M)/I_{6300} + 0.2\}^{-1},$$

where I_{5577}(M) is the mesopause-region contribution. In an analysis of storm-induced particle precipitation effects on the airglow emissions, Sahai *et al* pointed out that F-region contribution to the total OI 5577 Å line emission intensity is about 20% of the OI 6300 Å emission intensity. R increases with the increase in I_{6300} which varies inversely with virtual height ($h'F$).

Based on the analysis of simultaneous satellite measurements of the intensities of emissions at λ 3371 A and λ 5577 A, interrelationship of these two emissions have been derived in analytical form and it has been inferred therefrom that the primary source of excitation of 5577 Å below 180 kms is the reaction $N_2^* + O \rightarrow O(^1S) + N_2$ [85].

There are many such works regarding the interrelation of variations of airglow emission intensity for study [86 - 89].

Chemical reactions , kinetics and excitation mechanisms for four main airglow emissions

Airglow emissions are electromagnetic (em) radiations emitted by excited atomic or molecular species which can be quantitatively and qualitatively realized and understood only by means of quantum theory. According to this theory, radiations are emitted as a result of transition of any such atomic or molecular species from its excited energy level to any of its lower energy levels. Transitions, spontaneous or by absorption of radiation, do not occur between any two energy levels of an atom. Instead, it has to obey selection rules governed by the quantum theory and the general fundamental quantum selection rule for a multi-electron atomic species to undergo electric dipole radiative transitions

$$LSJM \rightarrow L'S'J'M' \text{ is } \Delta J = O,\ \pm 1;\ J + J' \geq 1,$$

Odd term $\leftrightarrows$ Even term.

The selection rule is valid as long as the spin orbit interaction is small. For neutral atoms and ions too, magnetic dipole and electric quadrupole transitions are inherently much weaker than electric dipole transitions. Magnetic and higher order electric transitions are therefore commonly known as Forbidden Transitions. Transitions between terms of different multiplicities, the so-called intercombination transitions, are also forbidden [79].

The most easily observed forbidden emissions are those for which the upper energy state is metastable where there are no transitions to lower energy levels allowed by electric dipole selection rules. Most observed forbidden transitions are produced by transitions within the ground state configurations

because for most of the atom and ions, all levels of the ground state configurations lie below all corresponding excited state configurations and consequently, are all metastable. Airglow emissions are produced both through allowed and forbidden transitions although most important ones are produced through forbidden transitions. Transitions are possible only when the atomic or molecular species undergo the process of excitation. The action-reaction schemes *via* energetics that paves the way of excitation are collectively known as the excitation-mechanism.

Chemical Kinetics is the branch of Physical Chemistry which deals with the speed of reaction or reaction rate, factors that influence the rate and reaction mechanism. The reaction rate depends on the nature of reacting species, concentration of each such species, ambient temperature, presence of extraneous bodies and energising em waves.

Reactions occurring entirely within one phase are known collectively as homogeneous reaction while reactions, in which phase transformation takes place on the surface of catalyst or of the container wall, are collectively known as heterogenous reactions [90] . Rate of a reaction is defined as

$$R = -\{dc/dt\} = \{dx/dt\},$$

where 'c' is the concentration of the reacting species at any time 't' and 'x' is the concentration of the product-species at the same time 't' . The order of reaction is the number of concentration terms on which reaction rate depends. The first order reaction rate is 'kc' where 'k' is the rate constant and 'c' is the concentration of a reacting species ; similarly, second order reaction rate is 'kc^2' and so on.

The reactions of charged particles play a major role i controlling the composition and physicochemical characteristi of the upper atmosphere.

Principal neutral species present in space between altitude of 50 kms and 500 kms are N_2,O_2, O, Ar and N and the princip ions of each type are NO^+, O_2^+, O^+ and NO_2^-, O_2^-, and O^- [91 All possible reactions are given in chart 1.

The most important possible results of collisional process excluding those that involve charge exchange or ionization ar as follows [78] :

(i) $A^*(m) + B$ (Elastic scattering) ,

(ii) $A^*(m') + B$ (depolarization),

(iii) $A^{**}(m') + B$ (Intraatomic excitation transfer c sensitized fluorescence),

(iv) $A + B^*$ (Interatomic excitation transfer or sensitize fluorescence),

(v) A+B+ Kinetic energy (quenching),

(vi) $AB + h\nu$ (Associative de-excitation) .

Further details of the processes mentioned above, are give in Refs. [78,79,92,93]

A typical pattern of gross variation of three importa ionospheric parameters [91]

A generalized reaction a A + bB + products is found to proceed with a rate proportional to [A] $[B]^{\beta}$———— . A,B,C ..... are different reacting species whil

Chart 1. Classification of reactions of ions which take place within terrestrial atmosphere.

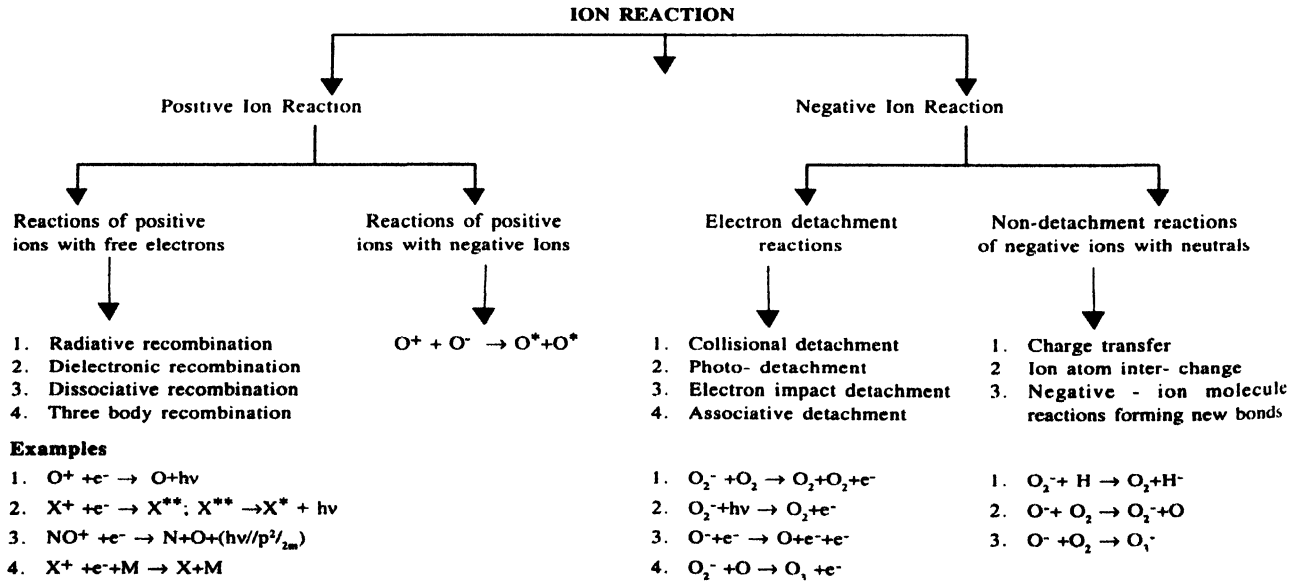

Physical quantity / Height	Temperature	Pressure	Electron density
50 Km	Decreases ↓ 250 K	1 mm of Hg	10 electrons / c c.
90 Km	↓ 180 K		↓
100 Km	Increases ↓	Decreases ↓ 10^{-4} mm Hg	Increases ↓
200 Km		10^{-6} mm Hg	
500 Km	↓ 2500 K	10^{-8} mm Hg	10^{6} electrons/ c.c.

the order of reaction being given by $\alpha+\beta+\gamma$ ———— = η and the atomicity or molecularity of the process is the sum a +b +c + ———— as expressed in the chemical reaction.

The constant of proportionality between rate of reaction and concentration terms is called the rate constant or rate coefficient. The mathematically rational procedure is to define a rate by the equation

$$\text{Rate} = -(1/a)\,(d[A]/dt) = -(1/b)\,(d[B]/dt)$$

$$= -(1/c)\,(d[C]/dt) = ------ = K[A]^{\alpha}[B]^{\beta}[C]^{\gamma} \ldots\ldots .$$

Defining reaction rate for an exemplary reaction will be more realistic and practical . Let us consider

$$2\,NO + Cl_2 = 2\,NOCl.$$

For this reaction, the rates are defined as

$$d[NOCl]/dt = K_1[NO]^2\,[Cl_2],$$

$$-d[Cl_2]/dt = K_1'[NO]^2\,[Cl_2],$$

$$-d[NO]/dt = K''[NO]^2\,[Cl_2].$$

For satisfying molecular requirement of the above mentioned reaction it is obvious that ;

$$K_1 = 2K_1' = K''.$$

Complications arise when several reactions occur simultaneously with one or more reacting species. The rate of chemical reaction usually varies with temperature and Arrhenius was the first person to give an equation for the temperature variation of rate constant as

$$K = A \exp.(-E_a/RT),$$

where K is the reaction-rate constant , E_a-the activation energy, T- the ambient temperature.

Activation energy may be simply defined as the minimum energy which any reacting species must possess in order to enable it to undergo the chemical transformation. Attempts for an ellucidation of the reaction mechanism led to two theories :

(i) The collision theory ,

(ii) The transition state theory .

A simplification in case of reactions with multiple steps is made by adopting the stationary state hypothesis which necessarily impose a quasi-realistic constraint for the intermediate species x :

$$d[x]\,/\,dt = 0\,.$$

The collision theory assumes that the reaction-partners are hard spheres and for reaction to take place, the reactants need to collide with an energy exceeding a critical value E_c and that the species possess a Maxwell distribution of velocity. The theory predicts a rate constant k given by,

$k = z \exp(-E_c/RT)$, where z is a collision frequency factor which is concentration-independent. For a two-species-reaction, 'z' is given by

$$z = \{(\sigma_A + \sigma_B)/2\}^2\,\{8\pi\,KT/\mu\}^{1/2}$$

where σ_A, σ_B are the collision diameters of reactants A and B and μ ' their reduced mass.

There are a large number of problems associated with collision theory due to its inherent fundamental assumptions and to overcome such problems (for actual determination of rate coefficients) another theory known as a Transition State theory (or Absolute Rate theory) was developed. This theory assumes that reactants A and B are in equillibrium with an activated complex or transition state AB* which remains at the maximum energy position on the pathway connecting the reactants and the products. Treating the equillibrium by means of statistical thermodynamics, the rate constant is found to be

$$k = (KT/h)\,(Q'_{AB*}/Q_A Q_B)\exp(-E_c/RT),$$

where Q'_{AB*} , Q_A and Q_B are the total partition-functions for AB*, A and B, respectively [94]. For the time rate of variation of vertical profile of species one can write

$$dn_i(z)/dt = P_i(z) - L_i(z) - (d\varphi_{i,z}/dz),$$

where $\varphi_{i,z} = n_i$, $P_i(z)$ is the chemical production rate for i'th species at an altitude 'z' and $L_i(z)$ is the net loss rate for i'th species at an altitude 'z' . The production and loss terms strongly couple the reactants and are of three basic types; unimolecular, bimolecular and termolecular [95]. For unimolecular reactions, the first order kinetics is suitably represented through a sequence of processes.

For example.

$$A + A \cdot \quad \rightarrow A^* + A \qquad \text{(activation)},$$

$A^* + A \xrightarrow{k_2} A + A^*$ (deactivation),

$A^* \xrightarrow{k_3} A + h\nu$ productions + radiations (reaction).

Application of the stationary state hypothesis for [A*] gives the result

$$-d[A]/dt = \left(k_1 k_3 [A]^2\right) / \left(k_2 [A] + k_3\right).$$

Normally, the system obeys the law of first order kinetics; but at sufficiently low pressure, the reaction becomes second order. Most of the chemical processes that take place within the atmosphere follow a third order kinetics and may be represented by a termolecular chemical reaction. A symbolical representation of such process is

$$A + B + M \cdot \quad \rightarrow AB + M ,$$

where M is the third body. This process can be thought to comprise a sequence of steps such as,

$$A + B \xrightarrow{k_4} \rightarrow AB^* ,$$

$$AB^* + M \cdot \quad \rightarrow AB + M ,$$

$$AB^* \xrightarrow{k_6} A + B .$$

Steady state transition theory gives the rate as [96].

$$d[AB]/dt = (k_4 k_5 [A][B][M]) / (k_5 [M] + k_6) .$$

This equation shows that the process is an equivalent second order reaction. But if $k_5 [M] << k_6$, this reaction becomes a third order reaction while if $k_5 [M] >> k_6$, the reaction becomes equivalent to a first order reaction.

In cases of fluorescence or similar radiation phenomena, the following scheme is a representative one :

$A + h\nu \cdot \quad \cdot A^*$ (absorption)

$A^* + M \cdot \quad \rightarrow A + M$ (quenching),

$\rightarrow A + h\nu$ (fluorescence).

Here, quenching means the process of coming down of an excited species to ground state by means of reaction with another body M called quencher and the quenching rate depends on the concentrations of both, excited species and quencher.

Quenching renders the intensity of emission or to say more practically, the volume emission rate decreased. In steady state, the quenched fluorescence-intensity is given by

$$I_{fluorescence} = k_r [A^*] = (k_r I_{abs}) / \left(k_r + k_q [M]\right).$$

Reactions which depend on the required threshold energy may, in general, be divided into two types :

(i) Thermal or dark reactions that occurs at the threshold of the order of 10 - 100 K. calorie (mainly kinetic energy of colliding species)

(ii) Photochemical reactions occur due to absorption of photons having λ ranging from 100 A to 10000 Å

There are two basic rules which govern all the photochemical reactions :

(a) *Grothus - Draper law* : Only those radiations which are absorbed , can be effective in producing the chemical change.

(b) *Einstein's Law* : Each quantum of radiation absorbed by a molecule, activates one molecule in the primary step of a photochemical process.

The rate of production of i'th species per unit volume ions at an altitude 'h' by photoionization is given by [15]

$$q_i(h) = \sum \varphi(\lambda, h)\, Q(\lambda, I)\, n_i(h) , \qquad (4$$

where n_i is the concentration of neutral atoms or molecules of i'th species, $\varphi(\lambda, h)$ is the flux of solar radiation of wavelength λ per unit area per second at height h, $Q(\lambda, I)$ is the photoionization crosssection of the neutral species for radiation of wavelength λ. If the solar zenith angle is ψ , then

$$\varphi(\lambda, h) = \varphi_0(\lambda) \exp\left[-\Sigma_m \sec\psi \int Q_\tau(\lambda, m) n_m(h) dh\right] \qquad (5$$

$Q_\tau(\lambda, m)$ is the total absorption crosssection of the neutral species m for radiation of wavelength λ , absorptions of radiation by all neutral species encountered are allowed, $\varphi_0(\lambda)$ is the incident flux of wavelength λ per unit area. It was shown by Bates and Massey [97] that the dissociative recombination is the most significant of all processes involving ion- electron recombination that occur within the terrestrial ionosphere.

$$XY^+ + e \rightarrow X + Y.$$

In this reaction, the electron recombines with a molecular ion and the excess energy released, dissociates the molecule. Variation of rate coefficient with temperature for such a reaction depends on the shapes of potential energy curves for XY and XY^+[98].

Chemical kinetic rate constants are primarily determined by laboratory experiments. Many of these rates are not determined with a great precision because of the difficulties of performing the experiments. Comprehensive tabulation of rate constant data are obtainable from the Refs. [99-106].

Excitation mechanism for four main airglow emissions

Each of the airglow lines has one or more specific mechanism of excitation. Amongst all probable and proposed mechanisms. only those are considered for which the rate coefficient and the volume emission rate are maximum.

Excitation mechanism for OI 6300 Å airglow emissions

OI6300 Å line emission is produced due to a forbidden transition [48]

$$O(^1D) \rightarrow O(^3P_2) + h\nu(6300\ \text{Å}).$$

(O^1D) may be produced in three different ways as follows :

(i) Dissociative Recombination $O_2^+ + e \rightarrow O_2 \rightarrow O^* + O^*$ (Unstable)

(ii) Photodissociation (Schuman Runge dissociation) [19] $O_2 + h\nu\ (\lambda < 1750\ Å) \rightarrow O(^1S) + O^*$

(iii) Photodetachment $O^- + h\nu \rightarrow O(^1D) + e.$

O* den s oxyge in ^1S or ^1D or in

Amongst the above three processes, the dissociative recombination is the most significant process to contribute to the production of OI 6300Å emission (airglow). Besides, the following are the principal reactions involved in the production of O* and O_2^+ and subsequent quenching [107, 108].

$O^+ + O_2 \rightarrow O_2^+ + O^*$, $O^+ + N_2 \rightarrow NO^+ + N$, $O_2^+ + e \rightarrow O^* + O^*$,

$O_2^+ + N \rightarrow NO^+ + O^*$, $O(^1D) + N_2 \rightarrow O(^3P) + N_2$,

$O(^1D) + O_2 \rightarrow O(^3P) + O_2$, $O(^1D) + e \rightarrow O(^3P) + e$,

$O(^1D) + O \rightarrow O(^3P) + O$,

$N(^2D) + e \rightarrow N(^4S) + e$, $N(^2D) + O \rightarrow N(^4S) + O$,

$N(^2D) + O_2 \rightarrow NO + O^*$.

Excitation mechanism for 5577 Å airglow emission :

OI 5577 Å line emission is produced due to the forbidden transition [48]

$$O(^1S) \rightarrow O(^1D) + h\nu\ (5577\ \text{Å}).$$

$O(^1S)$ may be produced in the following different ways (as proposed) :

Chapman's mechanism [109]

$$O + O + O \rightarrow O_2\left(X\,^3\Sigma g, v < 4\right) + O(^1S).$$

Barth's mechanism [110]

$$O + O + M \rightarrow O_2{}^* + M,$$

$$O_2{}^* + O \rightarrow O_2\left(X\,^3\Sigma g, v \le 4\right) + O(^1S).$$

Quenching occurs in either of the three ways :

$$O_2{}^* + M \rightarrow O_2 + M,\quad O_2{}^* + O \rightarrow O_2 + O\left(^1D\ or\ ^3P\right),$$

$$O_2{}^* \rightarrow O_2 + h\nu.$$

Other processes are as follows [111] :

Dissociative recombination $\rightarrow O_2^+ + e \rightarrow O_2^*$ $\rightarrow O + O(^1S)$,

Dissociative collisional excitation $\rightarrow O_2 + e$ (high-energy) $\rightarrow O_2{}^* + e \rightarrow O + O\left(^1S\right) + e$ (low energy),

Collisional deactivation of $N_2 \rightarrow N_2(A\ ^3\Sigma_u^+) + O(^3P)$ $\rightarrow N_2\left(X\ ^1\Sigma_g\right) + O(^1S)$.

Photodissociation $\rightarrow O_2 + h\nu \rightarrow O(^1S) + O^*$ (O^* means oxygen in ^1S or ^1D or ^3P state,

Collisional ion-atom interaction $\rightarrow N + O_2^+ \quad NO^+ + O(^1S)$ [112],

Dissociative recombination $\rightarrow NO^+\left(X\ ^1\Sigma^+\right) + e$ $\rightarrow N + O(^1S)$.

Evidences from aeronomical and chemical kinetic points of view show that Barth's mechanism is the most important source of $O(^1S)$ [113]

Excitation mechanism for Na 5893 Å airglow emission :

Na I 5893 Å line emission is produced due to allowed transition

$$Na(^2P) \rightarrow Na(^2S) + h\nu(5893 Å).$$

The followings are the most probable mechanism of production of Na (^{2}P) ;

(i) Resonance scattering by atmospheric sodium [114]

$Na(^2S) + h\nu(\lambda\ 5893\ Å) \rightarrow Na(^2P)$ (Sun to atmosphere)

$Na(^2P) \rightarrow Na(^2S) + h\nu(\lambda\ 5893\ Å)$ (atmosphere to Earth surface)

(ii) An alternative explanation was given in the works of Vegard and coworkers [115, 116]. Na atoms are released in the photodissociation of some compound of Na.

(iii) Free sodium is possibly formed by reduction mechanism [117, 118]

$$Na\ O^*(X\ ^2\Pi) + O(^3P) \rightarrow O_2(X\ ^3\Sigma_g) + Na(^2P)$$

(endothermic).

NaO* is formed following any one of the schemes given below :

$$Na(^2S) + O_3 \rightarrow NaO^*(X\ ^2\Pi) + O_2,$$

$$Na(^2S) + O + x \rightarrow NaO(X\ ^2\Pi) + x$$

$$Na(^2S) + O_2(X\ ^3\Sigma_g) + M \rightarrow NaO_2 + M,$$

$$NaO_2 + O(^3P) \rightarrow NaO^* + O_2.$$

Moreover, $NaO_2 + H \rightarrow NaH + O_2$ / $NaO^* + OH$

(iv) Another mechanism is also possible (Bates & Nicolet) [119]:

$$NaH(X\ ^1\Sigma) + O(^3P) \rightarrow OH(X\ ^2\Pi) + Na(^2P).$$

(v) Bates gave another possible mechanism ; [120,121]

$$NaH(X\ ^1\Sigma) + H(^2S) \rightarrow H_2(X\ ^1\Sigma g^+) + Na(^2p).$$

(exothermic)

On the basis of the rate coefficients and their dependence on temperature, the altitudinal distribution of relative abundances of different species and temperature are found out. Comparing those values with the observed values the most suitable mechanism is chosen for consideration while explaining various features concerned. Chapman's mechanism is the most important of all those mechanisms.

Excitation mechanism for OH airglow emission :

OH band emission occurs at different wavelengths due to the transition from vibrationally excited state down to vibrational ground states.

$$OH^* \rightarrow OH + h\nu.$$

OH* may, most practically, be formed in either of the following ways;

(i) Bates Nicolet theory [119]

$$O + O_2 + M \rightarrow O_3 + M,$$

$$O_3 + H \rightarrow OH^*(3.32\,ev) + O_2.$$

(ii) Krassovsky theory [122]

$$O_2 + O + M \rightarrow O_3 + M,$$

$$O + O_3 \rightarrow O_2^* + O_2^*.$$

$$O_2^* + H \rightarrow OH^* + O$$

(iii) Breig theory [123]

$$H + M + O_2 \rightarrow HO_2 + M,$$

$$HO_2 + O^* \rightarrow OH^* + O_2.$$

2. Ionospheric activities and their relation with airgl emissions

2.1 Classification of terrestrial atmosphere and ionosphere

2(1)(i) Nomenclature for different layers of atmosphere :

Attempts were made by many scientists to classify and nar the different layers of atmosphere primarily on the basis thermal properties and of responses to thermal energy- transf Among those scientists T.D. Bort was the pioneer [124]. early as 1898, with the help of balloon flights Bort became at to specify different sources of error in pressure-altitude-a temperature-determination and radiation- errors at some heig of atmosphere. Bort showed for the first time that above abo 11 kms., the temperature of the atmosphere during daytir becomes constant and for that reason, the layer above 11 kr (approximately) was named by Bort himself as 'isothermal laye Soon after that, Bort realized that the 'isothermal layer' was n perfectly isothermal and was found to show some kind stratification. Therefore, it could be better named as t 'stratosphere'. In this way, the different layers and sublayers terrestrial atmosphere were identified and named. A comparis of different standard nomenclatures which are in use, is giv below [Table 2 and Figure 12] [125] ;

Originally, two kinds of nomenclatures were proposed by panel appointed by the special subcommittee on the Upp Atmosphere of the National Advisory Committee f Aeronautics (NACA) of the U.S.A. These were

(i) General nomenclature (ii) Special nomenclature

Layer's Name	Approximate range of height	Specification / characteristics
(i) *General nomenclature* [22]		
Troposphere	0 - 12 km	
Stratosphere	12 - 80 km	
Mesosphere	80 - 100 km	The region of major minimum of temperature
Ionosphere	80 - 400 km	
Suprasphere	400 - 1000 km	
Exosphere	> 1000 km	Appreciable escap of air to outer space.

ii) *Special nomenclature :*

a) Based on temperature distribution

Troposphere	0 - 12 km	
Stratosphere	12 km < 100 km	From the top of troposphere to the region of minimum temperature.
Thermosphere	> 100 km	Region of increasing temperature, above the stratosphere.

b) Based on Composition :

Turbosphere	≈ Troposphere	Turbulent mixing surpasses the diffusion of different constituents of air.
Homosphere	20km < h < 120 km	Approximately uniform mean molecular weight.
Heterosphere	> 120 km	Dissociation of oxygen and other constituent.

c) Based on Ionization :

Ionosphere	80 ~ 600 km	Highly populated with electrons and ions which influence Radio wave propagation.
Neutrosphere	<80km	Electron or ion density too low to have any influence on Radio wave propagation.

(ii) Historical introduction to the discovery of 'Ionosphere'

Materials in the form of gas and plasma over the surface of Earth, bound by gravity, distributed according to their mean molecular kinetic energy and subject to solar terrestrial magnetic influences and their mutual interactions, constitute the terrestrial atmosphere or air. The whole atmosphere is conveniently thought to have several layers ,each of which has its own distinct physical characteristics. According to the altitudinal distribution of characteristic physical properties of the atmospheric content, the whole atmosphere is primarily subdivided into three parts such as the upper atmosphere, middle atmosphere and lower atmosphere.

With the invention of the balloon in 1783, people were able to fly high up in the terrestrial atmosphere. Initially, the balloon-flight was a kind of sport and gradually, it became the first kind of scientific probe for various atmospheric investigations. Balloon flights for recording several terrestrial atmospheric parameters such as humidity, temperature and terrestrial magnetism were made as early as 1804. Manned balloon flights are not capable of reaching altitudes greater than about 40 kilometers while the ceiling of the conventional airplane is considerably below that. Later, with the invention of liquid propellant rocket by R H Goddard in 1926, upper atmospheric investigation gained quite a bit momentum [124]. In course of time, with the help of such rocket and balloon flights, or more specifically, by means of scientific equipment and instrumentation carried thereby, the office of Naval Research Laboratory, Applied Physics Laboratory of Johns Hot University, the Air Force and the Army Signal Corps have been engaged in carrying out a wide variety of upper atmosphere research programs and projects. Therefrom, a large number of important, hitherto unavailable information regarding various physical characteristic parameters such as pressure, temperature humidity,air composition, electron and ion-densities,cosmic

Table 2. Different layers and sublayers of terrestrial atmosphere alongwith corresponding range of height and characteristic features.

Altitude (Km)	Goody		Flohn and Penndorf		Chapman			
					I		II	III
H<12	Troposphere		Advection layer		Troposphere			
H=12	Tropopause		Tropopause layer		Tropopause			
12<H<30	Lower		Isothermal layer		Stratosphere			
H=30					Stratopause		Homo-sphere	Neutro-sphere
30<H<58	Upper		Warm layer		Meso-incline			
H=58		Stratophere	Ozonopause	Stratophere				
58<H<75			Upper mixing		Meso-peak	Stratosphere		
			layer		Meso-decline			
H=75	Stratopause		Upper tropopause		Mesopause		Homopause	Neutropause
75<H<120	Ionosphere		Ionosphere		Thermosphere		Heterosphere	Ionosphere

radiation, ultraviolet radiation, vertical distribution of ozone and wind velocities have been obtained [125].

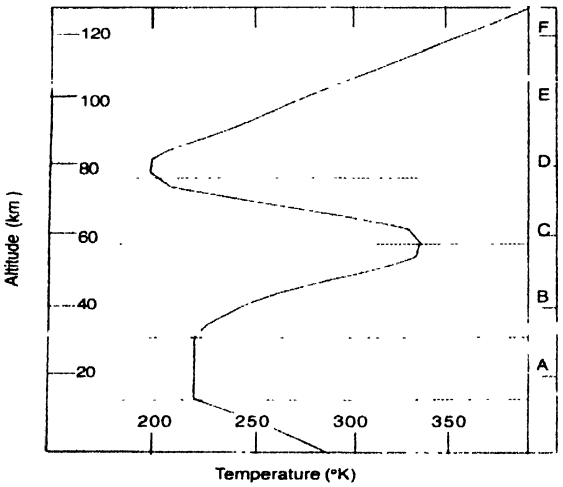

Figure 12. Approximate vertical temperature distribution in the troposphere in temperate latitude. Comparison with rocket atmosphere temperature data with curves adopted by the Rocket panel.

In 1901, Marconi discovered by sending wireless signals to a distant place that those signal waves propagated round a curved surface and that phenomenon could not be satisfactorily explained with the then-existing theory of diffraction. It was Kennelly and Heaviside in 1902 who, almost simultaneously, postulated the existence of a conducting layer in the upper region of terrestrial atmosphere and suggested that this layer might deflect the radio waves compelling them to traverse along a curved path. Heaviside proposed also that the conducting layer, full of electricity carriers *i.e* ions and electrons, might be produced due to the ionizing action of solar radiations. As early as 1878, Balfour Stewart postulated for the first time, the existence of a conducting strata in the upper part of atmosphere to establish his theory of the daily geomagnetic variation. The basic theory of propagation of radio waves through charged particles was first proposed by Eccles in 1912 and was later modified by Larmor in 1924. Eccles-Larmor theory [22] is thus the basic theory of radio wave propagation in the ionosphere according to which the refractive index of an ionized medium (without considering the presence of magnetic field) is given by

$$\mu = \left(\left\{ck^2/p\right\} + 1 - \left(4\pi N_e C^2\right)/\left\{m\left(p^2 + v^2\right)\right\}\right)^{1/2} \quad (6)$$

Here, c is phase velocity of the wave, p is the angular frequency of the wave, k is the absorption per unit length of path, v' is the frequency of collision per second, N_e is the number density of free electrons, e is the electronic charge and , m is the electronic mass [22].

The Eccles – Larmor theory was modified later by Appleton, Hartee and others which being known as the magneto-ionic theory, gives the refractive index of an ionized medium (in presence of magnetic field) as,

$$\mu = \left(1 + 2p_0^2 \Big/ \left[2\left(-p^2 + jpv\right) - \left\{\left(p^2 p_T^2\right)\Big/\left(p_0^2 - p^2 + jpv\right)\right\}\right.\right.$$

$$\left.\left. \pm\sqrt{\left\{\left(\left(p^2 p_T^2\right)\Big/\left(p_0^2 + jpv - p^2\right)\right)^2 + 4p^2 p_L^2\right\}}\right]^{-1} + jck/p\right)^{1/2} \quad (7)$$

where c- velocity of e.m. wave in free space , k- attenuation coefficient, N_e - electron density, p - the angular frequency of wave,

v- the collision – frequency, $p_0^2 = 4\pi N_e e^2/m$,

$p_L = H_L e/mc$, $p_T = H_T e/mc$,

H_L – component of imposed magnetic field along the direction of propagation and H_T- component of that magnetic field transverse to the direction of propagation. The above formula is well known as Appleton- Hartee formula.

The direct evidence of the existence of a conducting layer in the upper atmosphere was first established by Appleton and Barnett in 1925 [22]. Breit and Tuve in 1926 [22], published the important result of their experiment. They sent transient pulse-signal to a moderately distant receiver and reported that two (sometimes more than two) impulses were received instead of receiving only one impulse. One of those two were attributed to the directly traversed part of the emitted pulse and the other was due to the indirect wave or echo reflected from the conducting layer called ionosphere. This is perhaps the brief history of the discovery of the terrestrial ionosphere. According to the recommendations of a committee of the Institute of Radio Engineers [22], the terrestrial ionosphere is 'that part of the Earth's upper atmosphere where ions and electrons are present in quantities sufficient to affect the propagation of radio waves The ionosphere has been found to be stratified into a number of regions or layers of maximum ionization. According to the Wave Propagation Committee of the Institute of Radio Engineers, U.S.A, a 'region' within the ionosphere is a portion of the atmosphere in which there is a tendency for the formation of definite ionized layers and a 'layer' of the ionosphere is regularly stratified distribution of ionization which is formed in a region of the ionosphere and is capable of reflecting radio waves back to Earth. The existence of the different layers of ionosphere such as E, F_1, and F_2 within the ionosphere was discovered from a study of the variation of the equivalent height (at which a radio wave of a particular frequency range is reflected back) with frequency. It is usually observed that there are discontinuities in the curve at certain frequencies. At each of these frequencies, an ionospheric layer is penetrated. Ground-

based observation using sounding of radio waves at different altitudes essentially determined the altitude distribution of the electron concentration N_e, but with certain gaps corresponding to the penetration frequencies mentioned above. The three discontinuities in the figures [Figures 13 (a) and (b)] [15,22] thus give the three critical frequencies for the three regions of maximum ionization, E, F_1 and F_2 . As the formation of these regions are mainly due to the ionizing solar UV rays, it is obvious that the heights and the density of ionization will vary according to the hour of the day and season of the year. Average values of the minimum virtual heights of the three regions have been found to be near 120 km , 210 km and 300 km, respectively. Appleton [22] stated that in his early work, he used to write E for the electric vector of the wave reflected from the first layer he recognized. Afterwards, he identified another layer at a greater height and he wrote F for the field of the wave reflected from it. Splitting of the single F-layer into two parts such as F_1 and F_2 occurs in day time when solar ionizing radiations of high intensity are incident directly on the ionosphere and at night in the complete absence of the Sun, these two sublayers F_1 and F_2 coalesces together to produce a single F-layer at an intermediate

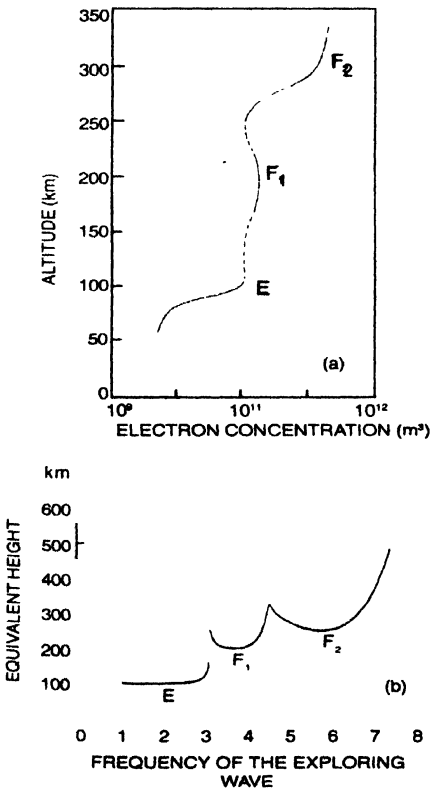

Figure 13. (a) Schematic representation of the variation of the electron concentration wiht height in the normal daytime terrestrial ionosphere. (b) Illustration of typical *h'-f* record indicating the stratification of the ionosphere.

height. Moreover, it is also quite possible for either stratifications to exist between or besides these three layers E,F_1 and F_2.

Probable existence of a new layer called the G-layer above the F_2-layer is hypothesized, although an alternate explanation of occassional observation of such great equivalent height is the multiple reflection between the bottom of F_2-layer and the top of F_1-layer.

There exists another layer below the E-layer which is not detectable by the ordinary pulse technique. This is because of the fact that this layer, later named D-layer, can not reflect back the medium or short waves at vertical incidences. The existence of this D-layer is inferred from (i) variation of signal strength of waves reflected from E and F-regions, (ii) variation of the strength of atmospherics from daylight to night, (iii) reflection of very long waves. Most probable height of maximum electron density for the D-layer is approximately near 70 km. Close to the heights of D and E layers, patches of intense ionization have been observed to exist irregularly and discretely at some places. Those regions are named the sporadic-D and sporadic-E regions, respectively [22]. E-layer and F_2-layer are also known as Kennely-Heaviside and Appleton layers, respectively.

2. 2 The Sun as the main source of various ionospheric activities:

Solar radiation and particle flux of ionospheric importance

The Sun is the source of electromagnetic (em) radiations at different wavelength ranges, high energy cosmic ray particles, solar magnetic field and the solar wind. All these four kinds of solar physical entities conjointly play the main role in the production and shaping of planetary ionosphere, especially terrestrial ionosphere. Thermonuclear processes are responsible for the production of solar radiations and of solar magnetic field and solar wind.

Solar em radiations are produced in two ways : (i) Directly from solar thermonuclear reactions and associated thermal features, (ii) Indirectly due to the electrodynamics of solar cosmic rays. High energy particles such as electron, protons and heavier nuclei are produced within the Sun due to solar flares. Secondary solar radiations emerge out as a result of interactions of solar cosmic ray particles with the matter and magnetic field of the solar atmosphere [128]. This radiation generally evolves in two phases. The first phase is characterized by impulsive burst of hard X-rays and microwaves and by Type III radio emissions. In the second phase, there are type II bursts , microwave and metric type UV emission and flare continuum radio emission. Hard X-ray and γ-ray lines are produced by interaction of high energy ions with the solar atmosphere. There are various energy sources and sinks, responsible for different ionospheric activities within and outside the Earth's atmosphere. The input of solar em radiations is characterized by specific processes that are compelled to take place within a limited part

of height above the Earth's surface by the absorption of solar UV radiations and it depends on solar conditions [129].

At an altitude of 90 km and above, the heat balance is primarily controlled by deviation from local thermodynamic equilibrium (LTE) of CO_2. In addition to solar energy, input gravity waves and Rossby waves together with atmospheric tides may be regarded as other possible energy sources in the E-region. Contribution of these additional energy sources to the total E-layer energy budget is regularly variable in space and time and are quite complex to be acurately determined [130]. Above 100 km within the thermospheric region, solar EUV radiation, tidal energy and atmospheric waves are supplemented by Joule heating and auroral particles' incidences as the energy sources on a global scale. The main source of energy above 400 km may be presumably, the electron cooling [130].

The solar radiation energy incident per sq. cm. of the Earth's surface is highly variable with season and latitude and can be determined with prior estimation of solar constant which according to Smithsonian Institute, varies daily by 1 to 2% . The spectral distribution of the solar radiation energy is more or less complex. Unlike the spectral distribution of radiations emitted by a black body, the solar radiation shows in its visible light spectrum an equivalent temperature of 6000 K. In the ultraviolet region of the solar radiations, due to the existence of a crowded gathering of many Fraunhofer lines, the smoothed out contour falls below that of a perfect black body at 6000 K [131]. There is indirect evidence that during the period of high solar activity, excess of short wave radiation may be emitted. Because of unsteady atmospheric absorption in IR region, more sophisticated techniques are required for measurement in this region of spectra. Quasiparallel beam of [125] solar radiation passes through the ionosphere with very little modification except the FUV which can be absorbed by oxygen and nitrogen. Below 50 km, ozone starts absorbing strongly in Hartley-Huggins-and Chappius- bands and the absorption has an important role to play in producing thermal equilibrium within the stratosphere. In the lower stratosphere, sufficient amount of water vapour and CO_2 alongwith ozone, absorb energy in the near infrared (NIR) bands. The total radiation absorbed by all atmospheric constituents is approximately 10% of the incident intensity although the exact amount depends on the zenith angle, water-vapour and ozone concentrations. Solar radiations get highly modified also through scattering within atmosphere as a consequence of which the stratosphere may be thought to be irradiated by a second diffuse stream of solar radiation coming from about 3 km above the Earth's surface with intensity equal to 40% of the incident radiation. Spectral distribution of this scattered radiation following the Rayleigh's λ^{-4}-law is not similar to that of the original solar radiations. The Earth's curvature, horizontal variations in the terrains, variable cloud cover, scattering of solar radiation are neglected and the incident solar radiation flux are assumed to be parallel. On the basis of these assumptions an ideal theoretical formulation can be considered for the evaluation of total flux of radiations at a altitude z. In this calculation Kirchoff's law and Lambert exponential law of absorption, that are strictly correct for purely monochromatic radiation, are used [125].

The rate of heating at altitude z is given by

$$dQ/dt = \rho_a c_p \, d\theta/dt = d\varphi(z)/dz \, ,$$

where

$$\varphi_z = \int_0^\infty \left[\varphi_\nu^S(z) + \varphi_\nu^E(z) + \varphi_\nu^A(z) + \varphi_\nu^B(z)\right] d\nu \, ,$$

where the purely original solar contribution

$$\varphi_\nu^S(z)\Delta\nu = -S_\nu \Delta\nu \cos\psi_3 \exp\left[-\int_z^\infty k_\nu(z')\rho(z')\sec\psi_3 \, dz\right.$$

The contribution of Earth surface is

$$\varphi_\nu^E(z)\Delta\nu = 2B_\nu(o)\Delta\nu \left\{\int_1^\infty e^{-x\sec\psi} \frac{d\sec\psi}{\sec^3\psi}\right\}$$

$$\left.\int_z^\infty k_\nu(z')\rho(z')dz'\right]$$

The atmospheric contribution from above z is

$$\varphi_\nu^A(z)\Delta\nu = \int_z^\infty 2\, B_\nu(z')\, \Delta\nu \frac{\partial}{\partial z}\left\{\int_1^\infty e^{-x\sec\psi} \frac{d\sec\psi}{\sec^3\psi}\right\}$$

$$\times\left[\int_z^\infty \rho(z'')k_\nu(z'')dz''\right.$$

and the atmospheric contribution from below z is

$$\varphi_\nu^B(z)\Delta\nu = \int_o^z 2\, B_\nu(z')\, \Delta\nu\rho(z')\, k_\nu(z')\left\{\int_1^\infty e^{x\sec\psi} \frac{d\sec\psi}{\sec^3\psi}\right.$$

$$\times\left[\int_o^z \rho(z'')k_\nu(z'')dz\right. \quad dz'$$

The interpretation of symbols used are as follows :

z, z′,z″ - vertical coordinate, *x*- horizontal coordinate, *e* - temperature, *ν*- frequency, ρ - density of absorbing gas, ρ_a - density of the atmosphere, c_p- speific heat at constant

pressure, ψ - Zenith angle, $S_\nu \Delta\nu$ - solar energy cm^{-2} sec^{-1} incident on the atmosphere in the frequency range ν to $\nu + \Delta\nu$.

$(1/\pi)\, B_\nu(\theta)\, \Delta\nu =$ energy cm^{-2} sec^{-1} per unit solid angle emitted in the frequency range ν to $\nu + \Delta\nu$ by a black body at temperature θ.

Solar short wave radiations (XUV) are the main source of photoionization of atmospheric atoms and molecules, mainly above 120 km and below the exosphere and also below 60^0 latitude in day time. Any exact correlation among the intensity, spectral distribution of solar XUV radiations and any of the usual solar indices such as 10.7 cm. solar flux, magnetic activity index *etc*, is yet to be established [15]. Solar extreme ultraviolet (EUV) radiations photoionize the upper atmospheric neutral constituents producing ions and electrons. Maximum ionisation at about 150 km. occurs mainly due to the absorption of radiation with wavelengths less than 796Å, the ionization threshold of the major neutral constituent of the atmosphere *i.e.* N_2. Photons having wavelengths in the range of 796 Å to 1027 Å, penetrate down to *E*-region. The most significant photoionization processes that occur within *E* and *F* regions are as follows [132],

$$N_2 + h\nu \rightarrow N_2^+ + e, \quad N_2 + h\nu \rightarrow N^+ + N + e,$$

$$O_2 + h\nu \rightarrow O_2^+ + e, \quad O + h\nu \rightarrow O^+ + e, \quad N + h\nu \rightarrow N^+ + e.$$

The following table (Table 3) gives the most important solar radiations which have significant contributions (the main role) in different ionospheric activities.

γ-ray bursts and solar nutrino production are also two important solar features that are observed and recorded with precision by means of sophisticated instrumentation. Theory of 'coronal equilibrium' helps us to understand many solar features including the production of various other spectral lines in the solar atmosphere through excitation by impact or collision of electrons and proton, non thermal emissions, other kinds of ionization and recombination and dielectronic recombination [133]. 10.7 mm. solar flux or 2800 MHz solar flux is produced by a free-free emission process and therefore, inspite of having no specific excitation mechanism or emission mode, its production is stongly associated with emissions that occur in frequent solar bursts or solar flares.

Table 3. Classification of electromagnetic radiation according to their wavelength range and the corresponding atmospheric layers of influence.

Radiation	Wavelength range	Layer of influence
IR	7800 Å< λ <1000 μm	Earth's surface
Near IR	λ <20 μ	
Far IR	λ >20 μ	
Visible	3800 Å< λ <7800 Å	Earth surface, E and F layer
UV	100 Å < λ <3800 Å	
EUV/XUV	2 Å< λ <1040 Å	E-layer
Near UV	2000 Å< λ <3000 Å	O_3 in lower stratosphere and troposphere
Lyman α (H_α)	λ = 1216 A	Mesosphere
X-Ray	0.1 Å < λ <100 Å	
Hard X-ray	λ <15 A	D-layer
Soft X-ray	λ >15 A	E and F layer

Different solar activity parameters or solar indices of importance

The solar data that are usually regularly observed and recorded comprise the following solar activity parameters [134] :

(i) sunspot area, (ii) sunspot blocking function, (iii) apparent solar diameter, (iv) total solar irradiance, (v) 10.7 cm. solar flux, (vi) Zürich and relative sunspot number, (vii) flares (γ -ray, X-ray, H_α , microwave, proton, energetic electron, solar flare-index), (viii) plage index (example, calcium plage), (ix) aurorae (solar), (x) solar flare number (xi) solar magnetic field index.

The three main solar features that are primarily concerned with the above-mentioned solar parameters, are the sunspot and solar flare-event and solar faculae. The most important primitive solar activity parameters are the Zurich sunspot number , the solar flare number and the 10.7 cm. solar flux all of which have been observed to have appreciable influence on the ionospheric activities [135-140]. At present, Zurich sunspot number has been replaced by relative sunspot number and solar flare number has been replaced by solar flare index (Sawyer-index, Kleczec-flare index) [141,142] and the 10.7 cm. solar flux has been coexisting with its variable component which is nothing but its original value minus the constant part of its own in its linear regression-relation with sunspot number [143]. Solar bursts are taking place on the solar surface mainly due to thermal energy imbalance and magnetoplasmodynamic instability in the hot plasma there, giving rise to the phenomenon of visible appearance of a long trail of hot bright gas-bulk jumping out of solar surface and then falling back. This is called solar flare. Associated with it are all generations of γ-ray, X-ray, H_α, microwave and high energy particles . In earlier days, solar flare numbers were used to be counted each hour of a day and each day of an year and were thought to represent an important solar activity index which affect some specific ionospheric activities. Later, it was realized by scientists that some more specific and more effective and useful flare index can be defined precisely to study solar influence on some specific ionospheric activities. Sawyer's solar flare index is such an index which is given by

$$I_f = 0.76 \Sigma A_d^2 / T^*,$$

A_d - individual flare area measured in millionth of solar disk, T^*- the effective observing time in minutes. Another flare index for evaluating daily flare index is the Kleckzec flare index [141] which is given by $q = it$, i represents an equivalent intensity scale (importance), t the duration (in minutes) of the flare.

Sunspots are, as known now-a-days , produced due to local thermal cooling on the solar surface caused by plasmaspheric rotational equillibrium and associated solar magnetic field connections. As the production of sunspots is inherently related to local rotation on the solar surface they appear prominently to possess certain periodicities. Sunspots are always observable in multitude on the solar surface and bear strong relationship with various terrestrial atmospheric features. Therefore, sunspots have been considered as the most important solar parameter to have influence on different ionospheric activities. In recent past, another solar activity index has been defined on the basis of modelling by the use of ground based photometric observation and is known as the photometric sunspot index (PSI) which is given by [144]

$$PSI = \alpha \sum A_i \mu [(3\mu + 2)/2].$$

Different solar periodicities

The temporal behaviour of solar activity, manifested especially in sunspots, has long been discussed and debated. Among the different solar periodicities observed from the Earth, some are of purely solar origin while the rest are produced as a consequence of relative angular speed of rotation (axial and orbital) of the Earth and their dependence on latitude and the angle of axis and orbit with respect to the solar ecliptic. Solar periodicities of purely solar origins are 11 years, 22 years, 152 days(5 months), 564 days (18.5) months , 26 months and also other short term periodities [145-152].

2.3 Ionospheric physics and chemistry for different layers of ionosphere

Depending on the specific nature of thermal, dynamical, gravitational and solar energy-input processes that prevail within the whole of the terrestrial ionosphere, the ionosphere is conveniently classified in two different ways:

(i) Altitudinally classified layers such as, D,E,F

(ii) Latitudinally divided sectors such as, low latitude, mid latitude and high latitude.

At first, the physical and chemical processes which take place within different layers will be considered . Until now, there has been no successful modelling of the day time quiet D-region which can explain how the initially formed ions like NO^+ get converted into oxonium ions H_3O^+, $(H_2O)_x$. Polar cap absorption (PCA) or solar proton event (SPE) has been successfully utilized in modelling the disturbed D-region which is characterized by the effective recombination coefficient which is directly proportional to the fourth power of the total neutral species concentration.

$$\alpha_{eff} = q/[e]^2 = L(A)^2/q$$

where, α_{eff} is the effective recombination coefficient, q is the ionization rate, [e] is the free electron concentration and L(A) is the electron loss rate.

Electron precipitation, sporadic meteor effects, cosmic X-ray are also some probable sources of ionization in D-region particularly at night. Although photo-detachment and associative detachment are the two main direct processes responsible for the negative ion formation in D-region, minor neutral gas species also have appreciable effects on it [153]. Absorption of radio waves within D-region which is related to ionization, varies appreciably throughout the year as well as with solar cycle. In winter in mid latitude D-region, the absorption is strongly enhanced for a period of several days. This phenomenon is known as the 'winter-anomaly'. During solar flares, the ionization in the D-region is enhanced and hence the absorption of radio waves is increased. As a consequence, radio transmission through the ionosphere may be seriously interrupted [154,155]. Populated with O_2^+ and NO^+ ions, the E region has been successfully modelled in which the electron recombination coefficient is written as

$$\alpha_{\mu R} = \left\{\alpha(NO^+)[NO^+] + \alpha(O_2^+)\left[O_2^+\right] + \alpha(M^+)[M^+]\right\} / \left([NO^+] + \left[O_2^+\right] + [M^+]\right).$$

Here, $[NO^+]$, $[O_2^+]$ and $[M^+]$ are the concentrations of NO^+ O_2^+ and atomic metallic ions, respectively and α's are the corresponding recombination coefficients.

Determining α_{eff} the effective recombination coeficient in relation with α_M , the coefficient of recombination with metal ion M^+ from bulk analysis in cases of meteor-caused ion production, poses great problem especially at night. Building up of ions in mid-latitude-sporadic E-regions is believed to take place mainly by the action of winds and wind shears in conjunction with the presence of Earth's magnetic field. The minor neutral gas NO is an important constituent in the E-region because the process $O_2^+ + NO \rightarrow NO^+ + O_2$ is generally competitive with electrons . But the distribution of NO in this region is not well understood [154]. Soft X-ray (λ_2 10-100 Å) are absorbed by N_2 and O_2 in the lower ionosphere as a consequence of which O_2^+, N_2^+, N^+ and O^+ ions are produced. Being very weak during the quiet state of the Sun and relatively stronger during the disturbed state of the Sun, the solar X-ray produces sudden ionospheric disturbances (SID) only in the high solar

ıctivity period. In the lower E-region, the atomic ions are quickly :onverted to molecular ions before transport process starts ıffecting their profile. Atomic ions that do not undergo rapid on-molecule reactions to form molecular ions, do generally have ong lifetimes and are subject to the influence of transport ıroces s. Long-lived metallic ions produced by meteor-ablation, :an have noticeable effect on the E-region electron density [155].

Ranging approximately from 100 km to 1000 km, F-region of he ionosphere constitutes of mainly O_2^+ and NO^+ in its lower ıortion (F_1) and O^+ and H^+ in its upper portion (F_2). Under ·ertain condition, He^+ also may be an important ion in F_2-region. The three transport equations, the equation of continuity, the nomentum equation and the energy equation need to be solved ımultaneously for electron gas and ion gas comprising of O_2^+, NO^+, O^+ and H^+ for developing a successful F-region model 155] . Photoionization of neutral constituents of F-region by olar Extreme Ultra Violet (EUV) radiations takes place. The ·alues of the absorption and ionization crosssections can be ıbtained from DNA Reaction Rate Hand book [156] while the olar photon flux can be obtained from the work of Donally and ?ope [157].

The main *F*-region ion-neutral reactions are given below :

$O^+ + O_2 \rightarrow O_2^+ + O$	$K_1 = 1.6 \times 10^{-11}\ cm^3\ s^-$	
$O^+ + N_2 \rightarrow NO^+ + O$	$K_2 = 6 \times 10^{-13}\ cm^3\ s^{-1}$	[156]
$O^+ + H \rightarrow H^+ + O$	$K_3 = (9/8)\ K_4$	
$H^+ + O \rightarrow O^+ + H$	$K_4 = 4 \times 10^{-10}\ cm^3\ s^{-1}$	
$N_2^+ + O_2 \rightarrow O_2^+ + N_2$	$K_5 = 5 \times 10^{-11}\ cm^3\ s^{-1}$	[156]
$N_2^+ + O \rightarrow NO^+ + N$	$K_6 = 1.4 \times 10^{-10}\ cm^3\ s^{-1}$.	

Around 500 km altitude, the following relation approximately ıolds good [156] .

$$n(H^+) = 9/8\ (n(H)/n(O))\ n(O^+)\ .$$

The main F-region ion-electron reactions are given below :

$N_2^+ + e^- \rightarrow N + N,$	$K_7 = 2.7 \times 10^{-7}\ (T/300)^{-0.2},$
$O_2^+ + e^- \rightarrow O + O,$	$K_8 = 2.1 \times 10\ (T/300)^{-0.7},$
$NO^+ + e^- \rightarrow N + O,$	$K_9 = 4.0 \times 10^{-7}\ (T/300)^{-0.5}.$

The existence of an F_2 peak can not simply be explained with he help of photochemistry. Processes in which electron-ion ransport takes place, need to be included also. Ambipolar liffusion is the most important process for such transport. Neutral winds play an important role in the diurnal variation of F_2 layer. The meridional wind component is directed towards he pole at day and towards the equator at night. F_2 layer is owered by wind in the day and is raised by it at night. Though lectric field-induced plasma-drift is unimportant for mid-latitude-onospheric transport process, it is extremely important for xplaining equatorial F-region anomaly (electron density crest at about 15° latitude). From aeronomical point of view, F-region is the best understood area. Yet no single model has been developed for explaining all the F-region features satisfactorily. For developing an effective model of F-region, the following problems will be of great concern, the details of which can be obtained from the Ref. [154].

(i) Thermospheric model problem ,

(ii) Neutral wind problem ,

(iii) Boundary value problem ,

(iv) EUV problem ,

(v) Ion chemistry problem ,

(vi) Electron temperature problem ,

(vii) Summer Morning problem .

The above-mentioned ion-neutral species reactions are the resonant charge transfer processes which result in a complete exchange of energy between the colliding systems without any change in the relative kinetic energy The resonant charge exchange cross section Q_E at the relative impact energies of importance can be approximately given by the formula,

$$Q_E = (A - B \log_{10} E)^2$$

where E is the relative kinetic energy [158].

The critical frequency and virtual height :

The wave equation that is usually considered is ,

$$\nabla^2 E - \left\{(\mu k/c^2)\left(\partial^2 E/\partial t^2\right)\right\} - \left\{\left(4\pi\ \sigma\mu/c^2\right)(\partial E/\partial t)\right\} = 0$$

Now considering $\sigma \approx 0$ and $\mu \approx 1$ 1 for a radio wave propagation through a uniformly ionized medium with no magnetic field the wave equation may be written as

$$\nabla^2 E - \left(k/c^2\right)\left(\partial^2 E/\partial t^2\right).$$

The oscillating E field sets electrons in motion. When these electrons collide with each other with a collision frequency ν_c , two significant phenomena take place. The amount of energy emitted as electromagnetic radiation is diminished and the electron's motion lag behind the phase of the incident wave. Thus, the use of complex exponentials to treat phase will lead to a real (negative) exponential which can be identified with the absorption coefficient of the atmosphere. The equation of motion of an electron is

$$m\left\{d^2x/dt^2\right\} = -eE_0 \exp(i\omega t) - m\nu_c\left\{dx/dt\right\} = \text{net force} +$$

net momentum transfer rate.

The steady state solution of this equation is

$$x = \left\{-i/(\nu_c - i\omega)\right\}\left\{e/\omega m\right\}\ Eo \exp(-i\omega t)\ .$$

The dielectric constant is given by

$$d.c. = k = 1 + 4\pi\{p/E\} = 1 - (4\pi\ N_e ex)/E$$

$$= 1 + (i4\pi\ \sigma_p)/\omega\ ,$$

where

$$\sigma_p = \left(N_e e^2 (\nu_c + i\omega)\right)/\left(m(\omega^2 + \nu_c^2)\right)$$

is the complex conductivity (The polarisation current replaces the conduction current j) [19].

The plane wave solution of Eq. 2(iii) is

$$E(z,t) = E_0 \exp\left[-i\omega\left\{t - \left(k^{1/2} z\right)/c\right\}\right],$$

where z is the distance along the path of propagation. The real part 'k' is

$$k_0 = 1 - \left(4\pi\ N_e e^2\right)/\left(m(\nu_c^2 + \omega^2)\right) = 1 - \omega_0^2/\left(\omega^2 + \omega_c^2\right),$$

where ω_0 = the plasma frequency. The real part of the refractive index 'n' for $n^2>0$ and $\omega_c << \omega$, can be written as

$$n = k_0^{1/2} = \left\{1 - \left(\omega_0^2/\omega^2\right)\right\}^{1/2}.$$

Waves with $\omega_0 \geq \omega$ will not enter the region of ionosphere due either to refraction or to reflection. For angle of incidence equal to θ_0 and obeying Snell's law $n = \sin\theta_0$, the ray will be reflected by the corresponding electron density. For the vertical incidence $\theta_0 = 0$, critical reflection occurs for $\omega^2 = \omega_0^2$ and $n = 0$. The maximum value of frequency $(\omega/2\pi)$ for an em wave to be reflected from an ionized layer, equal to the maximum value of natural plane wave plasma-frequency of the layer concerned and is called the critical frequency of that layer.

$$f_0 = \{(\omega_0)_{max}/2\pi\} = \left\{\left(4\pi\ N_{e\,max} e^2\right)/m\right\}^{1/2}.$$

The pressure law that holds good within an atmosphere in equilibrium, is given by

$P = P_0 \exp(-mgh/KT)$ = the pressure at height 'h' for gas of mean molecular mass 'm' at a constant temperature $T°K$. The quantity (KT/mg) is of the dimension of height and is called the scale height 'H' which may also be defined as the 'height at which the pressure diminishes to negative exponential times its value at the surface ($P = P_o e^{-h/H} = P_0 e^{-1}$)'.

A simple method of exploring the ionosphere is to send a series of short radio frequency wave trains in a vertically upward direction which can be varied. The time-delay between emission and reception after reflection from the ionosphere is to be recorded too. The time delay (t) is expressed as the equivalent or virtual height (h') at [15,24] which the wave would have been the reflected if it had travelled all the way with free space velocity of em wave 'c' so that $h' = (ct/2)$.

Starting with day-time ionosphere at $t = 0$ and setting the photoionization rate equal to zero, O^+ density disribution in the F-region is studied and found to decrease with time. The corresponding time constant approximately equals to the inverse of O^+ loss frequency at the height of F_2 peak. This decay takes place while ionization does not occur. This does not necessarily represent the nighttime F-region, because ionization in the nighttime F-region is indirectly maintained by its downward flow from the high altitude plasmasphere [132].

Critical frequency of F_1 layer (f_0F_1) varies with seasons. The behaviour of F_2 layer is described in terms of the extent of its departure from that of a hypothetical Chapman layer, the departure being named 'anomaly'. Geographic amomaly, diurnal anomaly, seasonal anomaly, winter anomaly are some of such anomalies observed usually in the experimental measurement of f_0F_2 (Critical frequency of F_2-layer) [159- 163]. Eclipses have been found to have no specific influence on F_2-layer parameters such as, f_0F_2 and $h'F$ (and also n_mF_2) to an appreciable extent [164]. The theory of ionospheric storm is capable of explaining the basic features in the behaviour of negative phase at the commencement of a disturbance on the basis of firmly established link between electron density and the ratio of densities of atomic oxygen and nitrogen molecule. Three dimensional models of the storm circulation with the inclusion of wind induced diffusion are needed to explain in detail the storm-time negative F_2-phase. All the morphological features of F_2-region can not be explained with the help of any one of the three existing mechanisms, namely, horizontal wind-induced drift electric field and protonospheric fluxes. As there are reasons to assume that positive disturbances are linked to entirely different regions and processes in the magnetosphere from Joule heating in the auroral oval, there are reasons to think of soft particle precipitation in the region of the daytime cusp as a possible source of positive disturbances [165].

Terrestrial ionosphere shows significant variations with altitude, latitudes longitude, universal time, solar cycle, season and geomagnetic activity. These variations are produced as a result of competition between the variation of forces acting within and on the ionosphere. Of special mention are the forces due to atmosphere-ionosphere-magnetosphere coupling through currents, energetic particles, electric fields and atmospheric drag. Not corotating with the 'Earth', the high latitude plasma moves under the action of electric fields of magnetospheric origin. Topside thermal plasma is capable of escaping from the topside ionosphere along open geomagnetic field lines. This process of escape is termed as the 'polar wind'

[132]. The cross-tail potential (CTP) difference is the electrical potential difference generated across the magnetospheric tail by means of interaction of shocked solar wind with the geomagnetic field. CTP can vary typically from 20 kV to 120 kV depending on the level of geomagnetic activity. Most of the time, the ring current effectively shields the plasma, within the plasmasphere and therefore, only the high latitude ionosphere is influenced by magnetospheric electric field. At all ionospheric altitudes, the frequency of electron-neutral atom collision is much less than the electron cyclotron frequency and therefore, the combined effect of the perpendicular field E and geomagnetic field B is to induce an electron drift in $\boldsymbol{E} \times \boldsymbol{B}$ direction. At F-region altitude, both ions and electrons drift in the $\boldsymbol{E} \times \boldsymbol{B}$ direction 2]. The corotation velocity, although much low, is added with drift for the E-field-induced two-cell drift pattern which is appreciable within the high latitude ionospheric plasma. There occurs an ionization hole, a low density-low temperature-region that appears during quiet geomagnetic activity.

At mid-latitudes, the geomagnetic field lines are inclined to the vertical direction. The effect of meridional wind (north south) is to compel the F-region ionization to move up or down the field lines depending on the direction of wind. The equatorward wind at night therefore, has an important role to play in maintaining F-layer ionization. Mid-latitude ionosphere exhibits another type of transport process which is the plasma-flow along different geomagnetic field lines. During geomagnetic storms, high density cold plasma in the plasmasphere comes into contact with low density hot plasma in the ring current. Energy, either of any one or of both of the Coulombic collision and wave-particle interaction, transforms ring current particles into thermal electrons within the interaction region. This energy is then conducted to the lower ionosphere along geomagnetic field lines which gives rise to an elevated electron temperature. Hot electrons at an altitude range of 300-400 km. have got sufficient energy to collisionally excite atomic oxygen as a result of which OI 6300 Å red line is emitted. Produced in this way, the oxygen red line emission is generally found over a narrow band of latitude on the equatorial side of the auroral oval which is well known as stable auroral red arc (SAR-arc).

At low latitudes, the quasi-horizontal geomagnetic field lines produce some unique transport processes, the most interesting of which is the equatorial fountain [132]. Another source of transportation is the expansion and cooling of ionospheric plasma on the summer side of the equator and compression and heating of the same on the winter side of the equator.

The existence of ionospheric structures with scale sizes of tens of kilometers or smaller than that are collectively known as the small scale irregularities [166]. These can be primarily caused by the onset and evolution of different types of instability. Evolving from large scale ionospheric configurations, these instabilities are generally mutually superimposed. The two most important small scale irregulatities are:

(i) The steepening and subsequent recurrential splitting of barium clouds released in the ionosphere, after being driven by the gradient drift instability.

(ii) The formation and buoyant rise of low density 'bubbles' of plasma, after being driven by the collisional Rayleigh-Taylor instability in the nighttime equatorial ionosphere, is known as equatorial spead F (ESF).

These effects have bearing on the magnetic field intensity and are therefore latitude dependent too [166].

Peak electron density $n_m(e)$ is another important ionospheric parameter which affects airglow emission significantly, because of its intrinsic relation with the critical frequency and to some extent, with the virtual height. The peak electron density $n_m(e)$ or n_mF_2 is related to f_0F_2 according to the well known equation [167]

$$n_m(e)\,(cc^{-1}) = 1.24 \times 10^4\,[f_0F_2(MHz)]^2\,. \tag{9}$$

Peak electron density n_mF_2 is so strongly correlated to f_0F_2 both from purely theoretical and empirical points of view that one is computed from the value of the other. $n_m(e)$ is very often computed from f_0F_2 [168, 169]. Sometimes, zenith airglow intensity for different important airglow emissions are directly computed from their relation with $n_m(e)$ [170]. Ionization profile in the F_1 region is different from that of F_2 because of the following reasons [80];

(i) F_2-region ionosphere is optically thin to most ionizing radiations and if the atmosphere in this region can be considered to be isothermal, the general rate of photoionization for incident monochromatic radiation (for single ionizable constituent) can be written as,

$$q(z, \mu) = \pi\, F_\nu \sigma_\nu N(z_0) \exp\left[-(z - z_0)/H\right]. \tag{10}$$

(ii) The recombination term being directly proportional to n_e, the electron density under the chemical equillibrium would increase indefinitely with height.

(iii) But indefinite increase of n_e with altitude can not be realistic. Hence, F_2 can not be treated with chemical equilibrium only. Dynamics is also an essential feature in F_2-region. Ambipolar diffusion stops that indefinite increase of n_e with height.

Kimura *et al* [171] have shown on the basis of Diffusive Equilibrium (DE) model and SUPIM analysis (discussed later) that the latitude dependence of global electron can approximately be represented by an oscillatory function of latitude.

2 .4 Interrelation between ionospheric activities and airglow emissions:

From our previously discussed sections regarding the basic physics of airglow, related chemical kinetics and excitation mechanism and above all, the ionospheric physics and chemistry, it is obvious and easy to comprehend that there exists a direct relationship, either of complex or of straightforward nature between ionospheric parameters and airglow emissions. Considering eqs. Eq. 1- 4,8 and 9 simultaneously, one can mathematically prove that,

$$\text{airglow intensity} \propto \left[f_0F_2\right]^2 \exp\left[-(z-z_0)/H\right].$$

Barbier [172] was the first to establish a semiempirical formula for OI 6300 Å airglow emission which is given by,

$$Q_{6300} = A\,(f_0F_2)^2 \exp\left[-(h'F-200)/H\right] + B,$$

where H is the scale height in terms of oxygen and was assumed by Barbier himself to be equal to 41.3 . Later, this relation due to Barbier was verified to an extraordinary level of satisfaction by Carman *et al* [173]. Barbier's equation has been used by several workers in their analysis of OI 6300 Å and OI 5577 Å airglow intensity variation with different solar geophysical parameters [174, 175]. Actually, the volume emission rate of different airglow radiations, which is directly proportional to the corresponding intensity, depends in general, on the electron density and the relative abundances of different atomic and molecular ionic species involved in all possible dominant modes of excitation. For oxygen green and red line airglow emissions , it is therefore deducible from the experimentally determined values of different rate-constants, quenching coefficients and transition probabilities that the airglow intensity for those two emissions is proportional only to the electron density and so the pattern of variation of OI 6300 Å and OI 5577 Å airglow emissions is mainly governed by the electron density profile, [48, 167, 169, 174] . Besides, there are many more works regarding the analysis of interrelation between different airglow emissions and corresponding ionospheric parameters [176 - 180].

2 .5 Ozone chemistry and its importance in airglow study :

In the UV and visible regions of solar spectrum between 2000 Å and 6600 Å , O_3 is the naturally occurring major atmospheric absorber. Intense Hartley band and weak Huggins and Chappius bands are among the principal spectral features of O_3 . Photolysis of O_3 in the visible spectral region leads to ground state products O_2 ($^3\Sigma^-_g$) and O (^{3}P) [181]. Photolytic production of O(^{1}D) in the reaction

$$O_3 + h\nu \rightarrow O_2 + O^*,$$

is possible in a spin conserved process at wavelengths $\lambda \leq 310$ nm. This reaction is the major source of O(^{1}D) , which on one hand, gives oxygen red and green lines emissions through forbidden transitions and on the other hand, is involved in reaction with H_2O, CH_4 and N_2O [182] . The basic atmospheric O_3 photochemistry theory, as developed by Chapman [182], involves two photochemical and three chemical reactions ;

$$O_3 + h\nu \rightarrow O_2 + O, \quad O_2 + h\nu \rightarrow O + O, \quad O + O_2 + M \rightarrow O_3 + M,$$

$$O + O_3 \rightarrow O_2 + O_2, \quad O + O + M \rightarrow O_2 + M.$$

Approximately, 80% of stratospheric O_3 produced by solar irradiation is not balanced by Chapman's removal scheme or by transport to lower altitudes. Reactions with trace amounts of N, H, C or halogen are important [182,183]. Midya [184] reports that O_3 plays an important role in the emission of OH (8,3) band airglow and there is a correlation between the two. Midya *et al* [185] have found out that both chemical kinetically and practically, Li 6708 Å line intensity decreases proportionally with dramatic depletion of ozone at two antarctic survey stations (Halley-Bay and Mc- Murdo) .

3. Well known features of terrestrial airglow emissions

Airglow intensity variation is one of the most significant airg features which can be broadly classified into two different ty

(i) Spatial variation ,

(ii) Temporal variation.

Spatial variation again has some specific varieties; Th are (a) Altitudinal variation or vertical profile, (b) Latitud variation and (c) Longitudinal variation. Temporal variation has certain varieties ; (d) Hourly and diurnal variation, (e) M monthly or seasonal, (f) Semiannual and annual; all these ty of variations are described briefly.

3.1 Altitudinal distribution or vertical profile :

Altitudinal distribution or vertical distribution of up atmospheric pressure, mean density, temperature, elect density and density of different neutral and ionic species h been determined through several rocket launching and satel launching missions, several times at different latitudes longitudes. Each time, the data have been modified to so extent. Based on these data, several airglow fluctuation mod have been developed by many scientists. F-region nightgl emission, dominated by oxygen green and red line emissi has been found to increase with altitude, being maximum ab 200 km and then to decrease again upto a certain height [48,18 Solomon *et al* [187] compared their model for 6300 Å airgl emission with corresponding satellite mission observation giv special stress to emission -altitude profile and they too show that the intensity of emissions increases with altitude to reac maximum at about 250 km and then decreases with altitude. M *et al* [188] analyse the different mission experimental result altitude profile of volume emission rate for 5577 Å , $O_2(0$

band and O_2 Herzberg band in which the same has been found to increase with height reaching a maximum above 100 km, and then to decrease. Takahashi *et al* [30] described in details, the altitude profile of all important airglow lines obtained from MULTIFOT experiment. Shepherd *et al* [189] describes the observed vertical distribution of 5577 Å emission near geographic equator.

3. 2 Latitudinal variation of airglow intensity :

The latitudinal variation of airglow intensity is difficult to be determined properly [24]. Many problems in determining the latitude-dependence of airglow emission intensity have been sorted out by many scientists in the early period of the study of airglow emissions.

Davis and Smith studied observed latitudinal variations of all important airglow emission lines and found that [190] 5577 Å and 6300 Å line intensities have in general, an oscillatory nature of variation with latitude, having a minimum at the geomagnetic equator. The maximum values of intensities of those lines in northern hemisphere is much greater than those in southern hemisphere. In case of Na 5893 Å line intensity, the findings are similar to those mentioned above except the fact that the maximum value of intensity in southern hemisphere is much more than that in northern hemisphere. Chandra *et al* [170] too studied latitudinal variations of airglow emission coupled with seasonal and other variations and they inferred that electron content profile has little to control OI 6300 Å airglow emission values. Zuzic *et al* [191] use (N_2/O) ratio to indicate the thermospheric composition changes and isolating geomagnetic activity effect from ESRO4 satellite data, they find out the latitude profile of that ratio. This may give useful data for obtaining analytically latitudinal structure of airglow emission profile. Kimura *et al* [172], in their model-based calculations, have computed and studied the latitudinal variation of electron density and other ion densities, which may help us to develop a model for latitude variation of different airglow emissions. Hickey *et al* [192] discuss the latitudinal variations of geocoronal hot oxygen and compared it with other type of variations. Ghosh and Midya [193] explained the latitudinal variation of 5577 Å night airglow emission with the help of latitudinal variation of air density.

3 .3 Longitudinal variation :

Mukherjee [194] identifies a westward penetrating electric field at low and equatorial latitudes that affects the excursions in '*H*' which may indirectly influence the corresponding airglow emissions. Su *et al* [195] made a modelling study of the longitudinal variations in the north south asymmetries of the ionospheric equatorial anomaly. Actually, the longitudinal variation of airglow emission is both theoretically and practically, insignificant and little work on that type of variation has therefore been done.

3.4 Hourly and diurnal variation of airglow intensity and SZA :

Regular temporal observations of airglow emissions have been dominated by such temporal recording of airglow data all over the world. Ghosh and Midya [196] reported their observation of morning twilight airglow emissions at Kolkata where all three airglow lines' intensities [5577 Å , 5893 Å & 6300 Å] were found to be increase exponentially with time and then reaching a peak within 15-20 minutes from the start of enhancement, decay down to an average range of intensity. Only the 6300 Å line intensity did not show any peak .Ghosh and Midya [90] studied also the evening twilight enhancement of 5893 Å line intensity at Kolkata and obtained successive enhancements and decays as exponential fuctions of time. But for this case, they obtained a typically prominent two-peak feature, one of which occurred before the local sunset and the other, a little lower than first peak, occurred with certainty after the local sunset time. Similar observations were discussed in the perspective of different excitation mechanisms by the same authors [81] . Low *et al* [197] discussed the INDII/ UARS observations of twilight hydroxyl airglow at mid-latitude equinox in which they observed that during the early hours after sunset, the volume emission rate on the bottom side of the layers appears to decay exponentially with time having a time constant that varies from 1.1 h at 78 km to 2.9 h at 82 km. They also showed that the value of this time constant is related to the process of excitations involved. Mukherjee *et al* [198] studied 6300 Å nightglow they observed made from 17° latitude and showed that in the geomagnetically quiet night, the 630nm airglow intensity varies more or less similarly at two stations, Kolhapur (lat. 16°8 N, long. 74°2E) and Ahmedabad (lat. 23°.0 N long. 72°6E). The intensities were found to decay almost exponentially with time showing a two peak feature. But it is interesting to see that during geomagnetically disturbed night, the 6300 Å airglow intensity oscillates with time and decays exponentially. The dawn to dusk asymmetry in volumetric intensity of 5577 Å airglow emission was identified from AE-C satellite-measurements. Kiselev [199] explained that assymmetry on the basis of an analysis of the excitation mechanism and its dependence on solar zenith angle (SZA) . In his model-based- calculations of the OI 844.6 nm airglow emission during the period of evening twilight, Singh (200) found that the calculation as a function of solar zenith angle (SZA) gives the corresponding line intensity in fair, agreement with the measurementm, only for a range of SZA. Tanabe *et al* [201] disscussed in detail, the airglow observation program of Tokyo Astronomical Observatory where observation was made regularly on Moonless clear nights of every month since the International Geophysical Year (IGY), (1957-8) at Mainuyama,

Dodaira, and Kiso stations. Hickey *et al* [192] described the diurnal variation of geocoronal hot oxygen in details. Kagan and Frolov [202] reported the diurnal variations of decay time of heater-induced small- scale irregularities in the mid-latitude ionospheric F-layer measured by means of diagnostic stimulated em emissions (DSEE) and analysed the results.

Bhaumik *et al* [203] reported their observation on morning twilight airglow emissions of OH [7,2] and Li 6708 Å line, in which the intensity for both emissions was found to increase exponentially with time.

3.5 Dynamical coupling :

Variety of dynamical processes are involved in coupling the motions of middle atmosphere with that of lower ionosphere. Classifying in general those processes as either advective, wave-like or diffusive, Hocking (204) discussed various aspects of the those process detail.

3.6 Barium cloud feature :

Detailed investigations on the ionization and airglow of Ba in the early stage have been made and expansion of the Ba cloud in the field of solar radiation has been reported by Priyatkin *et al* [205] . Kinetic processes involved in the excitation and ionization of barium atoms by suprathermal electrons formed at the time of short radio waves, influence on barium cloud and have been analysed by Grebnev *et al* [206] .

3.7 Seasonal variation of airglow intensity:

Monthly mean values of airglow emission intensities, often termed as seasonal airglow data, are of great importance in airglow research. Ghosh and Midya explained the seasonal variations of 5577 Å and 5893 Å night airglow emission at Calcutta on the basis of their consideration of density of air and related compositions as functions of time. For explaining the seasonal variations, they considered Chapman's mechanism and Jacchia's relations [207]. Seasonal variation of the low latitude OI 630.0 nm nightglow and its strong correlation with solar activity and solar cycle have been presented by Sahai *et al* [208] . Seasonal variation of 6300 Å airglow line intensity has been obtained by Midya and Ghosh [82] who found an oscillatory mode of variation against month. Seasonal variation of OH(8,3) airglow band intensity distribution has been considered and explained in terms of air density fluctuations by Bhaumik *et al* [209]. Midya *et al* [210] considered seasonal variation of 5893 Å airglow intensity at Calcutta and found that the same is correlated with solar flare index Hickey *et al* [192] discussed the seasonal variations of geocoronal hot oxygen in terms of fluctuations of its new sources. McNeil *et al* [211] found that the main contribution to the seasonal variation of sodium nightglow comes from the temperature dependence of the reaction that recycles atomic sodium from $NaHCO_3$. Seasonal variations in the atmospheric minor species including ozone are secondary effects at best. With the help of calculations based on spectrographic observation of the OH atmospheric emission (9,4) , (6,2) , (5,1) and O_2 (0,1) bands, seasonal variation of temperature at 88.95 km height has been established by Toroshelidze [212].

3.8 Semi-annual and annual variations :

Estimating variation of wind velocity due to turbulence in inertial subrange, the vertical eddy diffusivity in the troposphere, stratosphere and also in mesosphere have been studied and seasonal, semi- annual and annual variations of diffusivity parameter K has been confirmed by Kurosaki *et al* [213]. The effect of O_3 depletion on OH (8,3) band emission on the basis of Bates - Nicolet theory has been described and the annual variation of the same at Halley Bay station during the period 1973 to 1984 has been presented by Midya [184]. Takahashi *et al* [214] found that 5577 Å , 5893 Å and OH (9,4) band emissions in upper mesospheric and lower thermospheric airglow show strong semi-annual oscillations with maxima at equinoxes and minima during the solstices. They suggested that such oscillations may be caused by the effects either of one or of both seasonal variations in vertical eddy transport and meridional circulation. Burnside and Tepley [215] in their meridian- scanning observations of the intensities of the OI emissions 558 nm and 557.7 nm, noticed that the ratio between 558 nm intensity to the North and to the South of Sutherland, underwent an annual variation with the largest ratios being observed during Southern winter.

3.9 Hydrodynamical oscillation type variation :

Pertsev reports the identification of a new types of hydrodynamic oscillations revealed by airglow fluctuations [216].

3.10 Rotational and doppler temperatures :

Molecular rotational energy expressed in terms of equivalent gas kinetic temperature is known as Rotational temperature. Similarly, the airglow spectral line broadening due to Doppler effect may be looked upon as to be conveniently expressed in terms of an equivalent temperature called the Doppler temperature. They are of immense significance in aeronomy and airglow study [10].

3.11 Limb view of Earth's airglow spectra :

Earth's airglow layer observed in the limb view, appears to be a composite spectral layer. Mende *et al* [217] described in detail, such limb view spectrum of Earth's airglow and compared it with a model of limb view spectrum.

4. Different atmospheric, thermospheric and ionospheric models developed by scientists from 1940's and onwards

4.1 Wulf's worldwide circulation system – 1945 :

It is believed that Wulf is the first person to successfully apply the Atmospheric Dynamo theory to the motions of upper atmosphere and predict for the first time the existence of vertical motions of air for which the concept of circulation wheels was needed. Wulf's model predicts also that a part of magnetic disturbance caused by the fluctuations in the upper atmospheric circulation produces a latitudinal and seasonal dependence of his disturbance. Wulf also hypothesized that the potential differences generated by zonal ionospheric winds which cut the Earth's magnetic field may be the primary source of excitation of airglow and aurora[20].

4.2 Vestine's wind systems of geomagnetic disturbance -1953:

In this model with the help of atmospheric dynamo theory the atmospheric electric current system is replaced by the equivalent atmospheric wind system which varries with the degree of electric polarization of the atmosphere and also with the intensity of toroidal or solenoidal electric currents likely to be caused by zonal winds. Dynamo air-flow-induced variation in E-region is found, in this model, to be independent of magnetic storm [20].

4.3 Goldie's average planetary circulation- 1950 :

On the basis of the assumption of an average condition within atmosphere upto a height 45 Km, regarding pressure and temperature obtained from radiosonde experiments, unequal heating in different latitudes, mass transport and on the basis of the assumption that actual velocities have the same direction as the acceleration, Goldie proposed a model applying which Goldie himself deduced the following informations : (i) there exist two major frictionally driven vertical circulations running in opposite senses in meridian plane. (ii) reversed secondary circulation with subsidence in the tropic may be primarily caused by unequal heating and convection along meridional plane [20].

4.4 Kellog- Schilling model of stratospheric circulation – 1950 :

The important assumptions which this model is based on are as follows :

(i) Stratospheric winds over the equator are easterly with cross-isobaric components;

(ii) In the lower ionosphere *i.e.* in the region of *D* and *E*-layers, winds are assumed to be variable yielding strong diurnal variations while in the upper ionosphere, mean meridional currents are more towards poles.

(iii) The entire circulation between tropopause and ionosphere reverses itself semiannually. The important results obtained from this model were as follows :

(a) meridional temperature distributions were found to be related with mean zonal winds.

(b) The role of concentrated ozone in ozonosphere as the main solar radiation-absorbing constituent, especially in winter solstice may eventually cause the reversal of the general circulation.

(c) Some other important ionospheric features such as cooling in a part of the stratosphere in summer, have generally agreed with this model [20].

4.5 Yerg's ionospheric wind system (1951) :

Based on the observation of temperature lapse-rate from electron recombination coefficient and a proposed large scale vertical distribution of viscous stress in the F-region of ionosphere, Yerg [20] proposed a model of circulation for the ionosphere between 100 and 300 km. altitude and with the help of this model, he explained the longitudinal variations in electron concentrations for the F_2-layer.

4.6 Deb's model of ionospheric circulation (1953) :

On the basis of a synthesis of theoretical reasoning and then-available experimental data, Deb [20] proposed another model for atmospheric circulation above 100 km . This model gives the following results ;

a) Wind is south–west in the E and F_1 regions and north east or east in the F_2-region of ionosphere.

b) Wind velocity rises with height and undergoes seasonal variation [20].

4.7 Brasefield's empirical wind system – 1954 :

On the basis of wind data obtained from rocket and balloon-flight, Brasefield constructed a theoretical model which was proposed to be valid for a very limited range of altitude and latitude [20].

4.8 Palmer model of circulation in the lower stratosphere – 1954 [20] :

Palmer is the first person to present a coherent model of tropospheric and stratospheric wind system which is based on the wind and temperature data and a critical study of various atmospheric dynamics including the tropical regions. Palmer's

model had the following achievements over the then-existing other models of atmospheric circulation :

(a) There exists big circulations which eventually mask the cross equator-drift.

(b) There is a fundamental difference between the circulations over the two poles.

(c) The model agrees fairly well with empirical datas that were known at that time.

(d) This model shows the way to extend 'general circulation models' so as to give a true synoptic picture of meteorological conditions on a daily basis. (Figures 14 - 18)

An ideal atmospheric model is actually a set of numbers that is intended to represent the physical properties of the atmosphere independent of the period of observation [218]. There are

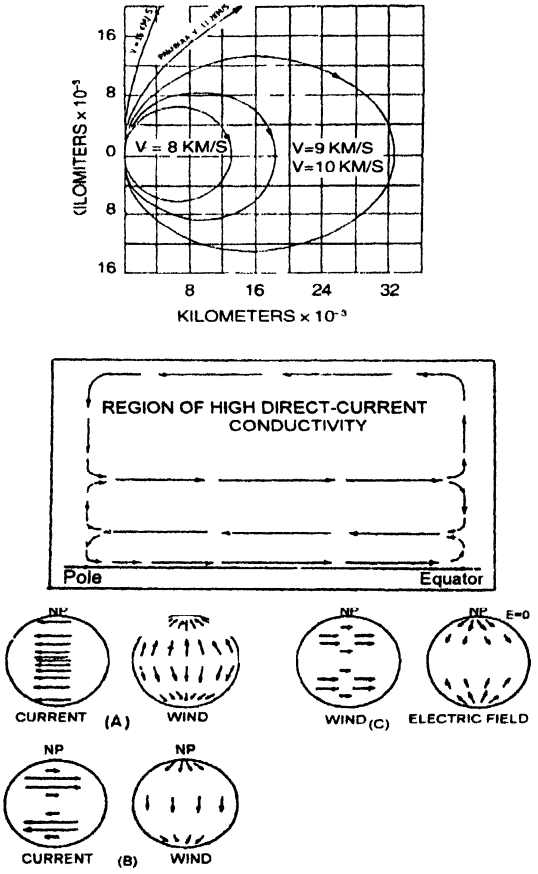

Figure 14. (a) Orbits in the Earth's field ; (b) Schematic representation of meridional component of large-scale atmospheric circulation ; (c) Schematic wind and current systems, thin spherical shell : (A) for daily means, symmetrical part of disturbance (B) for seasonal change in daily means, sinusoidal part of disturbance (C) electrical field for eastward zonal wind.

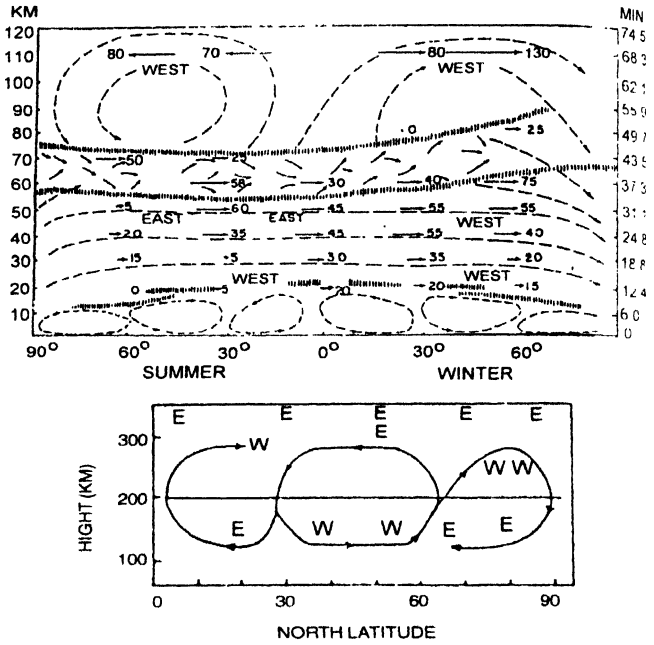

Figure 15. (a) Schematic representation of general circulation in meridional cross section for Northern Summer (Rossby) [20] ; (b) Proposed (Yerg) [20] circulation for ionosphere

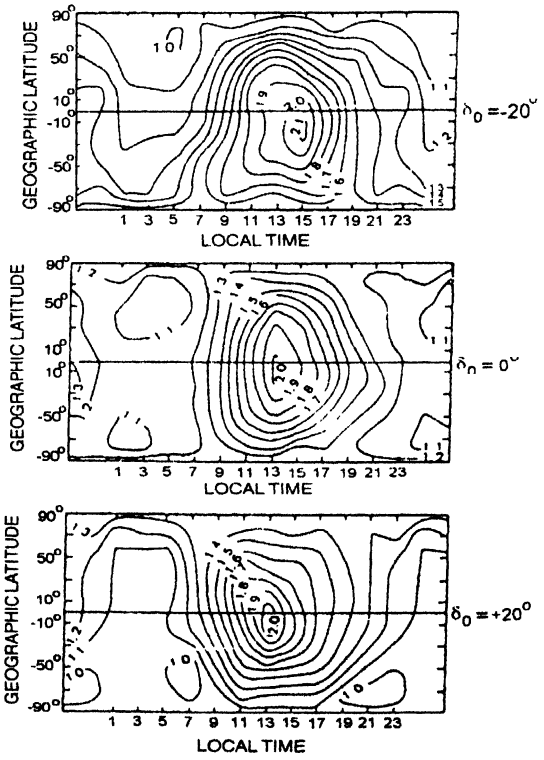

Figure. 16. Diagramatic vertical meridional cross section between 10 km and 60 km through the central pacific (Palmer) [20].

essentially three types of atmospheric models in reality used for our partial understanding of the upper atmosphere : (i) Purely theoretical model, (ii) Semi-empirical models and (iii) Empirical or Experimental models.

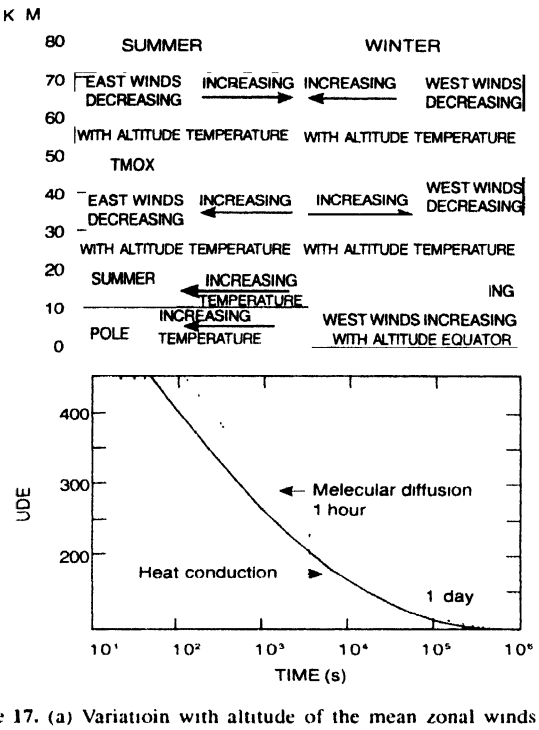

Figure 17. (a) Variatioin with altitude of the mean zonal winds and the poleward temperature gradient [Brassfield] [96] , (b) Comparison between diffusion time and heat conduction time in the mean CIRA.

4.9 CIRA Model :

In purely theoretical models, rigorous solutions of some basic equations including the fundamental conservation theorems along with some appropriate boundary conditions, produce results that are fairly comparable with experimental data. A collection of such useful theoretical models have been analytically discussed by Blumm *et al* [219] in COSPAR International Reference Atmosphere or CIRA [218]. It can be shown from CIRA model that the electron density is 100 times that of O_2^+ ions and hence, the stratospheric ozone concentration guided by reaction of O_2^+, depends primarily on the density of O_2^+ , ions [196] .

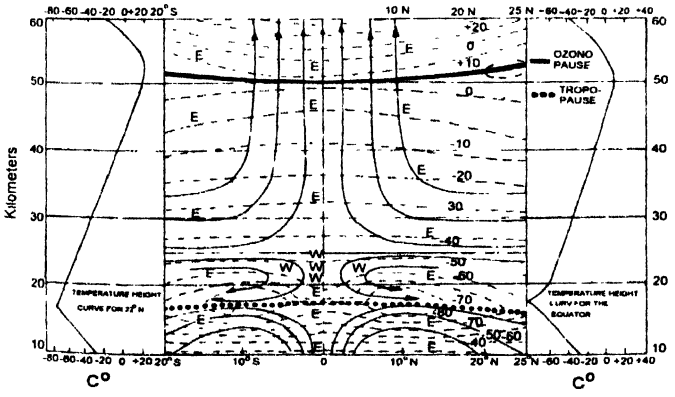

Figure 18. Ratio at 280 km between observed densities and th enighttime minimum density of Jacchia (1971) [20] as a function of local solar time and latitude. The solar declination is respectively - 20°, 0° and + 20°.

4.10 Jacchia model :

Atmospheric models due to Jacchia [220] fall in the category of semi- empirical model. Being based experimentally on satellite drag data and theoretically on diffusive equilibrium hypothesis, Jacchia's model gives a number of relations such as, latitudinal, altitudinal and seasonal variations of density of air.

For example , semi-annual and altitudinal variation of density of air, as given by Jacchia-model is

$$\log [\ \Delta \text{ (air density) }] = f(z)\ g(t),$$

$$f(z) = [\ 0.04\ \{z/100\}^2 + 0.05\ ] \exp(-0.25\ z/100),$$

and $$g(t) = 0.0284 + 0.382\ [\ 1 + 0.467 \sin(2\pi\tau + 4.14)\ ] \sin(4\pi\tau + 4.26),$$

$$\tau = \varphi + 0.954\ [\{\ \tfrac{1}{2} + \tfrac{1}{2} \sin(2\pi\ \varphi + 6.04)\}^{1.65} - \tfrac{1}{2}\ ],$$

$$\varphi = (t - \text{Jan1}) / 365,$$

where z = altitude in km, t = time of the year concerned.

The latitudinal variation of air density, as given by Jacchia model is,

$$\log [\ \Delta \text{ (air density) }] = \varphi/|\varphi|\ \text{S.P.} \sin^2 \varphi,$$

$$S = 0.014\,(z - 91) \exp\{-0.0013\,(z - 91)^2\},$$

$$P = \sin(2\pi\psi + 1.72),\ \varphi = \text{latitude concerned},$$

ψ = fraction of year = $(t - \text{Jan1})/365$, t in days

z = altitude in km.

Klostermeyer's observation of the fact that geomagnetic disturbance-caused gravity waves can cause an increase in temperature, agrees fairly well with satellite drag data of Jacchia. Barlier *et al.* established the fact that there exists a definite north-south asymmetry in the thermosphere which can also be found in Jacchia (1971) model [218].

IR emissions respectively of O at 63 km, of O_3 at 9.6 km, of CO_2 at 15 km play significant role in the heat budget of mesosphere and lower thermosphere and therefore need to incorporated into the atmospheric models [218].

4.11 MSIS Hedin :

Purely experimental or empirical modelling is an act of representing directly physical parameters that are measured *in*

situ by satellites. Purely empirical model sometimes lead to a semi-empirical model. As for an example, Hedin's empirical OGO – 6 model gives a worldwide distribution of temperature and concentration which was obtained with the help of spherical harmonic analysis of measured data. Similarly, ESRO-4 data due to von Zahn presents another empirical model.

4.12 MSIS-86 :

Thermospheric model due to Hedin [221] is the most widely used empirical model that includes the temperature, density and composition. Using similar data from Dynamics Explorer satellite, this model gives in addition to the normal physical parameters, the geomagnetic activity effect both in quiet and disturbed conditions and also the concentrations of species like N, N_2, O_2, He, H and Ar *etc*.

4.13 MSIS – 90 (Hedin) [222] :

It is another modified version of MSIS-86(Hedin) model.

4.14 CHIU model :

Later another empirical model was proposed by Chiu [223] and known as CHIU empirical model which gives the densities of different component species of ions within the terrestrial ionosphere.

4.15 SLIM & FAIM :

More sophisticated semi-empirical model SLIM (semi-empirical low latitude ionospheric model) was developed by Anderson *et al* [224] and this model was transformed into a much more effective semi-empirical model FAIM (Fully Analytic Ionospheric Model) by Anderson *et al* in 1989 [225]. Those semi-empirical models are based on the solution of the time-dependent continuity equation which considers only the dominant O^+ ions and takes into account $E \times B$ drifts and thermospheric winds. A successful application and a brief discussion of FAIM have been made by Mukherjee and Carlo [169].

4.16 CTIPM (Coupled Thermospheric Ionospheric Plasmasphere Model) :

This model is another useful model for application in cases of steady decrease or increase of atmospheric parameters including wind speed system mainly at high latitude sector [226].

4.17 TSMGCM (Troposphere- Stratosphere Mesosphere General Circulation Model) :

It is a global climate model with an upper level below 90 km. The model comprises 34 levels with a resolution of 3.5 km along the vertical height of atmosphere. In this model, the primitive GCM equations are solved and tropospheric parameterizations from ECHAM1 are used. This model is very effective in producing a realistic stratospause-semiannual oscillation with westerly winds during the equinoxes without a gravity wave drag parameterization [227].

4.18 QPS model :

It is another useful model concerning ionospheric profile developed jointly by Dyson, Benett , Baker and Lambert and used by Landeau *et al* to compare with a new model [228] .

4.19 EVF model:

Landeau *et al* in their model include E-layer , F-layer and joining valley layer. The behaviour of the E-layer is assumed to be determined as a function of time. E-layer parameterization follows another model known in the name of CCIR model [229]. EVF model has three free parameters and gives the time varying electron density in the lower ionosphere more accurately than QP model.

4.20 TDIM model :

Unlike the other models that are very useful for only low latitude sector, this model, developed at Utah State University (USU) and named as time-dependent ionospheric model or TDIM, has been proven to be very successful in the high latitude climatology. This is a numerical model which includes the physics of high latitude sector where ionosphere is driven both by magnetospheric and solar energy inputs [230].

4.21 SUPIM : Sheffield University Plasmasphere Ionosphere Model :

In this model, solutions of time-dependent equations of continuity are obtained on the basis of consideration of moments and energy balance for O^+, H^+, He^+, N_2^+ O_2^+ and NO^+ ion and electron cocentrations, field- aligned velocity and temperatures [231-233]

4.22 TIEGCM :

National Center for Atmospheric Research of USA developed thermosphere – ionosphere- electrodynamic general circulation model. It is a self- consistent set of solutions of the non-linear time dependent equations consisting of momentum, continuity, energy, hydrostatics and current density for the coupled thermosphere-ionosphere system along with the effects of tidal waves in the lower atmosphere [234].

4.23 FLIP model :

Field line Inter-hemispheric plasma model is another model useful for producing various ionospheric simulations as results. This model includes the photochemistry mainly of the F-region of the ionosphere [235-237] .

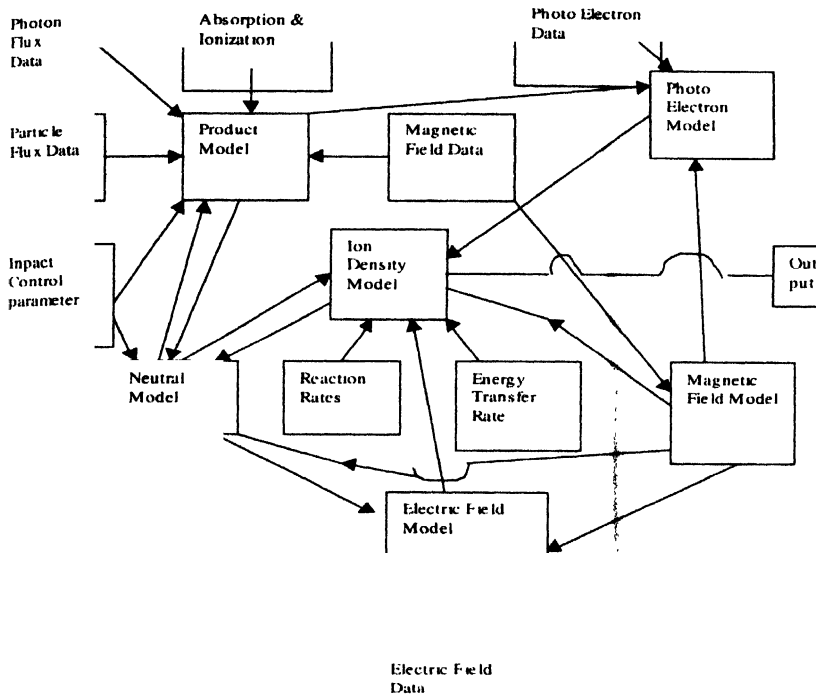

Figure 19. Flowchart showing th edetails of the comtructioin of Belikov model.

4.24 MWM :

Using the h_mF_2 and a comprehensive ionospheric model (FLIP model) to deduce thermospheric winds , Miller *et al* [238] developed a semi-empirical model which is known as Meridional Wind Model . This model is preferably applicable to mid-latitude ionosphere only because there is no provision for electric fields in this model. This model is based on the dependence of the height of the ionospheric F-region on the speed and direction of the meridional component of the neutral wind.

4.25 IRI Model :

International Reference Ionosphere Model is developed using similar expressions as that of Dudeney [239-241]. Various factors such as an extensive set of empirical coefficients' minimum or valley between *E* and *F* layers, h_mF_2 and n_mF_2 *etc* are included in this model.

4.26 Belikov model :

On the basis of numerical solution of the radiation transfer equation for a radially varying spherical atmosphere, Belikov developed a model which helped to resolve many interesting features related to multiple scattering of solar radiation by terrestrial atmospheres [242,243]. The various constituent part of this model is shown through a flow chart in Figure 19.

4.27 UBAIM model:

The University of Bern Atmospheric Ion Model is the first time dependent model of Ion chemistry applicable to the mesophere and lower thermosphere. The basic ion chemistry of UBAIM contains 311 reactions for 71 charged species. Ionization sources are X-rays, EUV radiation, resonant scattered Lyman α and β photons, and galactic cosmic rays. Densities of main and trace neutral atmospheric constituents are taken from a new version of the NCA model SOCRATES [244].

Theoretical model ionosphere circuitry shows the six basic theoretical model types and corresponding data -requirement [245].

It is noticable from the Table 4 that attempt to obtain ionospheric activities from theoretical model simulations is much more effective and realistic than attempt to obtain the same from purely empirical model simulation.

Table 4. Data requirement cum availability [245]

Nature of model	Parameters	Bits of information required	Approximate number of bits of information available
Empirical	D region (2)	10^7	600
	E region (2)	10^7	1×10^5
	F_1 region (2)	10^7	1×10^5
	F_2 region (2)	10^7	2.8×10^5
	F_2 above peak (2)	10^7	9×10^4
Theoretical	thermosphere	512	374
	mesosphere	200	100
	solar flux	256	192
	cross sections	1024	768
	Winds	256	192
	Electric fields	512	384
	Reaction Rates	400	300
	Particle fluxes	400	250
	Magnetic field	256	256

5. Missions and campaign related to airglow observation [Table 5]

Table 5. Missions and campaign related to airglow observatin

Misson Name / (Technique involved)	Description in short (purpose, place and result)	Year and persons involved
Rocket V-2 Differential Doppler	Ordinary air-pressure, density and temperature determination (from USA)	(1946 -1947) Reported by J.C Seddon [246]
Viking 10 Differential Doppler	Almost similar as that of V-2	(1959) , Reported by J.C Seddon *et al* [246]
Aerobee Hi Differential Doppler	Determination of electron density profile, sporadic E parameter absence of valley between E and F regions and also other atmospheric parameters	(1956 and 1959) , Jackson *et al* [246]
ARGO D - 4 Differential Doppler	Similar as that of Aerobee Hi (wallops island , Virginia)	(1961) , Jackson *et al* [246]
Satellite Transit 2A Differential Doppler	Dopper shift offset at the time of weak irregularities in electron density	(1960) , Mendonka [246]
Satellite Vanguard I Faraday Rotation	Equivalent thickness, Geomagnetic latitudes and longitude of subionospheric points (Jordell Bank)	(1960) Roger [247]
Satellite 1958 delta II Satellite Scintillation (polarization scintillation)	Scintillation index, heights of different active region (Kjeller)	(1960) Frihagen [248]
Satellites Sputnik3, Explorer 7, Discoverer- 32 and Transit 2A	Correlation possibilities between scintillation of signals coming either from satellite or from Radio stars with spread F and sporadic E parameters were explored	(1961, 1962) Liszka [249]
Satellite S-45 (Doppler shift detection, Faraday rotation, dispersive- Doppler, differential Doppler)	Electron density measurement, Correlation detection, Radio signal Scintillation (Durham, Weston)	(1958 on wards) Dieter [250]
Skylark rocket (Electronics aided spectrophotometry)	Photometric investigation of the oxygen lines at 5577 Å and 6300 Å The sodium D-line and the continuum at 5300 Å in the night airglow (Woomera, S Australia)	(1965 - 1967) Greer and Best [28]
U S N S. Eltanin (Ship board spectro- photometry)	Zenith observation of latitudinal and seasonal variations of OI 5577 Å , OH bands near 5893 Å (NewYork)	(1962) Davis and Smith [190]
Satellite OGO4 (OPEP spectrophotometry, UV -photometry,	Equatorial OI 6300 Å and OI 1356 Å airglow in relation with Ionospheric Geomagnetic Anomaly	(1967) , Chandra *et al* [170]
ISIS - II Satellite (photometry Ionosonde)	Equatorial OI 6300 Å red arcs over African and Asian Zones, during geomagnetic quiet and disturbed conditions, ESF bubble.	(1972 -1976) Bhatnagar *et al* [251]
ETS- II GSS (Polarimetry ionosonde, VLF-phase locked receiving system)	Influence of the great solar flare of 24 April 1984 on the ionospheric TEC and consequences (X in- Xians, Chong quing)	(1984 - 1986) Jian Min *et al* [252]
Atmosphere Explorer D- satalite	NOγ (1,0) band RS distribution and its inversion to generate meridional distribution of NO concentration	(1986) Gerard *et al* [253]
Chatanika Radar Program (Incoherent Scatter radar technique)	Integrated Hall and Pedersen conductivities, currents , Joule heating, effective D and E region recombination coefficients and information about total energy *etc*.	(1971) , Wickwar [254]
ESRO-4 Satellite (ion- spectrometry, auroral particle spectrometry)	Helium bulge, Argon bulge, ratio n(O)/ n (N_2) and its relation with plasma density, spatial structure of storm effects. Heating of neutral atmosphere during geomagnetic disturbances (ESOC)	(1972- 1974) , vonZahn [255]
UARS (HRDI)	High Resolution Doppler Imaging of O_2 atmospheric band nightglow and related features	(1994), Burrage *et al* [272]
OGO 6 (Spectrophotometry)	5577 Å airglow photometric data set and associated features.	1969, T M Donahue [256]
Black Brant VA (IR spectrometry) (I + II)	Long wave IR spectral measurement in Aurora Altitude profiles of 9.6μm (O_3) and 15 μm (CO_2) emissions , measurements of SWIR emissions from auroral arc.	1973 Stair(Jr.) *et al* [257]
Paiute-Tomahawk (IR Spectrometry)	Aurorally enhanced 4.3μm (CO_2), and 5.3 μm (NO) emissions.	1973 Stair(Jr.) *et al* [257

Table 5. (*contd.*)

Black BrantVA (III & IV) (IR spectrometry)	Background for auroral case, Auroral IR emission profile.	1974
Nike-Javelin	Background for auroral cases	1974
SPIRIT 1 Expt. (Spectral IR Interferometry)	Spectra of O_3 emission (Limb radiance profile)	1990, Adler Golden *et al* [258]
S3-4 Satellite (Spectro photometry)	NO, δ, γ band emissions, O_2 emissions, Herzberg I, II and III, N_2 LBH emissions.	1992, Eastes *et al* [259]
S-310-20 (rocket liquid N_2 cooled Ge sensor radiometry)	Altitude distribution of O_2 1.27 μm nightglow observation	1992, Yamamoto *et al* [260]
ATLAS - 1 Space Shuttle (Atmospheric Emission, Photometric Imaging device)	Imaging Earth's night airglow emission in the O_2, Atmospheric [O,O] bands at 702 0 nm which eventually absorbs all the Earth-reflected emissions Gravity waves' signatures are also detected	(1994) Mende *et al.* [262-265]
STS-39 Satellite (UV limb imaging expt., FUV Spectrometer)	H, O, N, and N_2 dayglow emissions' observations	(1991-1994) Budzien *et al* [266]
AIDA ACT '89 Campaign (MORTI)	The fluctuations in atmospheric $O_2(b\ ^1\Sigma_g^+)$ nightglow emissions induced respectively by gravity waves, evanescent waves and acoustic waves, are analysed	(1993) Hickey *et al* [267]
Black Brant XII Sounding Rocket (BEARS)	EUV emissions of atomic oxygen , molecular nitrogen dayglow features etc (Wallop Island, Virginia)	(1988 - 1993) Cotton *et al* [268]
NASA CRRES Satellite (Chemical Release Programme)	Emissions from spherically expanding neutral gas shells, released near perigee and below solar terminator were observed.	(1990-1994) Wescott *et al* [269]
NASA DC-8 Airborne lab (All sky video imaging)	Observations of upper atmospheric optical flashes and consequences (American Midwest).	(1993) Sentman *et al* [270]
SPIRE (IR spectrometry)	Comparison between non- LTE radiative transfer calculation and 4 3 μm Earth limb radiance data	(1994), Nebel *et al* [271]
Challenger Space lab2 (IRT)	IR consequences of excitation of low lying vibrational levels of H_2O by O (^3P) and implications	(1994),Maycrott *et al* [273]
ACTIVNY- Satellite (low light level imagers & Spectrograph)	Optical diagnostics in the visible and NIR detection of emission from satellite releases were examined	(1992) Wescott *et al* [274]
CIRRIS 1A Space shuttle Experiment (IR Spectrometry)	Absolute NO(v = *1, 2, 3*) column density derived from high resolution Earth limb IR spectra Production mechanism of subthermal NO spin orbit distribution tested	(1994) Lipson *et al* [261]
SONDA III rocket borne , MULTIFOT 92 payload (Airglow photometry)	Height profiles of airglow emissions O_2 Herzberg-band system, OI 557 7 nm NaD 589 3nm, OI 630 0 nm OH (8,3) band R branch at 724.0 nm , O_2 Atmospheric (O,O) band at 762 nm, sky background at 578 nm and 710nm , Sodium Lidar measured atomic sodium	(1992-1995) Takahashi *et al* [29-30]
Akebono satellite VLF instruments	Global electron density in the plasmasphere determined and found to be L value dependent. Determination of relative concentrations of H^+, He^+ and O^+ the reference altitude etc	(1775- 1997) Kimura *et al* [172]
San Marco 5 satellite Ion density & electric field measuring instrumentation)	Correlation of airglow bubbles with ion density depletion, and of additional airglow bubbles with enhanced AC electric field fluctuations	(1988 - 1997) Jahn *et al* [275]
FRONT Campaign (Radio and optical All Sky Imaging devices)	Travelling Ionospheric Disturbances (TID) in the OI 630 nm nightglow images over Japan and its structure's location in the mid-latitude lower F-layer were detected by the use of multipoint imaging network system	(1998-2000) Kubota *et al* [276]
ARGOS (HIRAAS)	Electron density determination by inversion of UV limb scans for a comparison with ionosonde data. A fair agreement was noticed.	(1999-2001) Dymond *et al* [38]
METEORS Sounding Rocket project (Airglow photometry)	Simultaneous measurements of $O_2(^1\Delta)$ and $O_2(^1\Sigma)$ airglow volume emission rate to derive ozone density profile in the daytime mesosphere.	(2001) Mlynczak *et al* [277]

6. Newly discovered airglow lines' features, newly proposed excitation mechanism and newly determined constants and coefficients.

Some of the relatively recently discovered airglow lines' features, newly proposed excitation mechanisms and newly determined constants and coefficients are described below :

6.1 O (^1D) rate constants and their temperature dependence:

Streit *et al* [104] gave absolute rate constants and their temperature-dependence for the deactivation of O(^1D) by five atmospheric gases O_2, N_2, CO_2, O_3 and H_2O. Photolysis of O_3 at 266 nm [104] produces O (^1D), which in the transition O(^1D) $\rightarrow$ O(^3p) gives 630 nm radiation. Gases O_2, N_2 and CO_2 ,the quenchers of O(^1D) are found to have a small negative temperature-dependence. Arrhenius expressions for the reactions measured and given by Streit *et al* [104] are O_2 (T= 104 – 354K) 0.29 exp (134/RT), N_2 (T = 104 –354k) 0.20 exp(214/RT), CO_2(T = 139 -200 K) 1.2 and (T= 200–354K) 0.68 exp(233/RT). The rate constants for O_3 and H_2O are 2.4×10^{-10} and 2.3×10^{-10} cm^3/ molecule, and over the ranges of 103-393K and 253 - 353 K , respectively.

6.2 New values of rate constants and branching ratio for N_2^+ + O reaction :

The branching ratio and the rate constant for the reaction N_2^+ + O were remeasured by Knutsen *et al* [278]. The resulting rate constant was found to be equal to $1.8(\pm 0.7) \times 10^{-10}$ cm^3 s^{-1} and branching ratio of $NO^+ : O^+ = 90(\pm 3) : 10(\pm 3)$ were found to be in good agreement with earlier measurements.

6.3 New value of Einstein's coefficient for spontaneous emission of the O_2 ($a\,^1\Delta_g$) state :

For the transition O_2($X\,^3\Sigma_g$ - $a\,^1\Delta_g$) at 1.2 μm, Einstein coefficient *A* for spontaneous emission of radiation has been found by Mlynczak *et al* [279] to be equal to 1.47×10^{-4} s^{-1}. The conventionally used value has been 2.58×10^{-4} s^{-1}. The new value of *A* coefficient implies that ozone concentrations, inferred from O_2 ($a\,^1\Delta_g$) emission, must increase significantly in existing data bases [279].

6.4 Revised cross-sections of O^+ 834 Å dayglow:

Assessment of O(^{3}P) photoionization, N_2 photoabsorption crosssections, O^+ oscillator strength and transition probabilities on OII 834 Å airglow emissions were made by Link *et al* [280]. The 834 Å intensities computed using the new parameters as mentioned above, agrees fairly well with rocket data. In contradicton to data that were used earlier, there new data indicate that besides being unique, N_mF_2 and h_mF_2 can vary by factors 2 and 50 km, respectively.

6.5 Carroll- Yoshino band problem :

Terrestrial airglow emissions near 958 Å and 980 Å corresponding to N_2 Carroll- Yoshino $c'_4\,^1\Sigma_u^+ - x\,^1\Sigma_g^+$ (O, O), I(OP) and (O, 1) Rydberg bands are found to be weaker than these inferred from c'_4 (O) excitation rate . For resolving this problem, Stevens *et al* [281] developed and discussed their resonant fluorescent scattering model for CY(*0,0*) and (*0,1*)

6.6 New finding about OI 844.6 nm emission mechanism .

Experimentally obtained twilight decay curves for thermospheric OI 844.6 nm emission was also represented by the field line interhemispheric plasma model. This model assumes only photoelectron-impact-excitation to be the only [282] production mechanism with a crosssection appropriate to an optically thin atmosphere. The model calculations were found to agree with the experimentally obtained results.

6.7 New quenching value of O(^1D) :

New value of rate coefficient for quenching of O(^1D) by O(^3P) was found out [283] as a function of temperature. which does not agree with the usually considered value.

6.8 Self absorption theory :

A self-absorption model using Holstein transmission function was developed [284] and applied successfully to UV fluorescent NO (*1,0*) γ - band emission.

6.9 New inference about Na nightglow excitation :

The potential energy surfaces of NaO+O reactionlead to excited Na* (*2P*) atoms which involve doublet rather than quartet spin configurations and have the branching ratio *f*~ 2/3 for the excited state of NaO [285].

6.10 On the analysis of geophysical data for an unknown constant :

Uncritical use of least square method of analysis of geophysical data is inappropriate and must be supplemented [286] with an error analysis. This fact has been exemplified with O^+ - O collision cross-section.

6.11 Inference about quenching rates for O_2 Herzberg I bands.

In agreement with the laboratory measurements, the values of quenching rates for O_2 Herzberg I band , O_2 Atmospheric band (O, O) and the green line have been newly found and is greater than 1×10^{-11}, the value usually considered [187].

6.12 Measurerment of rate constant for quenching CO_2 by atomic oxygen at low temperature :

Laboratory measurement of the rate constant for quenching CO_2 (*OI* ^1O) state during collisions of CO_2 molecules with O

atoms at temperatue range of 206-358 K has been made. The use of these new values of rate constant significantly decreased the rate of cooling by CO_2 15 ìm emission in the terrestrial lower thermosphere as compared to the previously obtained rate [287].

7. Effect of different physical factors on airglow emissions

Classification of factors that affect airglow emissions :

The factors that the terrestrial airglow emissions depend on, may be broadly classified into four types :

(i) Purely of solar origin

(ii) Lunar effects

(iii) Effects of other cosmic bodies

(iv) Terrestrial atmospheric features.

7.1 Purely solar effect :

Solar activities are the main sources of terrestrial ionosospheric features and have already been discussed in Sections 2.2 and 2.3. Study of correlations of terrestrial airglow and associated phenomen a with specific solar parameters started relatively later and has gathered momentum in recent past. Sahai *et al* [288] have shown that OI 630.0 nm low-latitude nightglow intensity is very strongly correlated with 10.7 cm solar flux and sunspot number. The correlations are generally found to be almost seven times in high solar activity period than in low solar activity period . Midya *et al* [289] have shown that Na 5893 Å nightglow intensity showed an oscillatory variation with solar flare number, relative sunspot number and variable component of 10.7 cm solar flux both in peak phase of 20th solar cycle at Mt. Abu and in non-peak phase of 21st solar cycle at Kolkata. They interpreted this variation in terms of similar variation of ozone as ozone's concentration is a major factor on which atmospheric sodium concentration and associated emission intensity depend. Terez and Terez [290] have established that the variation of global total ozone content is mostly the result of 10.7 cm. solar flux variation [291]. Labitzke and Loon [291] have established that the statistical correlation between ozone concentration and 10.7 cm. solar flux is highest between 5° and 30° latitude and the geopotential heights in ozone layer has a good correlation with 11 year sunspot cycle. Clemensha *et al* [292] analysed the atmospheric sodium measurements and concluded that the centroid height of the sodium layer shows its covariation with 10 year (?) solar cycle related oscillations. A good correlation of (OH) (8,3) band rotational temperature with 10.7 cm. solar flux has been obtained by Sahai *et al* [293]. Midya *et al* [210] obtained an oscillatory mode of variation in 5893 Å nightglow intensity as plotted against solar flare index given by Sawyer. Silbergeit [294] found a correlation between the geomagnetic storm and solar cycle length. Kolomittsev *et al* [295] studies theoretically the dependence of F-region electron density profile on solar activity expressed in terms of 10.7 cm. solar flux. Adler *et al* [296] established the fact that along with 10.7 cm solar flux and sunspot number, solar cycle length (SCL) is also a good indicator of long term changes in solar EUV radiations that affect strongly the terrestrial ionosphere, particularly the IEC. Midya and Midya [196] studied the correlation of monthly mean values of $h'F$ and f_oF_2 with each of three solar parameters, solar flare number, sunspot number and 10.7 cm solar flux. They studies the dependence of 5577 Å airglow intensity on solar parameters and found some useful regression equations. Smith and King [297] described in detail the long term relationships of sunspots and solar faculae with different ionospheric parameters. Correlation between O_3 concentration and solar flare index (Sawyer) has been found to be poor. Midya *et al* [298] found oscillatory modes of variations of 5577 Å line airglow intensity with each of sunspot number and 10.7 cm. solar flux both in peak phase (of 20th solar cycle at Mt. Abu) and in non-peak phase (of 21st solar cycle at Kolkata). Mikhailov *et al* [299] studied the dependence of post-midnight winter N_mF_2 enhancements on solar activity. Borovsky *et al* [300] explored the correlation between the amplitude of the MHD turbulence in the upstream solar wind and the amplitude of the Earth's geomagnetic activity indices. From fluid flow experiment, the terbulence effect is interpreted as an enhanced viscous coupling of the solar wind flow to the Earth's magnetosphere caused by an eddy viscosity that is controlled by the amplitude of MHD turbulence.

7.2 Purely lunar effects :

Lunar effects on Terrestrial airglow phenomena may broadly be classified into three types ; (a) Effect of background moon light, (b) L-variation and tidal effect (c) Effect of terrestrial magnetotail and reversal of electric field and related $E \times B$ drift. OI 6300 Å nightglow emission has been found to be affected by Moon's age less than 7 days or more than 23 days for $D > 50°$ [301]. Approximately, 7% of the incident light gets reflected from lunar surface; an appreciable amount of lunar thermal emission comes out of it [302-303]. Lunar radiations undergo short-period fading due to scintillation proportional to lunar libration and also long-period fading which is presumed to be caused by ionospheric irregularities associated with absorption, Doppler effect and Faraday effect within the atmosphere [304]. Lunar tidal variation of magnetic field (L-Variation) is high at the Newmoon phase at equinox and summer solstice. The electric current responsible for L-variation on the sunlit side of the Earth have intensity usually one tenth of that for S_q. [22,24] . Inspite of being weaker relative to the solar tidal effect, the lunar tidal effect is more readily determined and has been observed in D, E, F_1 and F_2 regions of the ionosphere [20]. Lunar tides leave signature in the mesopause region of upper atmosphere which is revealed by the characteristics of the variation of atmospheric emission with Moon's age [234] . The Earth on its night-side, has a

magnetic field extended beyond the lunar orbit and may therefore, interact with the lunar magnetic field [305] . The strong local-time-dependence of O(^{1}S) airglow emission at the geographic equator is presumed to be the result of tidal effect [189] . In the local solar time domain, the volume emission rate of oxygen and hydroxyl band airglow and their peak-height at the equator, undergo large tidal perturbation [44]. Fesen [234] has shown through TIEGCM simulation that F_2 peak electron density depends partially on the vertically propagating tide [234].

7.3 Effects of other cosmic bodies :

Meteoritic effects :

Analysis of IR airglow data obtained from on board USA FISTA aircraft indicates a small yet significant enhancement in OH airglow emission during the peak of the storm related to Leonid 1999 meteror shower [306] although no such influence on Na D airglow emissions was observed during the same meteor storm [307].

7.4 Terrestrial atmospheric features which the terrestrial airglow emissions depends on are mainly the following :

Gravity wave effects :

Mercier [308] reports some statistical results of observation on gravity waves within the ionosphere. This observation was made with the help of ground based radio inter- ferometers. Tarassick and Hines [309] explored the influence of gravity waves on airglow emissions elucidating the observable effects of such waves. Methods of distinguishing between evanescent waves and internal gravity wave modes and of determination of vertical wavelength were proposed by Tarassic *et al* Isler *et al* [310] obtained a closed-form solution for the integrated airglow response to linear gravity wave where all the higher order nonlinear response terms are retained. Wave-induced airglow fluctuations were shown to be much greater than the corresponding density fluctuations for major atomic species. Sobral *et al* [33] reported winter-time photometric perturbation of the nocturnal *F*-region atomic oxygen 630 nm red line intensity on southern hemisphere which they observed to be concurrent with apparent ionogram signatures of *F*-region gravity waves . Gravity waves act as a source of perturbation for initiating plasma bubble events during the month when the ambient ionospheric conditions provide favourable chances for growth of instability. Hines [311] proved a fundamental theorem of airglow fluctuations that are induced by gravity waves and also showed that gravity wave-induced airglow fluctuations do not depend on the minor species involved in the photochemistry of the corresponding emission process. Wang *et al* [312] generalized Hines-Tarassick's theory of gravity waves induced airglow fluctuations and compare their results of analysis with observed variations. Five years of photometric data of the 630 nm oxygen airglow emissions over Davis, Antarctica, have been searched by Innis *et al* [313] for obtaining evidence of periodic oscillations due to atmospheric gravity waves. Hetch *et al* [314] analysed the instability features in airglow caused by atmospheric gravity waves and found that if same is characterized by the aligment in a direction perpendicular to the atmospheric gravity wave (AGW) wavefronts. Observation made with the help of multicomponent instrument confirms the fact that such features are caused by convective instability.

Yao [315] established a two dimensional time-dependent nonlinear photochemical dynamical coupling gravitational waves model and he solved it using FICE method. Results of simulation from this model show that the gravity wave propagation can induce large change of the mean profiles of oxygen compound and hydrogen compound in the mesopause region.

Geomagnetic effects:

Numerical simulation of Monte Carlo (MC) solution of nonlinear Boltzman equation for chemically produced hot oxygen atoms is found to give number density and temperature of nonthermal oxygen atoms at equatorial latitudes which fairly agree with the observed results under the condition of low solar and geomagnetic activities [316,251]. The thermospheric temperatures obtained from Doppler broadening of OI 630 nm emissions and the mesospheric rotational temperatures obtained from OH (9,4) and $O_2A(0,1)$ band emissions during the recovery phase of geomagnetic storms were found to be lower than the corresponding values in the quiet geomagnetic conditions respectively [317] . Field and Rishbeth [318] express the disturbed to quiet ratio of N_mF_2 in terms of mean (DC) and local time (AC) variations for over 20 years' data from each of 53 stations between 70° N and 80° S and they found some important implications including a long term effect. They interpreted their results in terms of change of composition of F_2-layer due to storms . Saha [319] describes enhancement in the equatorial peak atomic oxygen density in the lower thermosphere and also the rise in OH (7-2) nightglow intensity following a geomagnetic substorm although no such enhancement of OI 6300 Å could be observed as compared to OI 5577 Å intensity rise. He interpreted the observational results on the basis of the concept that extra-ionospheric current increases the recombination rate. Regular all sky imaging observations of the F-region nightglow emission and mesospheric band emission during geomagnetic storm of February 12,2000 show that both OI 6300 Å airglow emissions and band emissions are enhanced along with several small scale intensity depletional structures which, as Sahai *et al* [320] suggest , might be caused by nonlinear interactions between TID and enhanced ionospheric anomaly.

Effects of lightning:

Boeck *et al* [321] described a transient luminosity observed at the height of airglow layer (~95 km) in coincidence with a lightning flash that took place directly beneath the layer in a tropical oceanic thunderstorm. Providing a new evidence of coupling between lightning and ionospheric events , this luminous event in the ionosphere was the only kind of its own observed during an examination of several thousand images of lightning records under suitable viewing conditions with space shuttle cameras.

Effect of earthquake :

Seismic activity produces F_2 region heating and thereby leaving signature of earthquake phenomena in the 5577 Å , 6300 Å and OH airglow emissions [322-324]. Seismogravity oscillations are enhanced before and at the time of earthquake and those oscillations affect the atmosphere immediately before earthquake. Internal gravity waves are generated and their group velocities have vertical components that may hit the ionosphere. A strong seismic radio emission may induce disturbance in the F-region aeronomical structures.

Non-LTE contribution :

Excess of atomic oxygen UV dayglow emissions which could not be obtained from standard thermosphere model calculations at exospheric altitudes, have been explained in terms of break down of the relative transfer model due to nonlocal thermal equilibrium above the exobase and a hot atomic oxygen geocorona [325] .

Thermosphere-ionosphere coupling :

Measurements of line shape of OI 630 nm and 557.7 nm emissions were used to obtain velocities of neutral atomic species and ion velocities in the *E* and *F* regions. Frictional heating obtained therefrom was interpreted as a result of dynamical coupling between ionosphere and thermosphere [322].

. Newly indentified airglow related features

8.1 Light Pollution :

'Light pollution', relatively newer discovery an interesting feature with nightsky brightness, is a term given to the phenomenon of emissions from the sky in excess of natural nightglow. This phenomenon has been observed in several metropoliton cities and in their surroundings throughout the world, where artificial light, scattered and reflected by the lower region of the atmosphere exceeds a certain limit so as to share a significant portion of nightsky-emissions observed there. Light pollution, from the viewpoint of its origin, depends quantitatively on two probable factors :

(a) Number and intensity of artificially produced light and

(b) Light reflecting air-pollutants.

Cinzano [327] studied the growth of light pollution in northern Italy for a period between 1960 and 1995 (35 years) and concluded that the mean annual increase in nightglow brightness was found to be 10% per year. Yet, as the airglow phenomena depend on the solar activity and as the light pollution is measured along with the airglow intensity, the actual increase in light pollution remains unresolvable during the solar minimum or solar maximum. Xiao-Jun *et al* [328] too studied the light pollution at Xinglong station and have inferred that the light pollution is not yet significant there.

8.2 Sprites :

Sprites' images were recorded by Nielsen *et al* [329] at 1 ms resolution and these images revealed several new sprite properties. Sprites appear to occur in a highly structured mesosphere and Nielsen *et al* suggested that the origin of some of those sprite structures are the sprites' activity themselves Sprites can be large with horizontal widths of more than 40 km, and they can extend from the clouds upto the lower ionosphere affecting a large volume of the atmosphere. Bell *et al* [330] mentioned that large quasi-electrostatic (QE) fields above thunderclouds produce an upward travelling beam of 1 Mev runaway electrons which may contribute to the production of optical emissions above thunderclouds called red sprites.

8.3. Radiation belt-particle contamination :

During the daytime flight of rocket skylark 12 upto an apogee of 830 km. over Natal (Brazil) specific non-electromagnetic contaminations of the concentrates in the detectors of EUV absorption cell spectrometers carried on board rocket skylark 12 were registered in addition to He I / HeII and O II emissions. Those were shown [331] to be caused by the particle-induced events associated probably with one or both of middle-energetic electrons and protons.

8.4 Disturbance of airglow measurements:

Spots in the Earth's upper atmosphere have been detected from which [332] airglow emissions are found to come with decreased intensity. It is shown that for observations from above a deposition rate of 1 kg/ sec. of gas approximately along the flux-direction, is sufficient to produce a substantial decrease of intensity in a spot ~ 50 km in diameter and those gas mass may be discharged from a space vehicle or the evaporated substance of a mini-comet. Three chemical groups of primary 'silicate' spheres, each less than 30ìm in diameter, of cometary origin were collected in the lower stratosphere [333].

8.5 Artificial satellite - space-vehicle -glow and laboratory modelling :

A glow around exposed surfaces of the space-shuttle facing the direction of orbital motion was first observed in 1983. The extension of this shuttle-glow was approximately 10 cm from the surface of the shuttle and was found to be maximum at the wavelength of 6800 Å. This, with a resolution of about 350 Å, formed a continuum. The most probable cause of such glow was found to be recombination [334] of fast oxygen atoms in the upper atmosphere with NO absorbed on the shuttle's surface. This forms excited NO_2 which radiates light as it desorbs. On the shuttle mission STS-39, four gases NO, CO_2, Xe and Ne were released for a plasma experiment. Unintentionally, so much gas was scattered on the surface of the shuttle-tail that when NO was released, a much more intense glow was observed. Under normal conditions the absorbed NO that causes the glow probably comes either from the surrounding or from the reactions that took place in the exhaust gas.

The N_2 LBH band is the only N_2 band system which has been identified in space-craft glow and is thought to be produced by recombination of N(*4s*) atoms on the spacecraft surface [335] . The absence of other bands is attributed to the higher kinetic energy in case of the spacecraft. Surface-mediated O + NO recombination, a key reaction in spacecraft-glow was investigated in the laboratory and the results obtained therefrom was used to provide a re-evaluation of Atmosphere Explorer glow [336]. A fast oxygen atom source was used to investigate the glow phenomena in the laboratory [337]. The hypothesized mechanism of recombination of O with surface-bound NO was verified positively. Spacecraft glow has also been observed in far ultraviolet region [338].

8.6 Space-shuttle-induced optical contamination :

The data obtained from CIRRIS 1A interferometric and radiometric experiments during the flight of STS-39 implies that water outgassed from the shuttle is highly excited by collisions with atmospheric O classifying it as a type of shuttle-induced glow [339]. Similar reporting about the optical contamination of natural airglow with shuttle-induced cloud glow has been made by other workers too [340] . An infrared contaminant model (IR model) had been developed by Zhou *et al* [341] for studying shuttle-induced excitation of and emission from water molecules outgassed from space shuttle. This model has been utilised in explaining various shuttle-induced glow-contamination features obtained from a large number of other missions. Kurskov *et al* [342] have shown that the calculations of efficiency of various mechanisms for the luminescence of the gaseous components of the intrinsic atmosphere of a spacecraft in IR band agree fairly well with the experimental result.

8.7 Travelling ionospheric disturbances :

Propagation of a medium scale travelling ionospheri disturbance in the OI 6300 nm nightglow imaging was observe in a campaign experiment with five all sky imagers that wer used for F-region radio and optical measurement. Th disturbance was observed to travel 2500 km a night in the ne moon period [276]

8.8 SNE or South to North propagating events :

Sobral *et al* [33] reports that there exists a feature of majo importance in case of airglow perturbations and that is travelling of airglow valleys or minima from South towards North The suggest that this South to North propagations of airglow minim are caused partially by the gravity wave modulation of airglo intensity. It is also mentioned that [321] travelling atmospheri disturbances may contribute to an early onset of the low-latitud perturbation. Thus, the delay between the disturbance peal and the associated effect on the atmosphere in an equatoria station, may cause the absence of OI 6300 Å peak as observe usually is.

8.9. Vertical propagation of atmospheric waves o disturbances:

Observations regarding the wavelength of atmospheri oscillation using Doppler shifts of OI 557 nm and OH (6 - 2 WINDII experiment indicate changes in atmospheric structur at the peak height of those emissions. This favours the presenc of long vertical wave mode near austral autumn equinox [34 Simultaneous measurements of large vertical winds in the uppe and lower thermosphere using a scanning F-P spectrometer wer made by Price *et al* [344] which showed the existence of a upwelling region with large horizontal scale.

8.10 SSL or sudden sodium layers :

Inspite of having sufficient knowledge of excitations and rate coefficients for loss processes of sodium for about a decad circumstances responsible for the sporadic occurrence of narrow intense layers of Na are not well understood. Driven by dynamical processes, ion-ion recombination between coincident layers of Na^+ and O^+ ions formed by e + O_2 reaction or a mixing between atomic oxygen layer and the layer of sodium makes the formation of SSL or (sudden sodium layers) possible [345] .

8.11 Features of ionospheric plasma depletion or IPD :

In an experiment with the help of all sky optical imaging system operated from Sriharikota rocket range, ionospheric plasma depletion was determined by means 630 nm and 777nm nightglow emission observations. Estimation of a number of plasma depletion parameters, such as degree of depletion, east -west extent, tilt with respect to the geomagnetic field interdepletion distance, drift velocity and plasma enhancements or brightness patterns were also made [346].

9. Application of airglow phenomena

9.1 Atomic oxygen profiles at midlatitude and equator derived from airglow observation :

Transition of lower thermospheric atomic oxygen in the Spring, has been searched with the help of long-term mid latitude airglow data and its statistical regression analysis . It has been inferred therefrom that rapid intensity changes do occur in other seasons too [347] . The volume emission rate was obtained from rocket observations of OI 5577 Å night airglow in the lower thermosphere at equatorial stations [348] and its large variability caused by the dynamical control of the atmomic oxygen was detected. Atomic oxygen density profiles were deduced from airglow data and were compared with available experimental data.

9.2 Recovering ionization frequency and oxygen atom density with the help of airglow data :

Using a synthetic data set and an inversion algorithm on a simple photochemical model involving O^+ ($^2D - ^2P$) transition, the possibility of obtaining informations about the thermospheric atomic oxygen density had been explored [344]. The unattenuated $O^+(^2P)$ ionization frequency was also obtained by inverting twilight observation of O^+ ($^2D - ^2P$) 732 nm airglow emission data [349].

9.3 Analysis of vibrational states of oxygen Herzberg I system using nightglow :

UV nightglow between 2670 And 3040 Å was observed from Whitesand missile range and was speculated from a synthetic spectra-data set of 41 spectral scans of the nightglow with the brightest feature given by O_2 ($A^3\Sigma_u^+ - X^3\Sigma_g^-$) Herzberg I system . The distribution of vibrational states observed therefrom, indicates that the vibrational levels were depleted and magnitude of vibrational shift much less than was predicted theoretically [350].

9.4 Atomic oxygen concentration from airglow data :

The atomic oxygen profiles were obtained from emissions from atomic oxygen and were used to test the photochemical mechanisms usually considerd for explaining the different emissions in the scenario of atomic oxygen recombination. The derived concentration data were compared with the concentrations actually observed in the same campaign [351] .

9.5 UV airglow and the knowledge of upper atmospheric conditions :

The fact that the Earth's UV airglow contains fundamental diagnostic information about the state of upper atmosphere and ionosphere has been reviewed on the basis of UV phenomenology within Earth's atmosphere. Concepts of various excitation mechanisms of atomic and molecular energy states are developed and discussed from the first principle and applied to selected examples of day and night airglow alongwith, a detailed review of radiation transport theory. A comprehensive examination of the current status of knowledge of the individual emission features seen in the airglow, alongwith their relationship to atomic physical theories relevant to atmospheric observations have been discussed. The use of airglow features as remote sensing observables has also been examined so that diagnostically useful species can be selected for collecting information about the state of thermosphere and ionosphere [352].

9.6 Procedure for extraction of precise airglow data in presence of strong background radiation :

Realizing the importance of ground -based measurement of terrestrial airglow for many applications in the field of aeronomy, a procedure for extracting automatically even very weak airglow emissions in the presence of strong background radiation has been described [353].

9.7 Ozone data from airglow observation :

Simultaneous measurements of the O_2 ($^1\Delta$) and O_2 ($^1\Sigma$) airglow volume emission rates were made in the daytime mesospheres and were used to derive ozone concentration separately from each airglow . The derived ozone profiles were found to be in fair agreement with the measured values within the measurement uncertainties [277]. There are several other reports the use of airglow data about the different states of the mesosphere and the ionosphere [354,35,31].

9.8 Electron density determination:

The inversion of electron density from Total Electron Content(TEC) measurement of Global Positioning System (GPS) radio occultation was investigated by means of simulated data from IRI-2001 and observations by the GPS/MET satellite experiment [355].

10. Non-terrestrial solar planetary aeronomy : facts and speculations

10.1 Mercury :

Having rlatively smaller gravitational mass and relatively much higher incident radiation temperature, the planet mercury possesses virtually no atmosphere [356] . Mercury has an appreciable magnetic field and an escape velocity of 4.4 km s^{-1} . It may contain Na in its atmosphere possibly derived from impact vaporization [357].

10.2 Venus :

Typical daytime exospheric temperature (TDET) of Venus is 280 K [358]. In addition to the major neutral component CO_2, the upper atmosphere of Venus contains also H, He ,O, C, CO and

probably N_2, Cl and S [359]. Venusian ionosphere has a prominent peak near 140 km identified as F_1 layer which appears both on the day and night side. An E layer near 125 km and possibly an F_2 layer near 179 km are also found to appear. Daytime ionosphere is explained in terms of absorption of solar radiation by CO_2,O and He. Direct interaction of Venusian atmosphere results in the formation of a bowshock [359]. UV spectra of Venusion nightglow is found to be dominated by the δ and γ band of NO which are speculated to be emitted in radiative collisions between N and O essentially by inverse predissociation, $N(^4S) + O(^3P) \rightarrow NO\ (a\ ^4\Pi\ ) \rightarrow NO(C^2\Pi,\ v'=0)$ [356]. Unstable neutral species such as CO and O are created in the venusian atmosphere by photodissociation of CO_2 [357]. Model-based calculations involving observational information regarding ionospheric constituents such as C^+, CO^+, N^+, N_2^+, NO^+ produce promising agreement with airglow observations on venus [356,359].

10.3 Mars :

Having TDET approximately equal to 150 k and CO_2 as the major neutral atmospheric constituent of its own, Mars interacts with the solar wind to produce a bowshock, the shock point of which varies in position. Possessing an O_2^+ ion- dominated ionosphere, Mars has got an equivalent F_1 layer right at the vertical height of about 140 km. The source of HO_x which catalyses to produce CO_2 recombination on Mars is H_2O and H_2. Observations of UV dayglow spectra made in the Mariner Missions, reveal that intense features on Mars are Cameron band of CO $\left(A\ ^3\Pi \rightarrow X\ ^1\Sigma^+\right)$, the fourth positive bands of CO $\left(A\ ^1\Pi \rightarrow X\ ^1\Sigma^+\right)$, CO_2^+ band system $\left(A\ ^2\Pi_u \rightarrow X\ ^2\Pi_g\right)$ and $\left(B\ ^2\Pi_u^+ - X\ ^2\Pi_g\right)$, OI ($^1S, ^3S, ^5S \rightarrow ^3P$) and the resonance lines of Cl at 156.1 and 105.7 nm [356-358].

10.4 Jupiter :

It has a probable value of TDET equal to 130 K if solar radiation is considered to be the only source of heat. But direct measurements by Voyger UVS stellar occultation measuring devices indicate that 1100K < TDET < 1600 K. Solar UV radiation is not the only source of heat for Jovian thermosphere. Some other possible sources of heat are upwardly propagating gravity waves, electrons' and ions' precipitations, frictional Joule heating due to electric fields generated in the magnetosphere by departure of the magnetospheric plasma from corotation [357]. The neutral components of Jovian atmosphere are H_2, He, CH_4,NH_3, CH_3D, C_2H_6, C_2H_2, PH_3, H_2O [360]. Jupiter has a strong magnetic field. C_2H_6, C_2H_2 and H_2 produced in different photochemical processes are transported downward and are eventually converted to CH_4 at high temperature that prevails below the visible cloud deck. The most abundant and important ion on Jupiter is H^+. The various important reactions that take place in the Jovian atmosphere or ionosphere (more specifically) may be classified into three categories : ion production by photolysis or electron impact, ion exchange reaction, ion removal or electron-ion recombination. Airglow radiation from Jovian atmosphere is yet to be detected prominently. 'He' has been detected in Jovian atmosphere from dayglow observations of resonace line at 584 Å.

10.5 Jupiter's satellite IO :

Being innermost of all satellites of Jupiter, IO is most exposed to Jovian radiation belt and magnetospheric interaction as a consequence of which Io modulates the Jovian decametric radio bursts [356,361]. Intense sodium D line emission has been observed to come from Io and its surrounding cloud. The Na is most likely sputtered from the satellite surfaces by intermittent bombardement of low energy protons. [361]. Pioneer 10 measured an electron density of almost 10^5 cm^{-3} on IO [358]. The ionosphere of Io contains probably Na^+ and SO_2^+ and electrons which are formed by photoionization of neutral species such as Na and SO_2 [358,362]. He 10830 Å line emission has also been observed to come from Io [362].

10.6 Saturn :

H_2 is the most abundant neutral species in Saturnian atmosphere. He, CH_4 and NH_3 are minor constituents of Saturn's neutral atmosphere [363]. TDET of Saturn's atmosphere was found to be approximately 900 K. Solar EUV radiation and impact inoization by energetic particles are the sources of ionization on Saturn. Electron density in the Saturnian ionosphere is of the order of 10^4 cm^{-3}.

10.7 Saturn's satellite Titan :

Voyger confirmed that Titan has a dense N_2 atmosphere. CH_4/N_2 mixing ratio on Titan, as measured by Voyger is about .05 and many other hydrocarbons have been detected in the Titan's atmosphere. Ionization, either by photolysis or by electron impact produces UV spectrum of excited N_2. A major ion in Titan's atmosphere is H_2CN^+ [358]. Limb brightening with N^+ (1085 Å) and $N_2C_4^-$ band emission caused 970 Å features are also observed [358].

10.8 Comet :

One of the remarkable features of the cometary spectra is that they consist mainly of emission bands of molecular ions. Bands of H_2O^+, CO^+, CO_2^+, OH^+, N_2^+ and CH^+ have been detected in the cometary spectra. Of all these, CO^+ bands are the strongest in the tail. H_2O^+, CH^+ and OH^+ bands are concentrated in coma. Na D lines, OI 6300 Å and bands of CN have also been detected in the cometary spectra [357].

10.9 Moon :

Na and K in lunar atmosphere may be produced by impact vaporization of the regolith by meteoritic collision. The calculated rate and observation together indicate that Na and K are probably lost mainly by escape of the hot impact product. Atomic oxygen is produced mainly by solar wind sputtering and desorption induced by solar photons' absorption. OH band emission at 2085 Å with intensity as much as 50 R at the sub-solar limb is predicted. Local Interstellar Medium (LISM) Ly α - photodissociation may limit the lifetime of H_2O ice in the shadowed region of moon [364,365].

10.10 Meteors :

Strong hydrogen emissions along with NO_2 yellow continuum, thermal red continuum and 50 atomic lines between 3700 - 9000 Å have been detected in the spectra of Leonid meteor train. The atomic lines within the meteor trace decayed in seconds. Lines FeI, MgI, CaI, CaI, CrI, MnI, KI and ALI along with OI 5577 Å were present [366] . Resonance Lidar measurements of Na density and consistent Na airglow observations were also made in the Leonid meteor train 2 [367].

References

[1] L Yntema *Publ. Ast. Groningen* No **22** 1 (1909)

[2] C T Elvy *Astrophys J* **111** 432 (1950)

[3] S Newcomb *Astrophys J* **14** 297 (1901)

[4] G J Burns *Astrophys J.* **16** 166 (1902)

[5] S D Townley *Publ Ast Soc Pacif* **15** 13 (1903)

[6] C Fabry *Astrophys. J* **31** 394 (1910)

[7] P J vanRhijn *Astrophys J.* **50** 356 (1919)

[8] Lord Rayleigh (R J Strutt) *Proc. Roy. Soc (London)* **A29** 458 (1930)

[9] I S Bowen *Astrophys. J.* **67** 1 (1928)

[10] J W Chamberlain *Physics of the Aurora and Airglow* (New York Academic) (1961)

[11] R Chattopadhyay *Bull IAPT (India)* **11** 9 275 (1994)

[12] D Barbier, J Dufay and D Williams *Ann. Astrophys.* **14** 99 (1951)

[13] K Chuvayev *Doklady Akad Nauk* (S.S.S.R) **87** 551 (1952)

[14] V I Krassovky *Doklady Akad. Nauk.* (S.S.S.R) **78** 669 (1951)

[15] D R Bates *Applied Atomic Collision Physics* **Vol. I** · *Atmospheric Physics and Chemistry eds.* H S W Massey and D R Bates, (New York: Academic) (1982)

[16] D R Bates and M Nicolet *J. Geophy. Res.* **55** 301 (1950)

[17] D R Bates and M Nicolet *Compt. rend.* **230** 1943 (1950)

[18] A Vallance Jones and A W Harrison *J. Atmos. Terr. Phys.* **13** 45 (1958)

[19] *Solar Terrestrial Physics, Principles and Theoretical Foundations* (eds.) R L Carovillano and J M Forbes (Dordrecht : D Riedel) (1983)

[20] Geophysical Research Papers No. 43 *Methods and Results of Upper Atmosphere Research* (ed) J Kaplan, (Geophysics Research Directorate, Airforce, Cambridge Research Centre)

[21] *Night Sky Radiations from the Upper Atmosphere* (Compendium of Meterology), (ed.) T F Malone, (1951)

[22] S K Mitra *The Upper Atmosphere* (2nd edn.) (Calcutta The Asiatic Society) (1953)

[23] *The Spectra of the Night Sky and the Aurora* (The Atmosphere of the Earth and Planets) (ed.) G P Kuiper (Univ. Chicago Press) (1952)

[24] *Physics of the Upper Atmosphere* (ed) J A Ratcliffe (New York Academic) (1950)

[25] F E Roach and L L Smith *Absolute Photometry of the Light of the Night Sky, the zenith intensity of Halekala [latitude N* 20.7°] *and at Fritz Peak [latitude N* 39 9°], Technical Note, No 214, (US Department of commerce, National Bureau of Standands) (1964)

[26] a) S N Ghosh, S K Midya and S Purkait *Mahavisva* **3** 31 (1982); b) S N Ghosh and S K Midya *Mahavisva* **6** (1985)

[27] G J Hernandez and A L Carrigan (eds) *Airglow Calibrations Symposium* (Airforce Cambridge Research Laboratories, Upper Atmosphere Physics Laboratory, Project 7661, Special Reports, No 22 AFCEL 65- 114, Office of Aerospace Research, United States Air Force) (1994)

[28] D Marlow and J C Pemberton *Rev Sci. Instrum.* **20** 724 (1946)

[29] F E Roach and D Barbier *Publ. Astr Soc Pacif* **61** 80 (1949)

[30] R G H Greer and G T Best *Planet. Space. Sci.* **15** 1857 (1967)

[31] H Takahashi, Y Sahai, B R Clemensha, D M Simonich, N R Teixeira, R M Lobo and A Eras *Planet Space Sci.* **37** 640 (1989)

[32] H Takahashi, B R Clemensha, D M Simonich, Stella M L Melo, N R Teixeira, A Eras, J Stegman and G Witt *J Atmos Terr. Phys.* **58** 16 1943 (1996)

[33] Stella M L Melo, H Takahashi, B R Clemensha, P P Batista and D M Simonich *J. Atmos. Terr. Phys* **58** 16 1935 (1996)

[34] M Mendillo, J Baumgardner, M Colerico and D Nottingham *J. Atoms. Sol Terr. Phys.* **59** 13 1587 (1997)

[35] J H A Sobral, G L Borba, M A Abdu, I S Batista, H Sawant, C-J Zamlutti, H Takahashi and Y Nakamura *J. Atmos. Sol. Terr Phys* **59** 33 1611 (1997)

[36] C B Cosmovici and R Stalio *NuovoCim* **15C** 703 (1992)

[37] S Chakraborti, T P Sasseen, M Lampton and S Bowyer *Geophys. Res Lett.* **20** 335 (1993)

[38] D J W Kendall, E J Leewellyn M R C, S B Mende, G R Swenson and R L Gattinger *Can. J. Phys.* **69** 209 (1991)

[39] M Yanhua, R N Peterson, S P Zhang, I C McDade, R H Wiens and G G Shepherd *Ann. Geophys.* **13** 189 (1995)

[40] K F Dymond, S A Budzion, S E Thonnard, R P Mcloy and R J Thomas *Geophys Res Lett* **28** 927 (2001)

[41] J Bishop, J Harlander, S Nossal, F L Roesler *J. Atmos. Sol. Terr Phys.* **63** 341 (2001)

[42] J W Duff and D R Smith *J. Atmos. Sol. Terr. Phys.* **62** 1199 (2000)

[43] J L Innis F A Philips, G B Burns, P A Greet, W J R French and P L Dyson *Ann Geophys. (Germany)* **19** 359 (2001)

[44] W Gant *Proc. SPIE - Int. Soc. Opt. Engg. (USA)* **430** 266 (2001)

[45] K Lierpka, M J Kosch, H Holma, A J Kavangly and T Hogfors *Geophys. Res. Lett.* **30** 6 (2003)

[46] S P Zhans, R Roble and G G Shepherd *J. Geophys. Res.* **106** A10 21381 (2001)

[47] R Chattopadhyay, S K Midya and U K De *Indian J. Phys.* **74B** 133 (2000)

[48] V L Peterson, T E Vanzandt and R B Norton *J. Geophys. Res.* **71** 2255 (1966)

[49] V I Krassovsky, N N Shefov and V I Yarin *Planet. Space. Sci.* **9** 883 (1962)

[50] P D Feldman and P Z Takacs *J Geophys Res.* **81** 260 (1976)

[51] K Misawa *Ionos Space Res Jpn* **29** 199 (1975)

[52] J W Meriwether (Jr), D Torr, J C G Walker and A-O Nier, *J. Geophys Res.* **83** 3311 (1978)

[53] J F Noxon *Planet and Space Sci* **26** 199 (1978)

[54] K Misawa and I Takeuchi *J Geophys Res* **82** 2410 (1976)

[55] W G Fastie and T M Donahaue *Space Res.* **4** (Amsterdam North Holland) p304 (1964)

[56] W H Brune, P D Feldman, R C Anderson, W G Fastie and R C Henry *Geophys Res Lett.* **5** 383 (1978)

[57] A B Christenson *Planet Space Sci. (Irb)* **23** 4 831 (1975)

[58] P D Feldman, D E Anderson (Jr), R R Meir and E P Gention *J Geophys Res* **86** 3583 (1981)

[59] J Frederick and D W Rusch *Astron Astrophys* **61** 635 (1977)

[60] J W Meriwether and J C G Walker *J Geophy Res* **82** 1855 (1977)

[61] J E Frederick and P B Hays *Planet and Space Sci (GB)* **26** 339 (1978)

[62] D Beran and E Suckfull *J Geophys* **44** 155 (1977)

[63] K Misawa *Report of Ionosphere and Space Research in Japan* **28** 134 (1974)

[64] L M Fishkova *Geomagn Aeron. (USA)* **16** 530 (1976)

[65] A L Broadfoot and A E Johanson *J Geophys Res* **81** 1331 (1976)

[66] C A Tepley *J Geophys Res* **86** 7781 (1981)

[67] M Dufay *Ann Geophys* **14** 391 (1958)

[68] A Vallance Jones *Ann Geophys* **14** 179 (1958)

[69] R S Narcisi *Proceedings of the Tenth Meeting of Air Committee on Space Research* (London) (1967)

[70] J M Young, C S Waller, C Y Johnson and J C Holmes *J. Geophys Res.* **76** 3170 (1971)

[71] J C Gerald and A Monfils *J. Geophys Res* **83** 4389 (1978)

[72] K M Kazakov *C R Acad Bulg Sci.* **31** 1301 (1978)

[73] A Vallance Jones *Planet Space Sci.* **10** 117 (1963)

[74] P Z Takacks and P D Reldman *J Geophys Res* **82** 5011 (1977)

[75] T M Donahaue and J B Kumar *J Geophys Res* **76** 145 (1971)

[76] J Delannoy and G Weill *Compt Rend* **247** 806 (1958)

[77] K Henrikson, C G Sivjee and C S Deehr *J Geophys. Res.* **85** 5153 (1980)

[78] W Hanle and H Kleinpoppen (eds) *Progress in Atomic Spectroscopy* (NewYork · Plenum) (1978)

[79] G Herzberg *Molecular Spectra and Molecular, Structure* **Vol.I** *Spectra of Diatomic Molecules* (New Jersey : D Van Nostrand) (1950)

[80] J W Chamberlain *Theory of Planetary Atmospheres · An Introduction to their Physics and Chemistry* (New York . Academic) (1978)

[81] S N Ghosh and S K Midya *Indian J. Radio Space. Phys.* **16** 277 (1987)

[82] S K Midya and S N Ghosh *Earth, Moon and Planets* **66** 145 (1994)

[83] Y Sahai *J. Geophys. Res* **86** 3657 (1981)

[84] Y Sahai, J A Bittencourt, H Takahashi, N R Teixeira, B A Tinsley and R P Rohrbaugh *J Atmos Terr Phys.* **52** 749 (1990)

[85] V A Kiselev *Geomagn. Aeron.* **31** 294 (1991)

[86] V Ramachandra Rao *Ann. Geophys (France)* **30** 291 (1974)

[87] H Takahashi *Planet. Space Sci.* **27** (1979)

[88] P Kulkarni and V R Rao *Indian J. Radio Space Phys* 2 26 (1973)

[89] K Misawa and I Takenely *Inons Space Res. Jpn* **30** 109 (197(

[90] P C Rakshit *Physical Chemistry* (Kolkata Sarat Book Hous (1980)

[91] W W Hunt (Jr) Research Note 80 (*Reactions of Ions in the Upp Atmosphere*), (Photochemistry Lab Project 7635, Air For Cambridge Research laboratory. Office of Aerospace Resear United State Airforce)

[92] I I Sobbelman *Atomic Spectra and Raidative Transitions* (Ne York : Springer-verlag) (1979)

[93] R D Cowan *The Theory of Atomic Structure and Spectra* (University of California press) (1981)

[94] R P Wayne in *Comprehensive Chemical Kinetics* **Vol. 182** (ed.) C H Bamford and C F H Tipper, (Amsterdam Elsvier) (1969)

[95] J R Winick *Solar Terrestrial Physics* p677 (eds) R L Carovillano and J M Forbes (Dordrecht D Reidel) (1982)

[96] *Atmospheres of Earth and the Planets* (ed) B M McCormac (Dordrecht D Reidel) (1974)

[97] D R Bates and H S W Massey *Proc Roy Soc* **A192** (1947)

[98] H S W Massey and H B Gilboy *Electronic and Ionic Impact Phenomena* (2nd edn) **Vol. 14** chap 20 (Oxford University Press) (1974)

[99] D L Baulch, R G Cox, R F Hampson (Jr) J A Kerr, J Troe and R T Watson *Physics and Chemistry Reference Data I* 295 (1979

[100] *NASA 1981 Chemical Kinetic and Photochemical Data for Use in Stratospheric Modelling Evaluation* No 4 JPL 81 (1981)

[101] P J Crutzen *J Geophys Res* **76** 7311 (1971)

[102] S C Solomon, P B Hays and V J Abreu *J Geophys Res* **93** A9 9867 (1988)

[103] D D Cleary *J Geophys Res* **91** A10 11337 (1986)

[104] G E Streit, C J Howard, A L Schmeltekopf, J A Davidson and H I Schiff *J Chem Phys* **65** 11 (1976)

[105] D Smith and R A Fouracre *Planet Space Sci* **16** 243 (1968)

[106] H I Schiff *Neutral Atmospheric Chemistry* (Introduction and review papers presented at the Summer Advanced Study, Institution of Physics and Chemistry of Upper Atmosphere) (University of Orleans, France) (1972)

[107] R Link and L L Cogger *J Geophys Res* **93** A9 9883 (1988)

[108] D R Bates *Planet Space Sci.* **26** 897(1978)

[109] S Chapman *Proc Roy Soc.* **A132** 353(1931)

[110] C A Barth *J Geophys. Res* **69** 3301 (1964)

[111] R G A Greet *Planet.Space. Sci* **27** 7 925 (1979)

[112] J E Frederick *J Geophys Res.* **81** 3923 (1976)

[113] D R Bates *Planet Space Sci.* **29** 1061 (1981)

[114] J W Chamberlain and B J Ngaard *J Atmos. Terr. Phys* **9** 169 (1956)

[115] L Vegard *Nature* **62** 300 (1948)

[116] L Vegard, G Kvifte, A Omholt and S Larsen *Geophys. Publik* 19 1 (1955)

[117] S Chapman *Meterorol. Mag.* **73** 137 (1938)

[118] S A Chapman *Astrophys J.* **90** 309 (1939)

[119] D R Bates and M Nicolet *J. Geophys. Res* **55** 235 (1950)

[120] D R Bates *Terr Mag.* **52** 71 (1947)

[121] D R Bates *J. Geophys Res* **55** 347 (1950)

[122] V I Krassovsky *Airglow and the Aurorae* (eds.) B Armstrong and A Dalgarno 197 (London : Pergamon) (1956)

[123] E L Breig *Planet Space Sci.* **18** 1271 (1970)

[124] J Gordon Vaeth *200 Miles Up* (New York : The Ronald Press)

[125] R M Good *The Physics of the Stratosphere* (University Press Cambridge) (1954)

[126] Institute of Radio Engineers *Standard on wave propagation, Definition of terms* 1950 *Proc IRE.* **38** 1264 (1950)

[127] R Silberstein *J Atmos Terr Phys* **13** 382 (1959)

[128] L A Fisk *Solar Terrestrial Physics* (eds) R L Carovillano and J M Forbes (Dordrecht . D Riedel) (201) (1983)

[129] A Egeland *Atmospheres of Earth and the Planets* (ed) B M McCormac (Dordrecht D Reidel) (1974)

[130] H I Schiff (ed) B M McCormac *Atmospheres of Earth and the Planets* (Dordrecht : D Reidel) (1974)

[131] E Durand *The Atmospheres of the Earth and Planets* (Chicago . University Press) (1949)

[132] R W Schunk *Solar Terrestrial Physics* (eds.) R L Carovillano and J M Forbes (Dordrecht . D Reidel) (1983)

[133] A H Gabriel and H E Mason *Applied Atomic Collision Physics* **Vol 1** (eds) H S W Massey and D R Bates (New York . Academic) (1982)

[134] M Carbonell and J L Ballester *Astron Astrophys* **255** 350 (1992)

[135] H W Newton *Geophys Suppl Mon. Not Roy Astron Soc* **5** 32 (1948)

[136] E Tandberg Hanssen *Astrophys J* **121** 367 (1955)

[137] J F Denisse *Ann Geophys* **8** 55 (1952)

[138] H W Dodson and E R Hedeman *J Geophys Res.* **63** 77 (1958)

[139] C S Warwick and R T Hansen *J Atm Terr Phys* **14** 287 (1959)

[140] D P Kanellakos *Radio Astronomical and Satellite Studies of the Atmosphere* (ed) J Aarons (Amsterdom North Holland) (1963)

[141] C B Sawyer *J Geophys Res* **72** 385 (1967)

[142] T Atac *Astrophys and Space Sci* **135** 201 (1987)

[143] *Solar Geophysical Data Book* (NOAA, Department of commerce, USA)

[144] G A Chapman, A M Cookson and J J Dobias *Astrophys J* **432** 403 (1994)

[145] A Ozguc and T Atac *Solar Phys* **123** 357 (1989)

[146] R E Howard *Solar Phys* **131** 327 (1991)

[147] R Oliver and J L Ballester *Solar Phys* **156** 145 (1995)

[148] J Javaraiah and M H Gokhale *Solar Phys* **170** 389 (1997)

R Oliver, J L Ballester and F Bandin *Nature* **394** 552 (1998)

[150] G W Lockwood, A S Brian, L B Sallie and R R Radick *Nature* **360** 653 (1992)

[151] S D'silva and R Howard *Solar Phys* **151** 213 (1994)

[152] J Javaraiah and M H Gokhale *Solar Phys* **154** 173 (1995)

[153] H S W Massey *Applied Atomic Collision Physics* **Vol. 1** (eds) H S W Massey and D R Bates (New York . Academic) (1982)

[154] W Swider *Atmospheres of Earth and the Planets* (ed.) B M McCormac (Dordrecht D Reidel) (1974)

[155] P Stubbe *Atmospheres of Earth and the Planets* (ed.) B M McCormac (Doordrecht · D Reidel) (1974)

[156] *DNA Reaction Rate Handbook* 1972 DOD (Nuclear Information Centre, General Electric, California) **93** 102 (1972)

[157] R F Donally and J H Pope *NOAA Technical Report ERL* 276 (1973)

[158] A Dalgarno *Phil. Trans. R. Soc. London Ser.* **A250** 426 (1958)

[159] J A Ratcliffe, E R Schmerling, C S G K Setty and J O Thomas *Phil Trans Roy. Soc.* **A248** 621 (1956)

[160] D F Martyn *Proc. IRE* **47** 147 (1959)

[161] D F Martyn *Phys. Soc. Rept. Ionosphere Conf.* **212** (1955)

[162] H L Lung *J. Geophys. Res.* **54** 177 (1949)

[163] F Mariani *J. Atmos. Terr. Phys.* **10** 239 (1957)

[164] J A Ratcliffe *Solar Eclipses and the Ionosphere* (Pergamon London) (1956)

[165] A D Danilov and L D Morozova *Geomag. Aeron* **25** 593 (1985)

[166] S T Zalesak *Solar Terrestrial Physics* (eds) R L Carovillano and J M Forbes 781 (Dordrecht D Reidel) (1982)

[167] Y Sahai, J A Bittencourt, N R Teixeira and H Takahashi *J Atmos Terr Phys* **51** 433 (1989)

[168] J G Moore and E J Weber *J. Atmos Terr Phys* **43** 851 (1981)

[169] G K Mukherjee and L Carlo *J Geomag Geoelectr* **46** 1029 (1994)

[170] S Chandra, E I Reed and B E Troy (Jr) *J Geophys Res* **78** 4630 (1973)

[171] I Kimura, K Tsunehara, A Hikuma, Y- Z. Su, Y Kasahara and H Oya *J Atmos Sol Terr Phys* **59** 1569 (1997)

[172] D Barbier *Compt. Rend* **245** 1559 (1957)

[173] E H Carman and B P Kilfoyle *J Geophys Res* **68** 5606 (1963)

[174] B S Salaria, N S Chauhan and H S Gurm *Indian J Radio and Space Phys* **16** 221 (1987)

[175] S K Midya and D Midya *Earth, Moon and Planet* **71** 1 (1995)

[176] D Barbier *Ann Geophys* **15** 179 (1959)

[177] P Lagos, W Bellew and S M Silverman *J Atmos Terr Phys* **25** 581 (1963)

[178] V L Peterson and W R Steiger *J Geophy Res* **71** 9 2267 (1966)

[179] S Jain, S D Mishra, S K Vijay and A K Gwal *Indian J Phys* **72B** (1) (1998)

[180] G K Mukherjee *Terr Atmos Oce. Sci* (TAO) **10** 265 (1999)

[181] R P Wayne *Physics and Chemistry of Upper Atmosphere* (ed) B M McCormac (Dordrecht D Reidel) 125 (1973)

[182] I T N Jones *Atmospheres of the Earth and the Planets* (ed.) B M McCormac (Doordrecht D Reidel) (1974)

[183] S N Ghosh and S K Midya *Indian J. Phys* **68B** (6) 473 (1994)

[184] S K Midya *Earth, Moon and Planets* **65** 1 (1994)

[185] S K Midya and H Sarkar *Czech J Phys* **51** 6 609 (2001)

[186] D M Packer *Ann Geophys* **17** 67 (1961)

[187] S C Solomon, P B Hays and V J Abreu *J Geophys Res* **93A** 9867 (1988)

[188] S M L Melo, H Takahashi, B P Clemensha and J Stegman *J Atmos Sol Terr Phys* **59**, 295(1997)

[189] G G Shepherd, C Mclandress and B H Solheim *Geophys Res Lett.* **22** 275 (1995)

[190] T N Davis and L L Smith *J Geophys Res* **70** 1127 (1965)

[191] M Zuzic, L Scherliess and G W Prolss *J Atmos Sol Terr Phys* **59** 711 (1997)

[192] M P Hickey, P G Richards and D G Torr *J Geophys Res* **100** A9 17377 (1995)

[193] S N Ghosh and S K Midya *Indian J Phys* **63B** (2) 212 (1989)

[194] G K Mukherjee *Indian J Radio Space Phys* **23** 393 (1994)

[195] Y Z Su, G J Bailey, K L Oyama and N Balan *J. Atmos Sol Terr Phys.* **59** 1299 (1997)

[196] S N Ghosh and S K Midya *Indian J. Phys.* **60B** 418 (1986)

[197] R P Lowe, L M LeBlanc and K L Gilbert *J Atmos Terr Phys* **58** 1863 (1996)

[198] G K Mukherjee, L Carlo and S H Mahajan *Earth, Planets Space (Japan)* **52** (2000)

[199] V A Kiselev *Geomag. Aeron* **31** 379 (1991)

[200] V Singh *Indian J. Radio Space Phys.* **21** 370 (1992)

[201] H Tanabe, A Takuchi, A Miyashita and K Tanaka *Ref. Nat. Astron Obs. Jpan* **1** 309 (1992)

[202] L M Kagan and V L Frolov *J Atmos Terr Phys* **58** 1465 (1996)
[203] D Bhaumik, J N Chakraborty, S K Midya and S R Chakraborty *Earth, Moon and Planets* **75** 169 (1996)
[204] W K Hocking *J. Atmos Terr Phy.* **58** 735 (1996)
[205] S N Priyatkm and E L Stupitskii *Cosm Res* **30** 204 (1992)
[206] I A Grebnev, A-V Gurvich, G P Millnevich and S Sh Nikolaishvilli *Cosm Res* **31** 92 (1993)
[207] S N Ghosh and S K Midya *Indian J Phys.* **63B** 913 (1989)
[208] Y Sahai, H Takahashi, J A Bittencourt, J H A Sobral and N R Teixeira *J Atmos Terr Phys* **50** 135 (1988)
[209] D Bhaumik, R Chattopadhyay, J N Chakraborty, S K Midya, K Sengupta and S N Ghosh *Proc Int. Symp Radio, Remote Sensing of the Atmos Environ CSIR*, NPL 385 (1990)
[210] S K Midya, G Tarafdar and T K Das *Indian J Pure and Appl Phys* **5** 183 (1993)
[211] W J McNeil, E Murad and S T Lai *J Geophys. Res* **100** D8 16847 (1995)
[212] T I Toroshelidze *Astophys Space Sci* **215** 11 (1993)
[213] S Kurosaki, M D Yamanaka, H Hashiguchi, T Sato and S Fukao *J Atmos Terr Phys.* **58** 727 (1996)
[214] H Takahashi, B R Clemensha and P P Batista *J. Atmos Terr. Phys.* **57** 407 (1995)
[215] R G Burnside and C A Tepley *Planet Space Sci* **38** 77 (1990)
[216] N N Pertshev *Akad Nauk, Fiz Atmos Okona (Russia)* **29** 608 (1993)
[217] S B Mende, S P Geller, E Murad and C P Pike *J Geophys Res* **98** 19117 (1998)
[218] G Kockarts *Atmospheres of the Earth and the Planets* B M McCormac (Dordrecht · D Reidel) (1974)
[219] P Blum, I Haris and W Priester *Cospar International Reference Atmosphere* (1972)
[220] L G Jacchia i) *Smithsonian Contribution to Astrophysics* **8** 215 (1965); ii) *Smithsonian Institute Astrophysics Observatory, Special Report* 332 (1971)
[221] A E Hedin *J Geophys. Res.* **92** A5 4649 (1987)
[222] A E Hedin *J Geophys Res* **96** A2 1159 (1991)
[223] Y T Chiu *J. Atmos. Terr. Phys.* **37** 1563 (1975)
[224] D N Anderson, M Mendillo and B Herniter *Radio Sci.* **92** 292 (1987)
[225] D N Anderson, J M Forbes and M Coderescu *J. Geophys Res.* **90** 1520 (1989)
[226] *STEP Handbook of Ionospheric Models* (ed) R N Schunk (Utah State University) p217 (1996)
[227] K M Muller, U Langematz and S Pawson *J Atmos Sci* **54** 2749 (1997)
[228] T Landeau, F Gauthier and N Ruelle *J. Atmos. Sol. Terr. Phys* **59** 125 (1997)
[229] CCIR model 1980 Kyoto, Supplement No 3 to Report 340 (IUT, Geneva) (1978)
[230] J J Sojka and R W Schunk *J Atmos. Sol. Terr Phys.* **59** 207 (1997)
[231] G J Bailey and R Cellek *Ann. Geophys.* **8** 171 (1990)
[232] G J Bailey, R Sellek and Y Rippeth *Ann. Geophys.* **11** 263 (1993)
[233] G J Bailey and N Ballan *STEP Hand Book on Ionospheric Model* (ed.) R W Schunk 173 (1996)
[234] C G Fesen *J. Atmos Sol. Terr. Phys.* **59** 1521 (1997)
[235] P G Richards and D G Torr *J. Geophys. Res.* **91** 9017 (1986)
[236] P G Richards and D G Torr *J. Geophys. Res.* **93** 4060 (1988)
[237] P G Richards *J. Geophys. Res.* **96** 17839 (1991)
[238] K L Miller, M Lemon and P G Richards *J. Atmos. Sol Terr Phys* **59** 1805 (1997)
[239] J R Dudeney *J Atmos. Terr. Phys* **45** 629 (1983)
[240] D Bilitza *Radio Science* **21** 343 (1986)
[241] D Bilitza *90-22 National Space Science Data Centre* (Green Belt MD) (1990)
[242] Yu E Belikov, Sh S Nikolaishvili and R K Peradze *Cosmic Res* 108 (1993)
[243] Yu E Belikov *J Atmos. Terr Phys.* **58** 1843 (1996)
[244] J Kazil, E K Opp , S Chabrillat and J Bishop *J. Geophys Res* 108 ACH-11-1-15 (2003)
[245] J S Nisbet *Atmospheres of the Earth and the Planets* (ed) B M McCormac (Dordrecht D Reidel) (1974)
[246] F de Mendonka *Radio Astronomical and Satellite Studies of the Atmosphere* (ed.) J Aarons (Amsterdam North Holland) (1963)
[247] R S Roger *Radio Astronomical and Satellite Studies of the Atmosphere* (ed) J Aarons (Amsterdam · North Holland) (1963)
[248] J Frihagen *Radio Astronomical and Satellite Studies of the Atmosphere* (ed) J Aarons (Amsterdam · North Holland) (1963)
[249] L Liszka *Radio Astronomical and Satellite Studies of the Atmosphere* (ed) J Aarons (Amsterdam · North Holland) (1963)
[250] C L Dieter *Radio Astronomical and Satellite Studies of the Atmosphere* (ed) J Aarons (Amsterdam : North Holland) (1963)
[251] V P Bhatnagar and G G Shepherd *J Atmos Terr Phys* **49** 950 (1987)
[252] M Jian Min and L Qi Li *Chin J Space Sci* **6** 137 (1986)
[253] J C Gerard and C E Noel *J Geophys Res* **91** A9 10136 (1986)
[254] V B Wickwar *Atmospheres of Earth and the Planets* (ed) B M McCormac (Dordrecht D Reidel) (1974)
[255] U Von Zahn *Atmospheres of Earth and the Planets* (ed) B M McCormac (Dordrech D Reidel) (1974)
[256] T M Danahue *Atmospheres of Earth and the Planets* (ed) B M McCormac (Dordrecht D Reidel) (1974)
[257] A T Stair (Jr), J C Ulwick, K D Baker and D J Bakar, *Atmospheres of Earth and the Planets* (ed.) B M McCormac (Dordrecht D Reidel) (1974)
[258] S M Adles -Golden, M W Matthend, D R Smith and A J Ratkoushi *J Geophys Res* **95** A9 15243 (1990)
[259] R W Eastes, R E Huffman and F J Leblanc *Planet Space Sci* 40 481 (1992)
[260] H Yamamidto, I Naito, T Makino and H Sekiguchi *J Geomagn Geoelect.* **44** 207 (1992)
[261] S J Lipson, P S Armstrong, J A Dodd, J R Lowell, W A M Blumberg and R M Nadile *Geophys Res Lett.* **21** 2421 (1994)
[262] S E Mende, G R Swenson, S P Geller and K A Spear *Geophys Res.Lett* **21** 283 (1994)
[263] D G Torr, M R Torr and P G Richards *Geophys Res. Lett.* **20** 519 (1993)
[264] S Chakraborti, T P Sasseen, M Lamptors and S Bowyer *Geophys Res. Lett.* **20** 535 (1993)
[265] M R Torr, D G Torr and P G Richards *Geophys. Res. Lett* **20** 531 (1993)
[266] S A Budzien, P D Feldman and R R Conway *J. Geophys. Res* **99** A12 23275 (1994)
[267] M P Hickey, G Schubert and R L Walterscheid *J. Geophys Res* **98** A8 13717 (1993)
[268] B M Cotton, S Chakraborti and G R Gladstone *J. Geophys. Res* **98** A12 21627 (1993)

[269] E M Wescott, H C Stenback-Nielser, D L Hampton and P A Delamere *J.Geophy. Res.* **99** A2 2145 (1994)

[270] D D Sentman and E M Wescott *Geophys. Res Lett.* **20** 24 2857 (1993)

[271] H Nebel, P P Wintersteiner, R H Picards, J R Winick and R D Sharma *J Geophys. Res.* **99** D5 10409 (1994)

[272] M D Burrage, N Arrin, W R Skinner and P B Hays *J. Geophys Res.* **39** A8 15017 (1994)

[273] R E Maycrott, G R Swenson, E L Sweitzer and D G Koch *J Geophys. Res.* **99** A9 17559 (1994)

[274] E M Wescott, H C Stenback-Nielsen and D L Humpton *Geophys Res. Lett* **19** 20 2079 (1992)

[275] J M Jahn, J LaBelle, J H A Sobral, T L Aggson and W B Hanson *J Atmos Sol Terr Phys* **59** 1601 (1997)

[276] M Kubota, K Shio Kawa, M K Ejiri, Y Otsuka, T Ogawa, T Sakanoi, H Fukunishi, M Yamamoto, S Fukao and A Sait *Geophys Res. Lett.* **27** 4037 (2000)

[277] M G Miynczak, F Morgan, J-H Yee, P Espy, D Murtagh, B Marshall and F Schmidlin *Geophys Res Lett* **28** 999 (2001)

[278] K Knutsen *et al, Planet. Space Sci* **36** 307 (1988)

[279] M G Mlynczak and D J Nesbitt *Geophys. Res. Lett* **22** 1381 (1995)

[280] R Link, J S Evans and G R Gladstone *J Geophys Res.* **99** 2121 (1994)

[281] M H Stevens, R R Meier, R R Conway and D E Strobel *J Geophys Res* **99** A1 417 (1994)

[282] F Bahsoma Hamade, R H Weings, G G Shepherd and P G Richards *J Geophys Res* **99** A4 6289 (1994)

[283] M J Jamieson, M Finch, R S Friedman and A Dalgarno *Planet Space Sci* **40** 11719 (1992)

[284] F G Eparvier and C A Earth *J Geophys Res* **97** A9 1372 (1992)

[285] D R Hershbach, C F Kolb, D R Worsnop and X Shi *Nature* **356** 6368 414 (1992)

[286] C O-Hines, H G Mayi and C A Reddy *J Atmos Terr Phys* **59** 181 (1997)

[287] G M Shred, L E Khvorostovskaya Igop, Yu Potekhin, V P Ogibalov and T V Vzyakova *Proc SPIE-Int SOC. Opt. Eng* (USA) **482** 106 (2003)

[288] Y Sahai, H Tashashi, J A Bittencourt, J H A Sobral and N R Teixeira *J Atmos. Terr. Phys* **50** 135 (1988)

[289] S K Midya, G Tarafdar and T K Das *Earth, Moon and Planets* **75** 177 (1996)

[290] E I Terez and G A Terez *J Atmos Terr. Phys* **58** 1849 (1996)

[291] K Labitzke and H VanLoon *J Atmos. Sol Terr Phys* **59** 9 (1997)

[292] B R Clemensha, P P Batista and D M Simonich *J Atmos Sol Terr Phys* **59** 131673 (1997)

[293] Y Saha, D H Giers, L L Cogger, P R Fagundes and G P Garbe *J Atmos. Terr. Phys.* **58** 1927 (1996)

[294] V M Silbergleit *J. Atmos. Sol Terr. Phys.* **59** 259 (1997)

[295] O P Kolomiitsev, B M Reddy and V A Surotkin *J. Atmos. Sol. Terr. Phys.* **59** 1287 (1997)

[296] N O de Adler, A G Elias and J R Manzano *J. Atmos Sol. Terr. Phys.* **59** 159 (1997)

[297] P A Smith and J W King *J. Atmos Terr. Phys.* **43** 1057 (1981)

[298] S K Midya, G Tarafdar and T K Das *Earth, Moon and Planets* **70** 135 (1997-1998)

[299] A V Mikhailov, M Froster and T K Legehins Koya *Ann. Geophys.* **18** 1422 (2000)

[300] J E Borovsky and W O Funsten *J. Geophys. Res.* **108** SMP 13-1-25 (2003)

[301] K Misawa *Ref Ionosph Res* **29** 162 (1975)

[302] O Struve *Elementary Astronomy* (New York Oxford University Press) (1959)

[303] J W Warwic *Radio Astronomical and Satellites Studies of the Atmosphere* (ed) J Aarons (Amsterdom North Holland) (1963)

[304] G N Taylor *Radio Astronomical and Satellites Studies of the Atmosphere* (ed) J Aarons (Amsterdom North Holland) (1963)

[305] V M Vsylinuas *Solar Terrestrial Physics* (eds) R L Carovillano and J M Forbes (Dordrechet D R Reidel) (1983)

[306] J Kristl, M Esplin, T Hudson, M Taylor and C L Siefring *Earth, Moon and Planets* **82-83** 525 (2000)

[307] K Biosch and O Shemmer *Earth, Moon and Planets* **82-83** 1 535 (2000)

[308] C Mercier *J Atmos Terr Phys.* **48** 7 605 (1968)

[309] D W Tarassic and C O Hines *Planet Space Sci* **38** 1105 (1990)

[310] J R Isler, T F Tuan, R H Picard and VcMaklouf *J Geophys Res* **96** A8 14141 (1991)

[311] C O Hines *J Atmos Sol Terr Phys* **59** 319 (1997)

[312] D Y Wang, W E Ward, Y J Rochou, G G Shepherd, S P Zhang, R H Weins, D Y Liang, W A Gault and B H Slheim *J Atmos Sol Terr Phys* **63** 35 (2001)

[313] J L Innis, P A Greet and D L Dyson *J Geophys Res* **106** A8 15489 (2001)

[314] J H Hetch, R L Walterschila and R H Viscent *J. Geophys Res* **106** D22 28189 (2001)

[315] Xu and Ji Yao *Proc SPIE-Int Soc Opt Eng* (USA) 4678 622 (2002)

[316] V I Shematovich, D V Bisikalo and J C Gerard *J Geophys Res* **99** A12 23217 (1994)

[317] P R Fagundes, Y Sahai, H Takahashi, D Gobbi and J A Bitten court *J Atmos Terr Phys* **58** 1963 (1996)

[318] P R Field and H Rishbeth *J Atmos Sol Terr Phys* **59** 163 (1997)

[319] S K Saha *Indian J Phys.* **75B** 285 (2001)

[320] Y Sahai, K Shiokawa, Y Otsuka, G Thara, T Ogauda, K Igarashi, S Miyazaki and A Saito *J. Geophys Res* **98** A12 21651 (1993)

[321] W L Boeck, O H Vaughan (Jr), R Blakeslee, B Vonnegut and M Brook, *Geophys. Res. Lett.* **19** 99 (1992)

[322] L M Fiskova, M B Gokhberg and V A Pilipenko *Ann Geophys* **3** 689 (1985)

[323] K Akmamedov *Geomag Aeron* **33** 135 (1993)

[324] G K Mukherjee *Bull IAPT (India)* **16** 303 (1999)

[325] D M Cotton, G R Gladstone and S Chakraborty *J Geophys Res* **98** A12, 21651 (1993)

[326] R J Sica, J P St Maurice, G Hernandez, G J Romick and T Sunoda *J Geophys Res* **98** A9 18667 (1993)

[327] P Cinzano *Mem Soc Astron. Ital* **71** 159 (2000)

[328] J Xiao-Jun, X Da -Wei and H Jing -Yao *Acta. Astro Phys. Sin* **19** 220 (1999)

[329] H C S- Nielsen, D R Moudry, E M Wescott, D D Sentman and F T S Sabbas *Geophys. Res. Lett.* **27** 3829 (2000)

[330] T F Bell, V P Pasko and U S Inan *Geophys. Res Lett.* **22** 2127 (1995)

[331] H J Fahr *et al, J. Geophys. (Germany)* **54** 219 (1984)

[332] Yu I Galperin and E I Gol' braikn *Cosm. Res.* **28** 619 (1990)

[333] F J M Rietmeijer *Earth, Moon and Planets* **82-83** 505 (1998)

[334] R A Viereck and E Murad *Nature* **354** 48 (1991)

[335] R E Meyerott and G R Swenson *Planet. Space. Sci.* **39** 469 (1991)

[336] W A D Greet, N H Pratt and J P W Stark *Geophys. Res. Lett* **20** 1731 (1993)

[337] G E Caledonia, K W Hotzclaw, B D Green and R H Krech *Geophys Res Lett.* **17** 1881 (1990)

[338] R G West, M R Sims and R Willingale *Planet Space. Sci* **42** 71-80 (1994)

[339] D A Dean, E R Huppi, D R Smith and R M Nadile *Geophys Res Lett* **21** 609 (1994)

[340] D K Zhou, W R Pendleton (Jr), G B Bingham, A J Stend and D A Dean *Geophys Res Lett* **21** 613 (1994)

[341] D K Zhou, W R Pendleton (Jr), G B Binghan, D C Thanson, U Raitt and R M Nadile *Geophys Res Lett* **99** A10 19585 (1994)

[342] A A Kurskov, A A Kitillov and A V Afonin *Sov J Opt Technol* **59** 8 472 (1992)

[343] G Hernandez, R Wems, R P Lowe, G G Shepherd, G J Fraser, R W Smith, L M Leblanc and M Clark *Geophys Res Lett* **22** 2389 (1995)

[344] G D Price, R N Smith and G Hernandez *J. Atmos Terr Phys* **57** 631 (1995)

[345] W Swider *Planet. Space Sci* **40** 247 (1992)

[346] H S S Sinha and S Raizads *Earth, Planets Space* **52** 549 (2000)

[347] K Shio Kawa and Y Kiyama *J Atmos Sol Terr Phys.* **62** 1215 (2000)

[348] D Gobbi, H Takahashi, B R Clemensha and P P Batista *Planet Space Sci* **40** 775 (1992)

[349] I C McDade, W E Sharp, P G Richards and D G Torr *J Geophys Res* **96** 259 (1991)

[350] D E Siskind and W E Sharp *Plant, Space. Sci* **38** 1399 (1990)

[351] M J Lopez- Gonzalez, U J Lopez-Moreno and R Rodrigo *Planet Space. Sci* **40** 929 (1992)

[352] R R Mier *Space. Sci. Rev.* **58** 1 (1991)

[353] W R Swift, D G Torr, M R Torr., C Hamilton, H Dongani, P G Richards and G G Sivjee *J Geophys. Res* **95** 15227 (1990)

[354] D Pallamraju, J Baumgardner, S Chakraborti and T R Pedersen *J Geophys Res* **106** 5543 (2001)

[355] K Hocke and K Igarashi *Earth,Planets Space* **54** 947 (2002)

[356] H S W Massey *Applied Atomic Collision Physics* **Vol. 1** (eds) (H S W Massey and D R Bates (New York : Academic Press) (1982)

[357] T E Cravens *Solar Terrestrial Physics* (eds) R L Carovillano and J M Forbes (Doradrecht D Reidel) (1983)

[358] S Kumar *Atmospheres of the Earth and the Planets* (ed) B M McCormac (Dordrecht D Reidel) (1974)

[359] L J Paxton *J Geophys Res* **93** 8473 (1988)

[360] M B Mcelroy *Atmospheres of the Earth and the Planets* (eds) B M McCormac (Dordrecht D Reidel) (1974)

[361] T D Parkinson *Atmospheres of the Earth and the Planets* (ed) B M McCormac (Dordrecht . D Reidel) (1974)

[362] Y L Young *Atmospheres of the Earth and the Planets* (eds) B M McCormac (Dordrecht D Reidel) (1974)

[363] G E Hunt *Atmospheres of the Earth and the Planets* (eds) B M McCormac (Dordrecht · D Reidel) (1974)

[364] D F Strobel, R R Meier, M E Summers and D J Strickland *Geophys Res Lett.* **18** 689 (1991)

[365] T H Morgan and D E Shemansky *J Geophys Res* **96** A2 1351 (1991)

[366] J Borovicka and R Jenniskens *Earth, Moon and Planets* **82** 399 (1998)

[367] C A Kruschavitz, M C Kettey, C S Gardner, G Swenson, A-Z Liu, X Chiu, J D Drum, W T Armstrong, J M C Plane, B W Grime and P Jenniskens *J Geophys Res* **106** 21525 (2001)

About the Reviewers

R Chattopadhyay

Dr. Rabindranath Chattopadhyay obtained M.Sc. (Physics) degree from Calcutta University in 1987 and Ph.D. degree in Upper Atmospheric Research from Jadavpur University in 2004. His field of specialization is airglow, solar terrestrial relationship and their consequences as rgistered in Terrestrial Ionospheric changes. He is at present an assistant teacher of Physics in Haripal G.D. Institution, Khamarchandi, Hooghly, West Bengal.

S K Midya

Dr. Subrata Kumar Midya is a senior Reader in Physics in the Department of Physics, Serampore College, Srampore, Hooghly. His field of specializaiton is airglow, O_3 depletion and interstellar molecules. He has published more than seventy research papers in different international journals. He is also an Honorary scientist at the Centre for Space Physics, 43 Chalantika, Garia station Road, Kolkata-84. He has supervised three successful Ph.D scholars and at present is engaged as referee of different research journals.